MIXED CONVECTION HEAT TRANSFER IN POWER LAW FLUIDS FROM A SQUARE CYLINDER

A Thesis Submitted

in Partial Fulfillment of the Requirements

for the Degree of

MASTER OF TECHNOLOGY

by

ANJAIAH NALAPARAJU

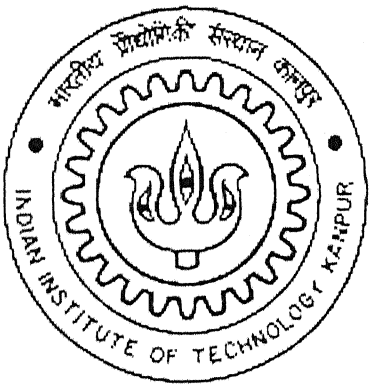

to the

DEPARTMENT OF CHEMICAL ENGINEERING

INDIAN INSTITUTE OF TECHNOLOGY KANPUR

April, 2005

Certificate

It is certified that the present work entitled "**Mixed Convection Heat Transfer in Power Law Fluids from a Square Cylinder**" has been carried out by Mr. Anjaiah Nalaparaju under my supervision and this work has not been submitted elsewhere for a degree.

Dr. R. P. Chhabra
Professor,
Department of Chemical Engineering,
Indian Institute of Technology,
Kanpur – 208016, India

April, 2005

Acknowledgements

I am deeply thankful to Dr. R. P. Chhabra for his valuable guidance, support and inspiration throughout the course of my research.

I would also like to thank my lab mates Sunil, Nanda kishore, Amit, Ravi, Ramprakash and Amrita for their immense help.

Lastly I would like to thank to all my class mates for making my stay at Kanpur truly memorable.

IIT Kanpur

Anjaiah Nalaparaju

Abstract

Combined forced and natural convection (Mixed convection) heat transfer from a cylinder of square cross section oriented normal to the direction of flow continues to be one of the important problems due to its fundamental nature as well as the many related engineering applications such as cooling of electronic components, compact heat exchangers, combustion chambers in chemical process and energy systems. Mixed convection flow around a square cylinder in cross flow will be highly complex because the velocity induced by thermal buoyancy will be normal to the forced flow direction and will distort the flow field around the body and hence the heat transfer. A wealth of information is available on the influence of buoyancy parameter (Ri) on the Drag and Lift coefficients, wake structure and time averaged Nusselt number on the cylinder when the flow is unsteady and the fluid exhibits the standard Newtonian flow behaviour. Incontrast, virtually no analogous results available for steady flow case even for Newtonian fluids and no prior study is available for the simplest type of non-Newtonian fluid behaviour, namely , shear thinning and shear thickening modeled by the usual two-parameter power-law fluid model.

In this study, the effect of combined forced and natural convection (mixed convection) on flow and heat transfer characteristics of steady, incompressible flow of power law fluids over a heated square cylinder placed normally to the approaching fluid is analyzed. A SMAC–type implicit scheme has been implemented on a staggered grid to solve complete Navier-Stokes and Energy equations for a two-dimensional laminar flow of a Boussinesq fluid over a square cylinder. Parametric calculations have been performed to determine the effect of Reynolds number (Re =5, 10 and 40), Richardson number ($0 \leq Ri \leq 0.5$), Prandtl number ($Pr \leq 10$), power law index ($0.5 \leq n \leq 1.4$) and Wall effects on hydrodynamic and thermal conditions for a blockage ratio of 1/15. The dynamics of flow and heat transfer are made visible by means of contour plots.

Contents

Nomenclature

A	projected area
b	Side of square cylinder
B	Blockage Ratio (b/H)
D	Divergence of velocity predictor
C_D	Total drag coefficient
C_{DF}	Friction drag coefficient
C_{Dp}	Pressure drag coefficient
C_L	Lift coefficient
C_{LF}	Friction lift coefficient
C_{LP}	Pressure lift coefficient
F_D	Drag force on the cylinder
F_L	Lift force on the cylinder
Gr	Grashof number
h	Local heat transfer coefficient
H	Height of the physical domain
i	Index used in x-direction
j	Index used in y-direction
k	Thermal conductivity of the fluid
L	Integer variable
L_d	down stream length
L_U	Upstream length
m	Power law consistency index
M	Number of cell in y-direction (including fictitious)
n	Power-law index
N	Number of cell in x- direction (including fictitious)
$<Nu>_f$	Average Nusselt number for front face
$<Nu>_m$	Overall average Nusselt number for square cylinder
$<Nu>_r$	Average Nusselt number for rear face
$<Nu>_t$	Average Nusselt number for top face

$<Nu>_b$	Average Nusselt number for bottom face
Nu	Local Nusselt number
p	Pressure
p'	Pressure correction (Chapter 3)
Pe	Peclet Number
Pr	Prandlt Number
q	Heat flux per unit length from the square cylinder
Re	Reynolds number based on side of square cylinder
Ri	Richardson number
T	Temperature
T_w	Temperature of square cylinder
T_∞	Temperature of free stream
U_∞	Uniform inlet velocity in channel
V_x	x-direction velocity
V_y	y-direction velocity

Greek Symbols

ψ	Stream function
ω	Vorticity
μ	Viscosity
ρ	Density of fluid
τ	Shear stress
Π	Second invariant of the rate of strain tensor
ϵ	Rate of strain tensor
υ	Momentum diffusivity
β	Coefficient of volumetric expansion

Superscripts

'	Dimensional variable
n	nth time step
*	Predicted values (Chapter 3)
'	Correction values (Chapter 3)

Chapter 1

INTRODUCTION

1.1 Introduction

Flow past a heated or a cooled cylinder of square cross-section with its longitudinal axis aligned normal to the direction of the approaching flow has attracted a great deal of attention over the years. Such studies have been motivated from two distinct but inter-related objectives. From a theoretical standpoint, such highly idealized model configurations are convenient for elucidating the fluid mechanical phenomena including drag and wake characteristics, vortex shedding frequency, etc. and their effect on the rate of heat transfer. On the other hand, this type of information is frequently needed for the technical problems associated with energy conservation, for structural problems in wind engineering, the prediction of aerodynamic forces acting on a body such as buildings and structures exposed to fluid flow wherever the flow induced vibrations are important and due to changing process and climatic conditions, one also needs to calculate heat transfer from such structures to select an appropriate material of construction. This type of flow is relevant to many practical applications like vortex flow meters, chimneys, compact heat exchangers, offshore platforms, the passages in equipments used for heat and mass transfer processes, suspension bridges, cooling of electronic components and equipments, flow dividers in polymer processing applications, etc.

Consequently, over the years a wealth of information on flow past a square cylinder has accumulated in the literature. From a careful scrutiny of the available literature, it is fair to summarize the current status as follows. Most of these studies relates to fluid mechanic aspects of steady and unsteady flow regimes and therefore an adequate body of information is available on the detailed flow field and on the time averaged drag and lift coefficient, Strouhal numbers, periodicity of flow, wake length, etc. for both confined and unconfined cases for Newtonian fluids like air and water. Depending on the Reynolds number, different flow regimes can be distinguished for a square cylinder. At very small Reynolds numbers ($Re < 1$), viscous forces dominate the flow and, no separation takes place at the surface of the cylinder in the so-called creeping flow. With increasing Reynolds number, the flow separates first at the trailing edges of the cylinder and a

closed steady recirculation region consisting of the two symmetric vortices is observed behind the body. The size of the recirculation zone increases with an increase in Reynolds number .When a critical Reynolds number is exceeded, the well-known von Karman vortex street with periodic vortex shedding from the cylinder can be detected in the wake. This transition occurs at about the value of Reynolds number in the range of 50-70.When the Reynolds number is further increased, the flow separates at the leading edges of the cylinder. The transition to three dimensionality takes place at a value of Reynolds number between 150 and 175 in an unconfined flow. Channel-confinement alters the critical Reynolds numbers for the transitions mentioned above, generally an increase in the blockage ratio leads to an increase in the critical values of Reynolds number relative to transition from steady to periodic flow.

In contrast, only limited numerical and experimental results are available on the heat transfer from a square cylinder to liquid flowing normally to its axis. Knowledge of the heat transfer coefficients is needed by the designers in the development of compact heat exchangers. The developments of new surfaces for compact heat exchangers have been attracting much attention in the engineering community motivated by the necessity to reduce the weight and volume of such equipment. The compact heat exchangers find application in automobiles, air conditioning, electronic cooling, spacecraft and aircraft. These devices usually operate in the laminar regime. This is because of the flow velocities and passage sizes are small and consequently the Reynolds numbers are low. Furthermore, the passage lengths are large, so the flow is fully developed in most of the channel. In order to enhance the heat transfer rates over the laminar fully developed values, devices that mix the main flow are introduced. A variety of such interruption devices have been proposed in the past. These have included placement of staggered and in-line baffles, louvers, and transverse vortex generators in the form of cylinders grooved channels (or) square bars. The flow in a channel with a built-in square cylinder can be assumed as one compact heat exchanger. Furthermore, this classical and practically interesting phenomenon has its implications in other applications ranging from heat exchangers to solar heating, combustion chambers, chemical processes and energy systems equipment, environmental control systems, cooling passages in turbine blades

and cooling of electronic packages. The geometry presents a simple yet essential paradigm for understanding the convection heat transfer in air-cooled passages containing bluff objects, as in the cooling of printed circuit boards. A number of engineering design parameters connected with fluid flow and heat transfer become important in these studies. Apart from the engineering relevance, a study of these mechanisms associated with the laminar flow past cylinders forms the first step towards understanding the vastly more complicated phenomenon. The rate of heat transfer is intimately dependent on the fluid dynamical behavior of the flow close to the surface. Through a laminar boundary layer, for example, the flow rate is much lower than if the layer were turbulent, and the variation of the heat flow rate with fluid velocity is very different in the two cases. To investigate this contrast, numerous experimental and theoretical studies have been conducted, especially in reference to the forced convection. Most of the heat transfer work reported in the literature pertains to the numerical investigation of the unsteady laminar flow pattern and forced convective heat transfer in a channel with a built-in square cylinder where the main thrust is to find the effect of von karman vortex street on the forced convective heat transfer and to find time averaged Nusselt number. Relatively little work has been done on temperature distribution in natural convection caused by isothermal horizontal square cylinder in an infinite quiescent fluid medium even with Newtonian fluids.

An examination of the available previous work shows that only limited numerical results are available on the forced convective heat transfer across a square cylinder in the steady flow regime. Paliwal et al. [16] investigated the 2D steady flow ($5 \leq Re \leq 40$) of power law liquids past a square cylinder for the range of Peclet numbers 5-400 by using the FDM on a uniform staggered grid arrangement in an unconfined configuration (β =1/15). The influence of the type of thermal boundary condition, i.e., the constant heat flux and the constant temperature at the surface of the cylinder has also been studied. While it is readily acknowledged that the values of Prandtl number up to ~ 100 are frequently encountered in chemical, petroleum and oil related industrial applications in the processing of organic liquids (glycols , glycerols) and petroleum fractions. Furthermore, owing to the generally high viscosity of process streams, the Reynolds numbers are not

excessively high and the assumption of 2D steady flow is therefore justified under these conditions.Gupta et al. [12] have investigated the 2D steady confined flow ($5 \leq Re \leq 40$; $\beta = 1/8$) of power law liquids past a square cylinder for the range of Peclet numbers 5-400 by using the FDM on a uniform staggered grid arrangement in a channel with parabolic velocity profile at the channel inlet. The shear- thinning behavior not only reduces the size of the recirculation region but also delays the wake formation, and shear- thickening fluids show the opposite effect on the wake formation. They also found the faster decay in the temperature field at high Peclet numbers in shear – thinning fluids, with the reverse behaviour being observed in shear-thickening. Overall, Shear-thinning fluid behaviour facilitates heat transfer whereas shear-thickening behaviour impedes it. Sharma and Eswaran[18] Presented a detailed examination of the flow structure and the effect of flow unsteadiness on the forced – convection heat transfer from the square cylinder, and heat transfer correlations between Nusselt number and Reynolds number, applicable in the two-dimensional regime ($Re \leq 160$), were proposed for both uniform heat flux and constant cylinder temperature boundary conditions. Dhiman et al.[9,10] have recently studied the effect of Peclet number ($0.7 \leq Pe \leq 4000$) on the heat transfer across a square cylinder in an unconfined and confined ($\beta = 1/8, 1/6$ and $1/4$) domain in the steady flow regime ($1 \leq Re \leq 45$). Heat Transfer from a square cylinder especially with viscous dissipation has been investigated by Nitin and Chhabra [15] in the Reynolds number range of 5 to 40, Peclet number 5 to 500 and Brinkman number 0.1 to 10 for both Newtonian and power law fluids. All the work mentioned above reveals that very few investigators to date have attempted the non-isothermal flow across a square cylinder for forced convection.

Situations may arise when the flow velocity is not very high and the temperature difference between the body surface and ambient fluid is large. The flow and heat transfer characteristics are then strongly influenced by the buoyancy forces, developed as the result of density gradients. Strictly speaking, in any convective heat transfer circumstance, natural convection effects are always, how so ever small to be present. Forced flow in which the buoyancy driven flow also affects the main flow is called mixed convection. The parameter that characterizes mixed convection is the Richardson

number, $Ri=Gr/Re^2$. Physically, the magnitude of Richardson number indicates the relative effect of buoyancy on forced convection. From a practical standpoint, the question is how large these effects are, and under what conditions they may be neglected as compared to forced convection effects. On the other hand, if the buoyancy effects are of greater relative magnitude, it is the question of when forced convection that may be neglected. A careful review of literature reveals that boundaries between natural and mixed convection, and between mixed and forced convection are not well established for several important geometries. Juma and Richardson [14] have found that free convection exerts a significant influence when Ri exceed about 0.2. The values of $Ri \rightarrow 0$ and $Ri \rightarrow \infty$ correspond to the forced and natural convection limits respectively. In mixed convection flows, one would normally expect enhancement of heat transfer between the fluid and the surfaces over the corresponding pure forced convection flow. However, flow separations will hinder this enhancement. Again the relative magnitude of Reynolds number and Grashof number will decide whether free convection has beneficial or adverse effects on heat transfer. The analysis of mixed convection flow usually requires a thorough understanding of the two limiting modes. Unfortunately, mixed convection is not simply the superposition of the two modes owing to the nonlinear and coupled governing equations. The complexity of the convection transport is caused largely by interaction of buoyancy forces and the force field. Depending upon the direction of the flow in relation to the obstacle, the free convection may assist or oppose or the two may be oriented in a cross direction. Mixed convection processes may be considered in terms of external flow over surfaces, in the free boundary flows (such as plumes and buoyant jets), and in terms of internal flows in tubes, channels, and enclosed flow regimes. The effect of buoyancy on heat transfer in a forced flow is strongly influenced by the direction of the buoyancy force relative to that of the flow.

Combined forced and natural convection heat transfer from a horizontal cylinder has been the subject of many experimental and theoretical investigations because of it numerous engineering applications. Most of the work on the mixed convection flow across a cylinder has been done for the circular cross-section when the forced flow is directed either vertically upward (assisting flow) or vertically down ward (opposing flow). The

main objective of these investigations is to find critical Reynolds number when the flow changes from a periodic to twin vortex pattern i.e. break down of von Karman vortex street for a heated cylinder and the initiation of vortex shedding for buoyancy opposing flow at low Reynolds numbers. Also, to delineate the extent of the influence of buoyancy on the Nusselt number, wake structures, temporal lift and drag forces. In contrast, only little work has been reported for the mixed convection flow around a cylinder of cross flow configuration when the mean flow is normal to the direction of gravity. This case is highly complex because the velocity induced by the thermal buoyancy is normal to the forced flow direction and thus distorts the flow filed around the body thereby altering the values of drag coefficient and heat transfer. One may encounter such mixed convection flows in a plate-fin heat exchanger with horizontally mounted tubes or heating elements. The subsequent literature survey focuses upon mixed convection from a horizontal cylinder in cross flow. A review of the earlier work on circular cylinder related to the current investigations is presented first. Numerous experimental studies have been performed on air in cross flow over horizontal cylinders, to develop general heat transfer correlations for mixed convection conditions (Hatton [13], Juma [14], Bennon[5]). Other efforts (Fand[11], Sharma[21]) have concentrated on identifying regions associated with natural, forced and mixed convection. The regions have been delineated in terms of a Grashof- Reynolds number ratio of the form Gr/Re^n , where n is typically in the range of 2 to 3. Virtually no analogous experimental results available for the square cylinder. Aside from correlation efforts, there appers to have been little analytical study of the problem. Badr[3] initiated the numerical investigation of mixed convection heat transfer from a isothermally heated circular cylinder using stream function – vorticity method to study the effect of cross- stream buoyancy, but limited his study to the steady flow regime in the range of Reynolds number ($1 < Re < 40$) and Grashof number up to 5 while keeping Prandtl number at 0.7 . He found that surface vorticity and accordingly the velocity gradient at the surface increases significantly with Richardson number, mainly due to buoyant forces aiding the flow around most of the cylinder surface resulting lower pressure and creation suction. The stream lines upstream of the cylinder have downward slope towards the point of minimum pressure. The reverse flow in the wake is also strongly influenced by Richardson number. It was found that at large values of

Richardson number, no reverse flow takes place in the wake and vortices completely disappear. With increasing Ri, while the maximum value of Nusselt number continues to occur near the forward stagnation point, the point of minimum Nusselt number moves upward from the rear stagnation point on the surface of cylinder and average Nusselt number increases. When Richardson number is small, the temperature field is almost symmetric about the horizontal centerline of cylinder, mainly governed by the imposed flow. With the increase of Richardson number, the point of plume separation moves upward and isotherm pattern changes accordingly. An analysis of mixed convection heat transfer from a circular cylinder dissipating a uniform heat flux under cross flow conditions was reported by Ahmad and Quershi [2].In the ranges of Reynolds number ($1 < Re < 40$) and the modified Grashof number $0 < Gr < 1.6 \times 10^4$ for Pr=0.7 .The normalizing scales for velocity and temperature were chosen depending upon whether the flow is dominated by forced convection or natural convection. The governing vorticity-transport equation along with appropriate boundary conditions was solved by a finite difference relaxation method. They found the flow and temperature fields to be similar to that reported by Badr[3]. They also reported the drag coefficient increased due to the buoyancy force, above that which would exist for a purely forced convection case at the same Reynolds number. Bassam and Hijleh [4] solved numerically the problem of laminar mixed convection from an isothermal cylinder. Several correlations were proposed to predict the Nusselt number in mixed convection regime from an isothermal cylinder at arbitrary angles of attack. Wang et al. [23] found that the heated circular cylinder has the same critical Reynolds number as the unheated cylinder for the onset of vortex shedding if the Reynolds number is defined based on a kinematic viscosity evaluated at an effective temperature. They also found a universal relationship between Strouhal number and effective Reynolds number applicable for a wide range of cylinder temperature.

In comparison with the circular cylinder case, there is significantly less work available on the cylinders of square cross section. The flow past a square cylinder resembles flow past a circular cylinder as for as the instabilities are concerned. But the separation mechanism i.e. the behavior of shifting separation points due to buoyancy is much different. Biswas

et al. [6] presented a numerical study of mixed convection in a horizontal channel with a built –in square cylinder symmetrically placed in the channel axis. Their study shows that mixed convection can initiate periodicity and symmetry in the wake at lower Reynolds numbers than forced convection alone and for a given Reynolds number, the heating of the fluid in the channel is improved by mixed convection up to a certain Grashof number and deteriorates if the Grashof number is further increased. Abbasi et al. [1] carried out a numerical investigation to study the mixed convection in a horizontal channel with a built –in triangular prism. At Re=100, the formation of convective cells is observed when Grashof number reaches ~ 5 X 10^3 . These cells result in an increase in heat transfer from the wall to the fluid. For Grashof numbers ranging from 5 X 10^3 to 10^4, the von Karman street is seen tilting towards the top wall, while for Gr >10^4, von karman street changes slant and becomes from the shedding area to the bottom wall. A numerical investigation was conducted by Turki et al.[22] to analyze the effect of thermal buoyancy on the flow pattern and heat transfer characteristics in a horizontal channel with a built-in heated square cylinder for Richardson number up to 0.1 and β =1/4. They found in mixed convection, the critical value of Reynolds number relative to transition from steady to periodic flow decreases with increasing Richardson number where as Strouhal number increases with Richardson number. The dominant effect observed is the deflection of most of flow toward the bottom of the body. When the buoyancy becomes significant, the heat transfer shows a remarkable increase in compared to those obtained in pure forced convection. They have also proposed correlations for global time averaged Nusselt number as function of Reynolds number. Recently, Sharma and Eswaran [20] numerically studied the effect of buoyancy on the flow structure and heat transfer characteristics of an isolated cylinder in horizontal cross flow for Re=100 and Ri= 0 to 1for Pr=0.7. The focus of this study was towards understanding the effect of cross-stream buoyancy on the onset and / or suppression of vortex shedding in the presence or absence of an adiabatic channel. Furthermore, the objective is to generate numerical data base for the flow and heat transfer parameters with respect to Richardson number and blockage ratio. All the work discussed above are for Newtonian fluids. Virtually no analogous results have been found for the Non-Newtonian fluids. The increasing use of Non-Newtonian fluids in chemical industries has necessitated understanding their behavior in

many transport processes (chhabra [7]). The prediction of heat transfer rates from non-Newtonian fluids, is therefore, of practical interest. While applying the numerical and analytical tools to solve the problems of fluid dynamics and heat transfer for non-Newtonian fluids, a number of complications arise due to the non-linear relation between the stress tensor and deformation strain tensor. There are various empirical models suggested in the literature for non-Newtonian fluids. If one ignores the effect of normal stresses in the generalized constitutive equation(Denn [8]), for a two dimensional flow, it reduces to a power-law model, is the one which is most commonly used.

A careful review of the above mentioned literature reveals that no numerical results are available to explore the effect of buoyancy on the flow and heat transfer from a square cylinder placed normally to approaching steady flow even for Newtonian fluids. And no prior study is available for the simplest type of non-Newtonian fluid behavior, namely, shear thinning and shear thickening modeled by the usual two-parameter power-law model. The objective of the present study is to fill this gap in the literature.

1.2 Objectives of the present work

The objective of this to study the effect of combined forced and natural convection (mixed convection) on flow and heat transfer characteristics of steady, incompressible flow of power law fluids over a heated square cylinder placed normally to the approaching fluid. To analyze this complete Navier-Stokes and Energy equations for a two-dimensional laminar flow of a Boussinesq fluid over a square cylinder is solved by implementing a SMAC- type implicit scheme on a staggered grid . Parametric calculations have been performed to determine the effect of Reynolds number (Re = 10 and 40), Richardson number ($0 \leq Ri \leq 0.5$), Prandtl number ($Pr \leq 10$), power law index ($0.5 \leq n \leq 1.4$) and Wall effects on hydrodynamic and thermal conditions for a blockage ratio of 1/15. The dynamics of flow and heat transfer are made visible by means of contour plots.

Chapter 2

MATHEMATICAL FORMULATION

This chapter presents the description of the physical problem of flow and mixed convection across a square cylinder, followed by approximations and idealizations made, and finally, the mathematical equations describing the flow togetherwith the relevant boundary conditions. The equations are non-dimensionalised in order to reduce the number of variables. Also, the auxiliary equations to calculate flow parameter (drag and lift coefficient), heat transfer parameter (Nusselt number), non-Newtonian viscosity, stream function and vorticity are also presented in this chapter.

2.1 Physical model

The problem being considered is the forced flow across a heated or a cooled square cylinder inducing upward or downward flow near the cylinder due to buoyancy force that occurs as a result of density changes arising from the temperature gradient near the cylinder. This buoyancy force is considered negligible for the forced convection case. Due to buoyancy, the flow is induced upward for a heated and downward for a cooled cylinder with the buoyancy force acting perpendicular to the horizontal-flow direction, representing the cross stream buoyancy case. In this case, the results obtained for a heated or a cooled cylinder will be similar symmetric; therefore, only the case of a heated cylinder has been considered in the present investigation.

2.2 Problem Statement

The geometry and the relevant dimensions considered for the present analysis are shown schematically in Figure 2.1(a) and 2.1(b) for the unconfined and channel-confined flow cases, respectively. In the unconfined flow case shown in figure 2.1(a), a fixed two-dimensional square cylinder with side b (which is also the nondimensionalizing length scale) maintained at a constant temperature T_w is exposed to a constant free-stream velocity U_∞ and temperature T_∞, respectively. In order to make the problem computationally feasible, artificial confining boundaries are placed around the flow, where "free-slip " boundary conditions are used. However, the boundaries are sufficiently far away from the body so that their presence has little effect on characteristics of the flow near the body.

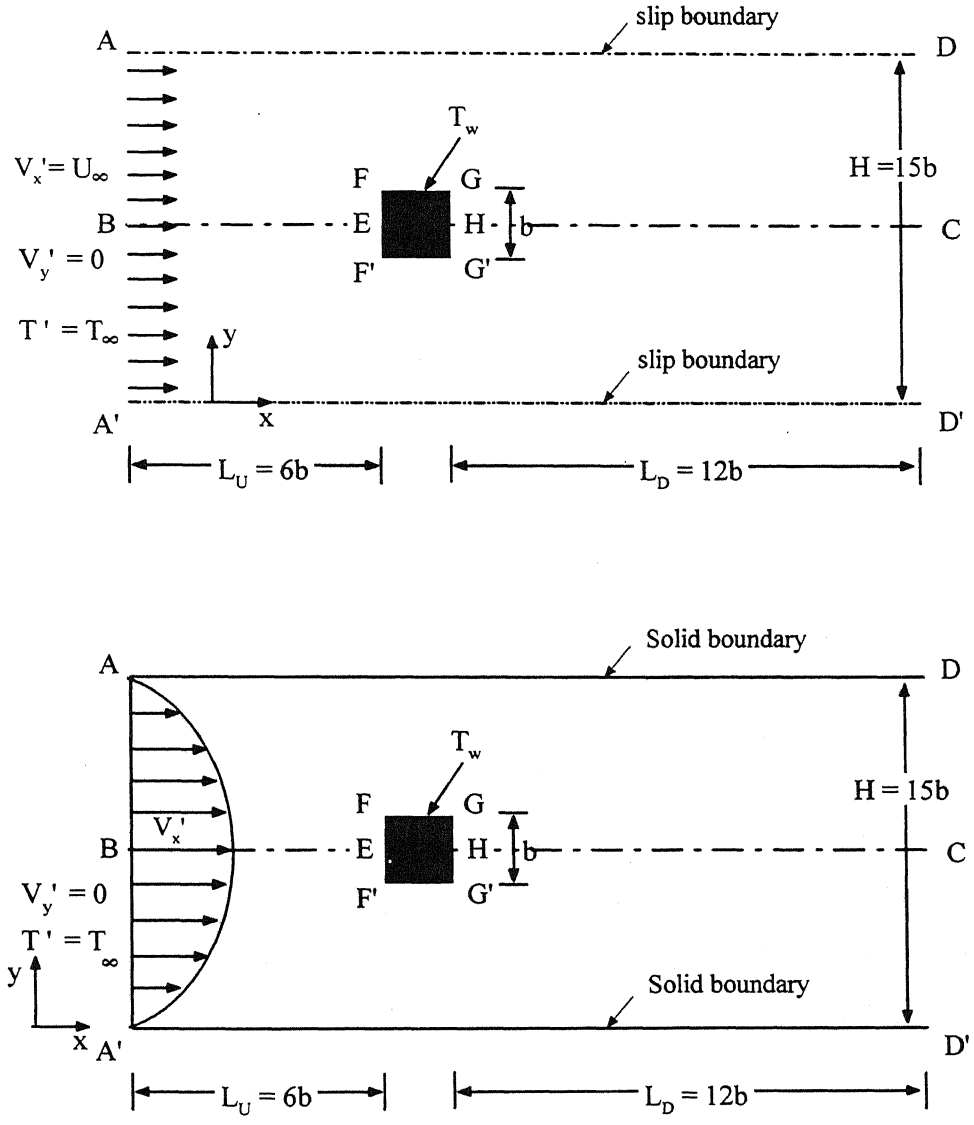

Figure 2.1: The physical model for (a) unconfined and (b) channel-confined horizontal-flow across a square cylinder and associated parameters.

The ratio of the width of the cylinder to the vertical distance between the top and the bottom boundaries, defines the blockage ratio of the confined flow. The channel confined flow case is obtained when "no-slip " boundary conditions are applied to the two adiabatic channel walls of finite length placed horizontally at a distance of H/2 on either side of the center of the cylinder, as shown in figure 2.1(b). It is assumed that the fluid enters the channel under fully developed conditions, i.e., with a parabolic velocity profile (with average velocity $U_{max} = U_\infty$) and temperature T_∞ . The results in this case are also applicable for the channel of infinite length with constant U_∞ inlet velocity profile. This allows us to compare the confined flow case with the unconfined flow case (where the inlet velocity profile is constant). The distance between the inlet plane and the front surface of the cylinder (upstream length) and the distance between the rear surface of the cylinder and the exit plane (downstream length) are represented by L_u and L_D respectively, as shown in figure. The fluid under consideration is assumed to be incompressible and of power law fluid. Since the maximum value of the Reynolds number considered in this work is 40, the flow is assumed to be two – dimensional and steady. Hence, there is no flow in the Z-direction and no flow variable depends upon the z-coordinate, i.e., $\partial(\ )/\partial z=0$. Furthermore, the thermo-physical properties (density, heat capacity, thermal conductivity, power law constants) are assumed to be independent of temperature except for the body force term in the momentum equation (the Boussinesq approximation). Thus the flow field is coupled with the corresponding temperature.

2.2.1: Boussinesq approximation

In flows accompanied by heat transfer, the fluid properties are normally functions of temperature. The variations may be small and yet be the cause of the fluid motion. If the density variation is not large, one may treat its variation only in the gravitational term. While all other thermo-physical properties of the fluid are assumed to remain constant, the density, associated with the buoyancy force, is assumed to vary linearly with temperature as per the relation: $\rho_\infty = \rho\ [1 + \beta\ (T - T_\infty)]$ where β is the coefficient of volumetric expansion at constant pressure, T_∞ is the temperature of the ambient fluid and ρ_∞ is the corresponding density. This is called the Boussinesq approximation. In most of

the analytical as well as numerical studies of natural/mixed convection flows, the classical Boussinesq approximation is customarily invoked.

2.3: Mathematical Model

A mathematical model consists of differential equations that govern the behaviour of the physical system and the associated boundary conditions. Employing these approximations and idealizations, the physical model described in the above section is simulated by an equivalent mathematical model involving the conservation of mass, momentum and energy, with appropriate boundary conditions. The mathematical model comprising the partial differential equations, along with suitable boundary conditions is presented in the following section.

2.3.1: Governing Equations

The laminar mixed convection is governed by three conservation equations; namely, continuity, momentum, and energy (in the absence of viscous dissipation) with Boussinesq approximation. A rectangular coordinate system is chosen for convenience. The velocity components in x – and y-directions are V_x' and V_y' respectively. The flow is assumed to be two dimensional and steady.

Therefore the velocity component in x, y and z –directions are given as

$$V_x' = V_x'(x', y'),\ V_y' = V_y'(x', y') \text{ and } V_z' = 0 \tag{2.1}$$

Under these conditions, the equation of continuity for an incompressible fluid reduces to:

$$\frac{\partial V_x'}{\partial x'} + \frac{\partial V_y'}{\partial y'} = 0 \tag{2.2}$$

And the corresponding x- and y-components of the Cauchy equations in terms of extra stress components are written as:

x-component:

$$\rho\left(\frac{\partial V_x'}{\partial t'} + V_x'\frac{\partial V_x'}{\partial x'} + V_y'\frac{\partial V_x'}{\partial y'}\right) = -\frac{\partial p'}{\partial x'} + \left(\frac{\partial \tau_{xx}'}{\partial x'} + \frac{\partial \tau_{yx}'}{\partial y'}\right) \tag{2.3}$$

y-component:

$$\rho\left(\frac{\partial V_y'}{\partial t'}+V_x'\frac{\partial V_y'}{\partial x'}+V_y'\frac{\partial V_y'}{\partial y'}\right)=-\frac{\partial p'}{\partial y'}+\left(\frac{\partial \tau_{yy}'}{\partial y'}+\frac{\partial \tau_{xy}'}{\partial x'}\right)+\rho g_y \tag{2.4}$$

(For heated cylinder flow due to natural convection is upward so $g_y = -g$)

From Boussinesq approximation $\rho_\infty = \rho\,[1 + \beta\,(T - T_\infty)]$

Above relation can be approximated as $\rho = \rho_\infty\,[1 - \beta\,(T - T_\infty)]$ (2.5)

where β is the coefficient of volumetric expansion at constant pressure, T_∞ is the temperature of the ambient fluid and ρ_∞ is the corresponding density.

From this relation and by replacing ρ by ρ_∞ on the left side y-component equation can be written as

$$\rho_\infty\left(\frac{\partial V_y'}{\partial t'}+V_x'\frac{\partial V_y'}{\partial x'}+V_y'\frac{\partial V_y'}{\partial y'}\right)=-\frac{\partial p'}{\partial y'}+\left(\frac{\partial \tau_{yy}'}{\partial y'}+\frac{\partial \tau_{xy}'}{\partial x'}\right)+\rho_\infty g\beta(T-T_\infty) \tag{2.6}$$

ρ_∞ is a constant , for simplicity denote it by ρ

where $\tau_{ij}' = 2\,\eta'\varepsilon_{ij}'$ (i,j = x,y) (2.7)

The rheological equation, which represents the power law fluid behaviour, is as follows:

$$\eta' = m(2\Pi_\varepsilon')^{(n-1)/2} \tag{2.8}$$

where η' is the non-Newtonian viscosity, m is the power law consistency index, n is the power law index and Π_ε' is the second invariant of the rate of strain tensor given by:

$$\Pi_\varepsilon' = \varepsilon_{xx}'^2 + \varepsilon_{yy}'^2 + 2\varepsilon_{xy}'^2 \tag{2.9}$$

Here ε_{ij}' is defined as the rate of strain tensor which is related to the velocity field, in rectangular coordinates, by

$$\varepsilon_{xx}' = \frac{\partial V_x'}{\partial x'} \tag{2.10}$$

$$\varepsilon_{yy}' = \frac{\partial V_y'}{\partial y'} \tag{2.11}$$

$$\varepsilon_{xy}' = \varepsilon_{yx}' = \frac{1}{2}\left(\frac{\partial V_x'}{\partial y'}+\frac{\partial V_y'}{\partial x'}\right) \tag{2.12}$$

$$\varepsilon_{zz}' = \varepsilon_{xz}' = \varepsilon_{zx}' = \varepsilon_{yz}' = \varepsilon_{zy}' = 0 \tag{2.13}$$

Evidently , $n < 1$ indicates the shear thinning behavior ; $n > 1$ shear thickening and $n = 1$ denotes the standard Newtonian fluid behavior.

The equation of thermal energy in terms of transport properties, for non-Newtonian fluids of constant c_p, ρ, k, neglecting the viscous dissipation terms, can be written as:

$$\rho c_p\left(\frac{\partial T'}{\partial t'}+V_x'\frac{\partial T'}{\partial x'}+V_y'\frac{\partial T'}{\partial y'}\right) = k\left(\frac{\partial^2 T'}{\partial x'^2}+\frac{\partial^2 T'}{\partial y'^2}\right) \tag{2.14}$$

Non-dimensionalization of the Governing Equations:

By using the following scaling variables, the continuity equation, the components of Cauchy equation and energy equation are non-dimensionalised:

$$V_x=\frac{V_x^1}{U_\infty};V_y=\frac{V_y^1}{U_\infty};x=\frac{x'}{b};y=\frac{y'}{b};t=\frac{t'}{\left(\frac{b}{U_\infty}\right)};\ T=\frac{T'-T_\infty}{T_w-T_\infty}$$

$$P=\frac{p'}{\rho U_\infty^2};\eta=\frac{\eta'}{\eta_o};\tau=\frac{\tau'}{\left(\frac{\eta_o U_\infty}{b}\right)};\Pi_\varepsilon=\frac{\Pi_\varepsilon'}{\left(\frac{U_\infty}{b}\right)^2}$$

$$\varepsilon_{ij}=\frac{\varepsilon_{ij}'}{\left(\frac{U_\infty}{b}\right)}\ ;\ \text{where},\eta_o=m\left(\frac{U_\infty}{b}\right)^{n-1}$$

Non-dimensionalized form of equations

Continuity :
$$\frac{\partial V_x}{\partial x}+\frac{\partial V_y}{\partial y}=0 \tag{2.15}$$

x-component:
$$\frac{\partial V_x}{\partial t}+V_x\frac{\partial V_x}{\partial x}+V_y\frac{\partial V_x}{\partial y} = -\frac{\partial p}{\partial x}+\frac{1}{\mathrm{Re}}\left(\frac{\partial \tau_{xx}}{\partial x}+\frac{\partial \tau_{yx}}{\partial y}\right) \tag{2.16}$$

y-component:
$$\left(\frac{\partial V_y}{\partial t}+V_x\frac{\partial V_y}{\partial x}+V_y\frac{\partial V_y}{\partial y}\right)=-\frac{\partial p}{\partial y}+\frac{1}{\mathrm{Re}}\left(\frac{\partial \tau_{yy}}{\partial y}+\frac{\partial \tau_{xy}}{\partial x}\right)+RiT \tag{2.17}$$

Energy equation:
$$\frac{\partial T}{\partial t}+V_x\frac{\partial T}{\partial x}+V_y\frac{\partial T}{\partial y}=\frac{1}{Pe}\left(\frac{\partial^2 T}{\partial x^2}+\frac{\partial^2 T}{\partial y^2}\right) \tag{2.18}$$

Where,

$$\mathrm{Re} = \frac{\rho(U_\infty)^{2-n} b^n}{m} \tag{2.19}$$

$$Gr = \frac{g\beta(T_w - T_\infty)\rho^2 U_\infty^{2(1-n)} b^{(2n+1)}}{m^2} \tag{2.20}$$

$$\mathrm{Pr} = \frac{c_p m}{k}\left(\frac{U_\infty}{b}\right)^{n-1} \tag{2.21}$$

$$Pe = Re * Pr \text{ and } Ri = \frac{Gr}{\mathrm{Re}^2} \tag{2.22}$$

The dimensionless non-Newtonian viscosity can be written as:

$$\eta = m(2\Pi_\varepsilon)^{(n-1)/2} \tag{2.23}$$

$$\Pi_\varepsilon = \varepsilon_{xx}^2 + \varepsilon_{yy}^2 + 2\varepsilon_{xy}^2 \tag{2.24}$$

$$\varepsilon_{xx} = \frac{\partial V_x}{\partial x} \tag{2.25}$$

$$\varepsilon_{xx} = \frac{\partial V_y}{\partial y} \tag{2.26}$$

$$\varepsilon_{xy} = \varepsilon_{yx} = \frac{1}{2}\left(\frac{\partial V_x}{\partial y} + \frac{\partial V_y}{\partial x}\right) \tag{2.27}$$

After substituting equations (2.23-2.27) and (2.15) in equations (2.16) & (2.17) and writing equations in the conservative form, we get:

x-component

$$\frac{\partial V_x}{\partial t} + \frac{\partial (V_x V_x)}{\partial x} + \frac{\partial (V_y V_x)}{\partial y} = -\frac{\partial p}{\partial x} + \frac{\eta}{\mathrm{Re}}\left(\frac{\partial^2 V_x}{\partial x^2} + \frac{\partial^2 V_x}{\partial y^2}\right) + \frac{2}{\mathrm{Re}}\left(\varepsilon_{xx}\frac{\partial \eta}{\partial x} + \varepsilon_{yx}\frac{\partial \eta}{\partial y}\right) \tag{2.28}$$

y-component

$$\left(\frac{\partial V_y}{\partial t} + \frac{\partial (V_x V_y)}{\partial x} + \frac{\partial (V_y V_y)}{\partial y}\right) = -\frac{\partial p}{\partial y} + \frac{\eta}{\mathrm{Re}}\left(\frac{\partial^2 V_y}{\partial x^2} + \frac{\partial^2 V_y}{\partial y^2}\right) + \frac{2}{\mathrm{Re}}\left(\varepsilon_{yy}\frac{\partial \eta}{\partial y} + \varepsilon_{xy}\frac{\partial \eta}{\partial x}\right) + RiT \tag{2.29}$$

Energy equation

$$\frac{\partial T}{\partial t}+\frac{\partial (V_x T)}{\partial x}+\frac{\partial (V_y T)}{\partial y} = \frac{1}{Pe}\left(\frac{\partial^2 \mathrm{T}}{\partial x^2}+\frac{\partial^2 T}{\partial y^2}\right) \qquad (2.30)$$

2.3.2 Boundary conditions:

The boundary conditions (in their dimensionless form) for governing equations are as follows:

- **Inlet boundary at AA':**

For the unconfined flow case

$$V_x=1, \quad V_y=0 \text{ and } \quad T=0$$

For the channel-confined flow case, parabolic inlet profile is used

$$V_x = \left[1-(2By-1)^{\frac{n+1}{n}}\right] \qquad \text{(for 1/2B < y <1/B) where (B=b/H)}$$

(This expression is used to calculate the upper half velocity profile, and with use of symmetry condition lower half velocities are calculated)

$V_y=0$ and $T=0$

- **Outlet boundary at DD':** The convective boundary condition given by

$$\frac{\partial V_i}{\partial t}+V_{conv}\frac{\partial V_i}{\partial x}=0, \quad (\mathrm{i}=\mathrm{x \text{ or } y})$$

$$\frac{\partial T}{\partial t}+V_{conv}\frac{\partial T}{\partial x}=0$$

The Orlanski boundary condition is used for right boundary, where V_{conv} was set equal to the maximum velocity $V_{max}$of the inlet profile. This condition ensures that vortices can develop and pass outflow boundary without significant disturbances or reflections into the inner domain.

- **Top boundary AD and Bottom boundaries A' D':**

Free slip boundary for the unconfined case :

$$\frac{\partial V_x}{\partial y}=0, \qquad V_y=0 \quad \text{and} \quad \frac{\partial T}{\partial y}=0$$

This implies a symmetric boundary condition for the temperature.

Channel walls for the confined case :

$$V_x=0, \quad V_y=0 \text{ and } \frac{\partial T}{\partial y}=0$$

This implies an adiabatic channel wall condition for the temperature, and no-slip conditions for the velocity.

- **Solid surface of the cylinder FGG'F':**

$$V_x=0, \quad V_y=0 \quad \text{(no-slip condition)}$$

And $T=1$ for the constant temperature on the surface of the cylinder.

2.4 Calculation of Drag and Lift coefficient

After solving equations (2.15), (2.28), (2.29) and (2.30) numerically, for $V_x(x,y)$, $V_y(x,y)$, $P(x,y)$, $T(x,y)$ the velocity field is used to estimate drag and lift coefficients. The total drag and lift comprises of individual components, i.e., friction drag and pressure or form drag.

The dimensionless drag and lift coefficients are defined as

$$C_D = \frac{F_D}{\left(\frac{1}{2}\rho U_\infty^2 b\right)} \text{ and } C_L = \frac{F_L}{\left(\frac{1}{2}\rho U_\infty^2 b\right)} \tag{2.31}$$

where F_D and F_L are the drag and lift forces exerted by the fluid on the cylinder, respectively. These forces are evaluated by integrating the pressure (normal) and viscous shear forces over the surface of cylinder. These forces are estimated by following expressions:

Pressure drag:

$$C_{DP} = 2\left[\int_{F'}^{F} p_f(y)dy - \int_{G'}^{G} p_r(y)dy\right] \tag{2.32}$$

Pressure lift:

$$C_{LP} = 2\left[\int_{F'}^{G'} p_b(x)dx - \int_{F}^{G} p_t(x)dx\right] \tag{2.33}$$

where $p(y)$ is the dimensionless pseudo pressure on the front(f) and rear(b) face and $p(x)$ is pressure on top(t) and bottom(b) face of cylinder respectively.

Friction drag:

$$C_{DF} = \frac{2}{\mathrm{Re}} \int_{F}^{G} \left(\eta \frac{\partial V_x}{\partial y} \right)_{FG} dx + \frac{2}{\mathrm{Re}} \int_{F'}^{G'} \left(\eta \frac{\partial V_x}{\partial y} \right)_{F'G'} dx \tag{2.34}$$

Friction lift:

$$C_{LF} = \frac{2}{\mathrm{Re}} \int_{F'}^{F} \left(\eta \frac{\partial V_y}{\partial x} \right)_{F'F} dy + \frac{2}{\mathrm{Re}} \int_{G'}^{G} \left(\eta \frac{\partial V_y}{\partial x} \right)_{G'G} dy \tag{2.35}$$

Therefore the total drag and lift coefficients are simply the sum of the pressure and friction components, given by the expression

$$C_D = C_{DP} + C_{DF} \text{ and } C_L = C_{LP} + C_{LF} \tag{2.36}$$

2.5 Calculation of Nusselt number

The Nusselt number is the non-dimensional temperature gradient averaged over the entire heat transfer surface, i.e., the cylinder. The local Nusselt number is defined in this study as

$$Nu_L = \frac{hb}{k} \tag{2.37}$$

where h is the local convective heat transfer coefficient and k is the thermal conductivity of the fluid .Depending upon the nature of the thermal boundary condition, the expression for the calculation of the Nusselt number will vary slightly. Expression for constant wall temperature condition is presented in the next section

2.5.1 Constant wall temperature condition

By equating the rate of heat transfer by conduction to that of by convection at the surface of cylinder yields:

For Top face FG :

$$q_{FG} = -k \left[\frac{\partial T'}{\partial y'} \right]_{FG} = h(T_w - T_\infty) \tag{2.38}$$

Where h is the local heat transfer coefficient at top face of cylinder.

Now, using equation (2.13), one can non-dimensionalize the above equation

$$-k\frac{(T_w - T_\infty)}{b}\left[\frac{\partial T}{\partial y}\right]_{FG} = h(T_w - T_\infty) \tag{2.39}$$

$$[Nu_x]_{FG} = \frac{hb}{k} = -\left[\frac{\partial T}{\partial y}\right]_{FG} \tag{2.40}$$

Similarly for bottom face F'G':

$$[Nu_x]_{F'G'} = \frac{hb}{k} = -\left[\frac{\partial T}{\partial y}\right]_{F'G'} \tag{2.41}$$

For front face FF' and rear face GG':

$$[Nu_y]_{FF' or GG'} = \frac{hb}{k} = -\left[\frac{\partial T}{\partial x}\right]_{FF' or GG'} \tag{2.42}$$

Equations (2.40-2.42) give the local Nusselt number over the all four faces for the constant wall temperature and constant wall heat flux, respectively. The average Nusselt number around each face for steady flow is evaluated by integrating the local Nusselt numbers over respective faces of the cylinder, so that:

For top face FG :

$$< Nu >_{FG} = \frac{1}{b}\int_F^G Nu_x dx \tag{2.43}$$

Similarly for bottom face F'G' :

$$< Nu >_{F'G'} = \frac{1}{b}\int_{F'}^{G'} Nu_x dx \tag{2.44}$$

For front face F F':

$$< Nu >_{FF'} = \frac{1}{b}\int_{F'}^{F} Nu_y dy \tag{2.45}$$

For rear face G G':

$$< Nu >_{GG'} = \frac{1}{b}\int_{G'}^{G} Nu_y dy \tag{2.46}$$

The overall Nusselt number for the square cylinder is evaluated by averaging the average Nusselt number of all faces.

2.6 Calculation of non-Newtonian Viscosity:

The dimensionless non-Newtonian viscosity is computed by non-dimensionalise equation (2.8), which obtained as

$$\eta = m(2\Pi_\varepsilon)^{(n-1)/2} \tag{2.47}$$

where

$$\Pi_\varepsilon = \varepsilon_{xx}^2 + \varepsilon_{yy}^2 + 2\varepsilon_{xy}^2 \tag{2.48}$$

$$\varepsilon_{xx} = \frac{\partial V_x}{\partial x} \tag{2.49}$$

$$\varepsilon_{yy} = \frac{\partial V_y}{\partial y} \tag{2.50}$$

$$\varepsilon_{xy} = \varepsilon_{yx} = \frac{1}{2}\left(\frac{\partial V_x}{\partial y} + \frac{\partial V_y}{\partial x}\right) \tag{2.51}$$

2.7 Calculation of stream function:

The stream function Ψ is defined as follows,

$$V_x = \frac{\partial \psi}{\partial y} \tag{2.52}$$

and it is calculated by integrating V_x velocity along y-axis as

$$\int_{\psi_1}^{\psi_2} d\psi = \int_{y_1}^{y_2} V_x \, dy \tag{2.53}$$

2.8 Calculation of vorticity, ω :

The vorticity is defined as,

$$\omega = \left[\frac{\partial V_y}{\partial x} - \frac{\partial V_x}{\partial y}\right] \tag{2.54}$$

Chapter 3

NUMERICAL METHODOLOGY

Numerical solution to the fluid flow and heat transfer problems can be obtained by two methods namely, Segregated and Coupled. The two methods differ in the calculation of temperature. In the so-called Segregated method momentum equation is solved first to obtain the steady state solution and then the velocity is used to obtain the temperature field by solving the energy equation. In the Coupled method momentum and energy equations are solved together for each time step up to the steady state. The choice of the method depends on the behavior of the temperature (passive or active) and the flow field (steady state or transient). A passive scalar does not affect the flow and is merely carried along by it but active scalar affects the flow. Temperature is passive for small temperature differences but active for large temperature differences as buoyancy begins to influence the flow. From the analysis it is found that the segregated method can be used only for steady state situation with passive scalars and the Coupled method should be used under other condition, i.e. steady state situation with active scalars and unsteady situation with active and passive scalars.

In this study, temperature is an active scalar so the Coupled method is used to solve the governing equations. A SMAC- type implicit scheme is implemented on a staggered grid to solve the complete Navier - Stokes and energy equations for a two-dimensional laminar mixed convection flow over a square cylinder in the cross-flow configuration. The convective terms have been discretized using the upwind scheme whereas the viscous terms have been approximated using the standard centre difference approach. A detailed description of the solution methodology is given in the subsequent sections.

3.1 Staggered grid

To solve the governing equations in the required flow domain, one needs to divide the flow domain into certain number of square or rectangular regions of equal size known as cell with a grid point located at the center of each cell. The type of grid depends upon the location of the scalars and vectors in the domain. For example, if all the scalars (pressure, viscosity and temperature) and vectors (velocity) are defined at the center of the cell, it is known as a normal or a collocated grid. While if scalars are defined

at the center of the cells and vectors are defined at the center of the cell faces on which they are normal, as shown in Figure 3.1, then it is known as "staggered grid". In such an arrangement, the pressure difference between any two adjacent cells is the driving force for the velocity component located between the interfaces of these cells. The finite difference approximation will accept a reasonable pressure distribution for a correct velocity field. This is physically more meaningful as compared to that for a collocated grid. Thus the pressure and velocity corrections are directly related to each other and the pressure velocity iterations converge quickly. Another important advantage is that transport rates across faces of the control volumes can be computed without interpolation of the velocity components.

As shown in Figure 3.1, grid points are labeled as (i, j), where i and j denote the numbering of grid as counted in x- and y- directions, respectively. Pressure and temperature are defined at the center of cell i.e. (i, j). V_x (i +1/2, j) is the component of velocity in the x-direction, which is defined at the midpoints of line joining (i, j) and (i+1,j). While V_y (i, j+1/2) is the component of velocity in the y-direction defined at the midpoint of line joining (i, j) and (i, j+1).

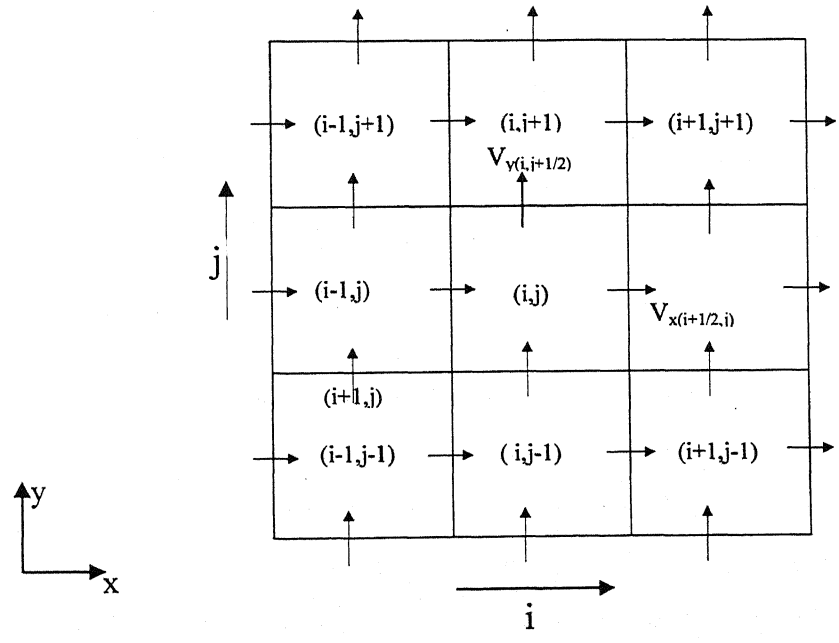

Fig 3.1 Two-dimensional staggered grid

In a staggered grid arrangement velocities are not defined at the cell center grid points so are determined by interpolations.

Figure 3.2 shows the computational domain for the present problem. The fictitious cells are denoted by dotted lines around the actual boundaries. Bold line denotes the square cylinder boundary surfaces. Boundary conditions are imposed on fictitious cells and the governing equations are solved for interior cells. The fictitious cells are used so that one can employ boundary conditions with second order accuracy.

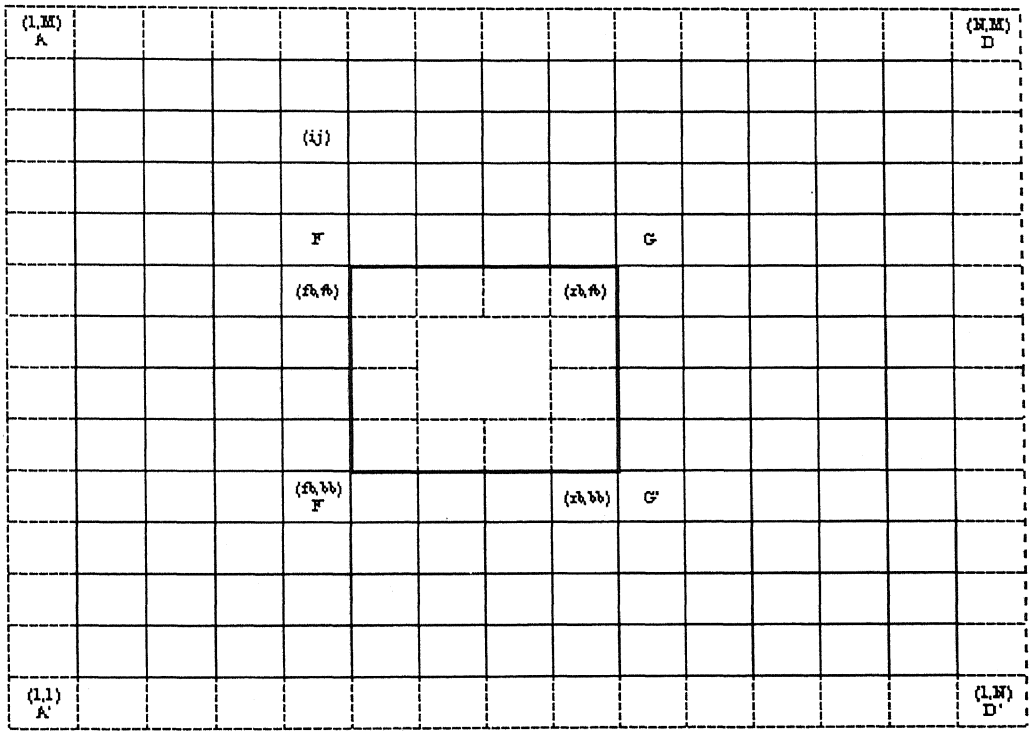

Figure 3.2 Grid Arrangement

As the present study is limited to a maximum Reynolds number of 40, the flow is steady and symmetric about the horizontal centerline of the flow domain. Thus, the upper half of the flow domain can be used as the computational domain for forced convection case. But in the case of mixed convection flow, due to buoyancy asymmetry will develop about the horizontal centerline even for small Richardson numbers. Therefore, computations have to be done for the full domain.

3.2 Finite difference discritisation:

Analytical solutions of partial differential equations provide us with closed-form expressions, which depict the variation of dependent variables in the domain. The numerical solutions, based on finite differences, provide us the values of the dependent variables at the discrete points in the domain, which are known as grid points. The basic philosophy of finite difference methods is to replace the derivatives of governing equations with a system of linear algebraic equations, which can be solved for the dependent variables at the discrete grid points in the flow field. Here the convective terms are discretized by first-order upwind differencing scheme and viscous terms by central difference scheme. Equations (2.15), (2.28), (2.29) and (2.30) can be written as

Continuity: $$\frac{\partial V_x}{\partial x}+\frac{\partial V_y}{\partial y}=0 \text{ or } \nabla.V=0 \tag{3.1}$$

x-momentum: $$\frac{\partial V_x}{\partial t}+[Conv_x]=-\frac{\partial p}{\partial x}+\frac{\eta}{\mathrm{Re}}[Diff_x]+\frac{2}{\mathrm{Re}}[Non_x] \tag{3.2}$$

y-momentum: $$\frac{\partial V_y}{\partial t}+[Conv_y]=-\frac{\partial p}{\partial y}+\frac{\eta}{\mathrm{Re}}[Diff_y]+\frac{2}{\mathrm{Re}}[Non_y]+RiT \tag{3.3}$$

Energy: $$\frac{\partial T}{\partial t}+[Conv_T]=\frac{1}{Pe}[Diff_T] \tag{3.4}$$

where [*Conv*], [*Diff*] and [*Non*] represent convective, diffusive and non-Newtonian terms and the subscript x, y, T corresponds to x-momentum, y-momentum and energy equations respectively.

They are given by the following expressions

$$[Conv_x]=\left[\frac{\partial(V_xV_x)}{\partial x}+\frac{\partial(V_yV_x)}{\partial y}\right] \tag{3.5}$$

$$[Diff_x]=\left[\frac{\partial^2V_x}{\partial x^2}+\frac{\partial^2V_x}{\partial y^2}\right] \tag{3.6}$$

$$[Non_x]=\left[\varepsilon_{xx}\frac{\partial\eta}{\partial x}+\varepsilon_{yx}\frac{\partial\eta}{\partial y}\right] \tag{3.7}$$

$$[Conv_y]=\left[\frac{\partial(V_xV_y)}{\partial x}+\frac{\partial(V_yV_y)}{\partial y}\right] \tag{3.8}$$

$$[Diff_y]=\left[\frac{\partial^2V_y}{\partial x^2}+\frac{\partial^2V_y}{\partial y^2}\right] \tag{3.9}$$

$$[Non_y]=\left[\varepsilon_{yy}\frac{\partial\eta}{\partial y}+\varepsilon_{xy}\frac{\partial\eta}{\partial x}\right] \tag{3.10}$$

$$[Conv_T]=\left[\frac{\partial(V_xT)}{\partial x}+\frac{\partial(V_yT)}{\partial y}\right] \tag{3.11}$$

$$[Diff_T]=\left[\frac{\partial^2T}{\partial x^2}+\frac{\partial^2T}{\partial y^2}\right] \tag{3.12}$$

3.2.1 Continuity:

The continuity equation, is discretised around grid point (i,j) given by

$$\left[\frac{\partial V_x}{\partial x}+\frac{\partial V_y}{\partial y}\right]_{i,j}=0$$

where ,

$$\frac{\partial V_x}{\partial x}\Big|_{i,j}=\frac{V_x(i+1/2,j)-V_x(i-1/2,j)}{\Delta x}$$

$$\frac{\partial V_y}{\partial y}\Big|_{i,j}=\frac{V_y(i,j+1/2)-V_y(i,j-1/2)}{\Delta y}$$

3.2.2 Momentum equations:

In this subsection, the finite difference discretization of each term of the momentum equations will be discussed separately. The center of discretisation for x- and y-momentum equations are grid points at (i+1/2, j), (i, j+1/2) respectively. The buoyancy term in the y-momentum equation (*RiT*) can be implemented as

$$T|_{(i,j+1/2)} = \left(\frac{T(i,j+1)+T(i,j)}{2}\right)$$

3.2.2.1 Discretisation of unsteady terms:

$$\left.\frac{\partial V_x}{\partial t}\right|_{(i+1/2,j)} = \frac{V_x^{n+1}(i+1/2,j) - V_x^n(i+1/2,j)}{\Delta t}$$

$$\left.\frac{\partial V_y}{\partial t}\right|_{(i,j+1/2)} = \frac{V_y^{n+1}(i,j+1/2) - V_y^n(i,j+1/2)}{\Delta t}$$

where, n is the n^{th} time step.

3.2.2.2 Discretisation of convective terms:

The central difference scheme for convection terms cause stability problem especially for the convection-dominated flows. To avoid this problem, first order upwind scheme is generally used, which uses constant extrapolation method to determine the value of the convected variable such that its value wherever needed is equal to that of its upstream neighbour. The upwind scheme is first order accurate and possesses both the conservative and transportive properties. In the convective terms of the x-momentum and y-momentum equations, the convected variables are V_x and V_y respectively. Whereas the convecting variable is V_x or V_y, depending upon the specific term being discretised in both the equations. Linear interpolation has been used to determine the convecting variable wherever needed.

Discretisation of [$Conv_x$]

The grid point for the discretisation of x-momentum equation is located at (i+1/2,j).

$$[Conv_x]_{i+1/2,j} = \left[\frac{\partial(V_x V_x)}{\partial x} + \frac{\partial(V_y V_x)}{\partial y}\right]_{i+1/2,j}$$

The corresponding finite difference representation is given by

$$\left.\frac{\partial(V_x V_x)}{\partial x}\right|_{(i+1/2.j)} = \frac{(V_{xav}V_{xup})_{(i+1/2,j)} - (V_{xav}V_{xup})_{(i,j)}}{\Delta x}$$

where,

$$\left.V_{xav}\right|_{(i+1,j)} = \frac{V_{x(i+3/2,j)} + V_{x(i+1/2,j)}}{2}$$

$$\left.V_{xav}\right|_{(i,j)} = \frac{V_{x(i+1/2,j)} + V_{x(i-1/2,j)}}{2}$$

$$\left.V_{xup}\right|_{(i+1,j)} = V_{x(i+1/2,j)} \quad if \quad V_{xav(i+1,j)} > 0 \quad \text{Else} \quad \left.V_{xup}\right|_{(i+1,j)} = V_{x(i+3/2,j)}$$

$$\left.V_{xup}\right|_{(i,j)} = V_{x(i-1/2,j)} \quad if \quad V_{xav(i,j)} > 0 \quad \text{Else} \quad \left.V_{xup}\right|_{(i,j)} = V_{x(i+1/2,j)}$$

$$\left.\frac{\partial(V_x V_y)}{\partial y}\right|_{(i+1/2.j)} = \frac{(V_{xup}V_{yav})_{(i+1/2,j+1/2)} - (V_{xup}V_{yav})_{(i+1/2,j-1/2)}}{\Delta y}$$

where,

$$\left.V_{yav}\right|_{(i+1/2,j+1/2)} = \frac{V_{y(i+1,j+1/2)} + V_{y(i,j+1/2)}}{2}$$

$$\left.V_{yav}\right|_{(i+1/2,j-1/2)} = \frac{V_{y(i+1,j-1/2)} + V_{y(i,j-1/2)}}{2}$$

$$\left.V_{xup}\right|_{(i+1/2,j+1/2)} = V_{x(i+1/2,j)} \quad if \quad V_{yav(i+1/2,j+1/2)} > 0 \quad \text{Else} \quad \left.V_{xup}\right|_{(i+1/2,j+1/2)} = V_{x(i+1/2,j+1)}$$

$$\left.V_{xup}\right|_{(i+1/2,j-1/2)} = V_{x(i+1/2,j-1)} \quad if \quad V_{yav(i+1/2,j-1/2)} > 0 \quad \text{Else} \quad \left.V_{xup}\right|_{(i+1/2,j-1/2)} = V_{x(i+1/2,j)}$$

Discretisation of [Conv$_y$]

The grid point for discretisation of y-momentum equation is located at (i,j+1/2).

$$[Conv_y]_{i,j+1/2} = \left[\frac{\partial(V_x V_y)}{\partial x} + \frac{\partial(V_y V_y)}{\partial y}\right]_{i,j+1/2}$$

Thus by discretising the above term

$$\left.\frac{\partial(V_x V_y)}{\partial x}\right|_{(i,j+1/2)} = \frac{(V_{xav}V_{yup})_{(i+1/2,j+1/2)} - (V_{xav}V_{yup})_{(i-1/2,j+1/2)}}{\Delta x}$$

where,

$$\left.V_{xav}\right|_{(i+1/2,j+1/2)} = \frac{V_{x(i+1/2,j+1)} + V_{x(i+1/2,j)}}{2}$$

$$\left.V_{xav}\right|_{(i-1/2,j+1/2)} = \frac{V_{x(i-1/2,j+1)} + V_{x(i-1/2,j)}}{2}$$

$$\left.V_{yup}\right|_{(i+1/2,j+1/2)} = V_{y(i,j+1/2)} \quad if\ V_{xav(i+1/2,j+1/2)} > 0 \quad \text{Else} \quad \left.V_{yup}\right|_{(i+1/2,j+1/2)} = V_{y(i+1,j+1/2)}$$

$$\left.V_{yup}\right|_{(i-1/2,j+1/2)} = V_{y(i-1,j+1/2)} \quad if\ V_{xav(i-1/2,j+1/2)} > 0 \quad \text{Else} \quad \left.V_{yup}\right|_{(i-1/2,j+1/2)} = V_{y(i,j+1/2)}$$

$$\left.\frac{\partial(V_y V_y)}{\partial y}\right|_{(i,j+1/2)} = \frac{(V_{yav}V_{yup})_{(i,j+1)} - (V_{yav}V_{yup})_{(i,j)}}{\Delta y}$$

where,

$$\left.V_{yav}\right|_{(i,j+1)} = \frac{V_{y(i,j+3/2)} + V_{y(i,j+1/2)}}{2}$$

$$\left.V_{yav}\right|_{(i,j)} = \frac{V_{y(i,j+1/2)} + V_{y(i,j-1/2)}}{2}$$

$$\left.V_{yup}\right|_{(i,j+1)} = V_{y(i,j+1/2)} \quad if\ V_{yav(i,j+1)} > 0 \quad \text{Else} \quad \left.V_{yup}\right|_{(i,j+1)} = V_{y(i,j+3/2)}$$

$$\left.V_{yup}\right|_{(i,j)} = V_{y(i,j-1/2)} \quad if\ V_{yav(i,j)} > 0 \quad \text{Else} \quad \left.V_{yup}\right|_{(i,j)} = V_{y(i,j+1/2)}$$

3.3.2.3 Discretisation of diffusion terms:

For the discretisation of the diffusion terms, the central difference scheme is used. The finite difference discretisation of the diffusive terms is represented as

Discretisation of [Diff$_x$]

The center for discretisation is (i+1/2,j). Thus discretisation of diffusive term, is represented as

$$[Diff_x]_{i+1/2,j} = \left[\frac{\partial^2 V_x}{\partial x^2} + \frac{\partial^2 V_x}{\partial y^2}\right]_{i+1/2,j}$$

where,

$$\left.\frac{\partial^2 V_x}{\partial x^2}\right|_{(i+1/2,j)} = \frac{V_{x(i+3/2,j)} - 2V_{x(i+1/2,j)} + V_{x(i-1/2,j)}}{(\Delta x)^2}$$

$$\left.\frac{\partial^2 V_x}{\partial y^2}\right|_{(i+1/2,j)} = \frac{V_{x(i+1/2,j+1)} - 2V_{x(i+1/2,j)} + V_{x(i+1/2,j-1)}}{(\Delta y)^2}$$

Discretisation of [Diff$_y$]

The center for discretisation is (i+1/2,j). Hence, the discretisation of diffusive term is represented as

$$[Diff_y]_{i,j+1/2} = \left[\frac{\partial^2 V_y}{\partial x^2} + \frac{\partial^2 V_y}{\partial y^2}\right]_{i,j+1/2}$$

where,

$$\left.\frac{\partial^2 V_y}{\partial y^2}\right|_{(i,j+1/2)} = \frac{V_{y(i,j+3/2)} - 2V_{y(i,j+1/2)} + V_{y(i,j-1/2)}}{(\Delta y)^2}$$

$$\left.\frac{\partial^2 V_y}{\partial x^2}\right|_{(i,j+1/2)} = \frac{V_{y(i+1,j+1/2)} - 2V_{y(i,j+1/2)} + V_{y(i-1,j+1/2)}}{(\Delta x)^2}$$

3.2.2.3 Discretisation of non-Newtonian terms:

The discretisation of the non-Newtonian terms is similar to that of diffusion terms using central difference scheme.

Discretisation of [Non$_x$]

The grid point for discretisation is (i+1/2,j). Thus discretisation of non-Newtonian term is represented as

$$[Non_x]_{i+1/2,j} = \left[\varepsilon_{xx} \frac{\partial \eta}{\partial x} + \varepsilon_{yx} \frac{\partial \eta}{\partial y} \right]_{i+1/2,j}$$

where

$$\varepsilon_{xx}\Big|_{(i+1/2,j)} = \frac{(V_{x(i+3/2,j)} - V_{x(i-1/2,j)})}{2(\Delta x)}$$

$$\frac{\partial \eta}{\partial x}\Big|_{(i+1/2,j)} = \frac{(\eta_{(i+1,j)} - \eta_{(i,j)})}{\Delta x}$$

$$\varepsilon_{yx}\Big|_{i+1/2,j} = \frac{1}{2}\left[\frac{\partial V_x}{\partial y} + \frac{\partial V_y}{\partial x} \right]_{i+1/2,j}$$

$$\left[\frac{\partial V_x}{\partial y} \right]_{i+1/2,j} = \frac{(V_{x(i+1/2,j+1)} - V_{x(i+1/2,j-1)})}{2(\Delta y)}$$

$$\left[\frac{\partial V_y}{\partial x} \right]_{i+1/2,j} = \frac{(V_{y(i+1,j+1/2)} + V_{y(i+1,j-1/2)} - V_{y(i,j+1/2)} - V_{y(i,j-1/2)})}{2(\Delta x)}$$

$$\frac{\partial \eta}{\partial y}\Big|_{(i+1/2,j)} = \frac{(\eta_{(i,j+1)} + \eta_{(i+1,j+1)} - \eta_{(i,j-1)} - \eta_{(i+1,j-1)})}{4(\Delta y)}$$

Discretisation of [Non$_y$]

The center for discretisation is (i,j+1/2). Thus discretisation of non-Newtonian term is represented as

$$[Non_y]_{i,j+1/2} = \left[\varepsilon_{yy} \frac{\partial \eta}{\partial y} + \varepsilon_{xy} \frac{\partial \eta}{\partial x} \right]_{i,j+1/2}$$

where,

$$\varepsilon_{yy}\Big|_{(i,j+1/2)} = \frac{(V_{y(i,j+3/2)} - V_{y(i,j-1/2)})}{2(\Delta y)}$$

$$\frac{\partial \eta}{\partial y}\Big|_{(i,j+1/2)} = \frac{(\eta_{(i,j+1)} - \eta_{(i,j)})}{\Delta y}$$

$$\varepsilon_{yx}\Big|_{(i,j+1/2)} = \frac{1}{2}\left[\frac{\partial V_x}{\partial y} + \frac{\partial V_y}{\partial x}\right]_{i,j+1/2}$$

$$\left[\frac{\partial V_y}{\partial x}\right]_{i,j+1/2} = \frac{(V_{y(i+1,j+1/2)} - V_{y(i-1,j+1/2)})}{2(\Delta x)}$$

$$\left[\frac{\partial V_x}{\partial y}\right]_{i,j+1/2} = \frac{(V_{x(i+1/2,j+1)} + V_{x(i-1/2,j+1)} - V_{x(i+1/2,j)} - V_{x(i-1/2,j)})}{2(\Delta y)}$$

$$\frac{\partial \eta}{\partial x}\Big|_{(i,j+1/2)} = \frac{(\eta_{(i+1,j+1)} + \eta_{(i+1,j)} - \eta_{(i-1,j+1)} - \eta_{(i-1,j)})}{4(\Delta x)}$$

3.2.2.4 Discretisation of pressure terms:

For the discretisation of pressure terms, the central difference scheme is used as given below:

$$\frac{\partial p}{\partial x}\Big|_{(i+1/2,j)} = \frac{p_{(i+1,j)} - p_{(i,j)}}{\Delta x}$$

$$\frac{\partial p}{\partial y}\Big|_{(i,j+1/2)} = \frac{p_{(i,j+1)} - p_{(i,j)}}{\Delta y}$$

3.2.3 Energy equation

The center for discretisation of energy equation is (i,j). The transient term, convective term and diffusive terms are discretized as follows

Transient term:

$$\frac{\partial T}{\partial t}\Big|_{i,j} = \frac{T_{i,j}^{n+1} - T_{i,j}^{n}}{\Delta t}$$

where n is the n^{th} time step.

Convective terms:

Convective terms are discretised using central difference scheme. The central difference scheme is second order accurate. The discretisation of convective terms are as follows

$$[Conv_T]_{i,j} = \left[\frac{\partial(V_x T)}{\partial x} + \frac{\partial(V_y T)}{\partial y}\right]_{i,j}$$

where,

$$\frac{\partial(V_x T)}{\partial x}\Big|_{i,j} = \frac{V_x T\big|_{(i+1/2,j)} - V_x T\big|_{(i-1/2,j)}}{\Delta x}$$

$$= \left[\frac{V_{x(i+1/2,j)}\left(\frac{T_{(i+1,j)} + T_{(i,j)}}{2}\right) - V_{x(i-1/2,j)}\left(\frac{T_{(i,j)} + T_{(i-1,j)}}{2}\right)}{\Delta x}\right]$$

$$\frac{\partial(V_y T)}{\partial y}\Big|_{i,j} = \frac{V_y T\big|_{(i,j+1/2)} - V_y T\big|_{(i,j-1/2)}}{\Delta y}$$

$$= \left[\frac{V_{y(i,j+1/2)}\left(\frac{T_{(i,j+1)} + T_{(i,j)}}{2}\right) - V_{y(i,j-1/2)}\left(\frac{T_{(i,j)} + T_{(i,j-1)}}{2}\right)}{\Delta y}\right]$$

In the above equation temperature is the convected variable and velocity is the convecting variable. The central difference scheme has been used for the convective term using linear interpolation for the temperature.

Diffusive terms:

The diffusive terms are discretised using the central difference scheme as

$$[Diff_T]_{i,j} = \left[\frac{\partial^2 T}{\partial x^2} + \frac{\partial^2 T}{\partial y^2}\right]_{i,j}$$

where,

$$\frac{\partial^2 T}{\partial x^2}\Big|_{i,j} = \frac{T_{(i+1,j)} - 2T_{(i,j)} + T_{(i-1,j)}}{(\Delta x)^2}$$

$$\frac{\partial^2 T}{\partial y^2}\Big|_{i,j} = \frac{T_{(i,j+1)} - 2T_{(i,j)} + T_{(i,j-1)}}{(\Delta y)^2}$$

3.2.4 Discretisation of Boundary conditions

Consider Figure (3.1) and (3.2) for understanding the discretisation of the boundary conditions. N and M are the number of cells in x- and y-direction including two fictitious cells in both directions.

Along AA':

Dimensionless boundary conditions along AA' are given as :

V_x=1 (for unconfined flow case)

and $V_x = \left[1-(2By-1)^{\frac{n+1}{n}}\right]$ (for confined flow case)

V_y=0, T=0 (for both confined and unconfined flow)

These boundary conditions can be discretised along AA' as

$V_x(1+1/2, j) = 1$ (for unconfined flow case) For j=2 to (M-1)

$V_x(1+1/2, j) = \left[1-(2By-1)^{\frac{n+1}{n}}\right]$ (for channel confined flow case) For j=2 to (M-1)

$$\frac{[V_y(2, j+1/2) + V_y(1, j+1/2)]}{2} = 0$$

or $V_y(1, j+1/2) = -V_y(2, j+1/2)$ For j=2 to (M-2)

$$\frac{[T(1, j) + T(2, j)]}{2} = 0$$

or $T(1, j) = -T(2, j)$ For j=2 to (M-1)

Along DD':

The dimensionless convective boundary conditions along DD' are given as:

$\frac{\partial V_i}{\partial t} + V_{conv}\frac{\partial V_i}{\partial x} = 0$ where (i = x or y) and $\frac{\partial T}{\partial t} + V_{conv}\frac{\partial T}{\partial x} = 0$

with V_{conv}=1

These boundary conditions can be discretised as:

$$\frac{V_x^{n+1}(N,j) - V_x^n(N,j)}{\Delta t} + \frac{V_x^n(N,j) - V_x^n(N-1,j)}{\Delta x} = 0$$

or $V_x^{n+1}(N,j) = V_x^n(N,j) - \frac{\Delta t}{\Delta x}[V_x^n(N,j) - V_x^n(N-1,j)]$ For j = 2 to (M-1)

Similarly, $V_y^{n+1}(N,j) = V_y^n(N,j) - \frac{\Delta t}{\Delta x}[V_y^n(N,j) - V_y^n(N-1,j)]$ For j = 2 to (M-1)

$T^{n+1}(N,j) = T^n(N,j) - \frac{\Delta t}{\Delta x}[T^n(N,j) - T^n(N-1,j)]$ For j = 2 to (M-1)

Along AD and A' D':

The dimensionless boundary conditions along AD and A' D' are given by

$\frac{\partial V_x}{\partial y} = 0$ (for unconfined flow)

and V_x=0 (for confined flow)

$V_y = 0$, $\frac{\partial T}{\partial y} = 0$ (for both confined and unconfined flow)

These boundary conditions can be discretised as:

Along AD:

$$\frac{V_x(i+1/2, M) - V_x(i+1/2, M-1)}{\Delta y} = 0$$ (for unconfined flow)

or $V_x(i+1/2, M) = V_x(i+1/2, M-1)$ For i =2 to (N-1)

and $V_x(i+1/2, M) + V_x(i+1/2, M-1) = 0$ (for confined flow)

or $V_x(i+1/2, M) = -V_x(i+1/2, M-1)$ For i =2 to (N-1)

$V_y(i, (M-1)+1/2) = 0$ For i =2 to (N-1)

$$\frac{T(i,M)-T(i,M-1)}{\Delta y}=0$$

or $T(i,M)=T(i,M-1)$ For i =2 to (N-1)

Along A' D':

$$\frac{V_x(i+1/2,2)-V_x(i+1/2,1)}{\Delta y}=0 \text{ (for unconfined flow)}$$

or $V_x(i+1/2,1)=V_x(i+1/2,2)$ For i =2 to (N-1)

and $V_x(i+1/2,2)+V_x(i+1/2,1)=0$ (for confined flow)

or $V_x(i+1/2,1)=-V_x(i+1/2,2)$ For i =2 to (N-1)

$V_y(i,1+1/2)=0$ For i =2 to (N-1)

$$\frac{T(i,2)-T(i,1)}{\Delta y}=0$$

or $T(i,1)=T(i,2)$ For i =2 to (N-1)

Obstacle FGG'F':

The dimensionless boundary conditions along the obstacle surface FGG'F are given as:

$$V_x=0\ ;\quad V_y=0\ ;\ T=1$$

Along F F':

$V_x(fb+1/2,j)=0$ For j = (bb+1) to tb

$$\frac{[V_y(fb,j+1/2)+V_y(fb+1,j+1/2)]}{2}=0$$

or $V_y(fb+1,j+1/2)=-V_y(fb,j+1/2)$ For j = (bb+1) to (tb-1)

For the constant wall temperature case:

$$\frac{[T(fb,j)+T(fb+1,j)]}{2}=1$$

or $T(fb+1,j)=2-T(fb,j)$ For j = (bb+2) to (tb-1) (3.13)

Along FG:

$$\frac{[V_x(i+1/2,tb)+V_x(i+1/2,tb+1)]}{2}=0$$

or $V_x(i+1/2,tb)=-V_x(i+1/2,tb+1)$ For i = (fb+1) to (rb-1)

$V_y(i,tb+1/2)=0$ For i=(fb+1) to rb

For the constant wall temperature case:

$$\frac{[T(i,tb)+T(i,tb+1)]}{2}=1$$

or $T(i,tb)=2-T(i,tb+1)$ For i = (fb+2) to (rb-1)

Along GG':

$V_x(rb+1/2,j)=0$ For j = (bb+1) to tb

$$\frac{[V_y(rb,j+1/2)+V_y(rb+1,j+1/2)]}{2}=0$$

or $V_y(rb,j+1/2)=-V_y(rb+1,j+1/2)$ For j = (bb+1) to (tb-1)

For the constant wall temperature case:

$$\frac{[T(rb,j)+T(rb+1,j)]}{2}=1$$

or $T(rb,j)=2-T(rb+1,j)$ For j = (bb+2) to (tb-1)

Along F'G':

$$\frac{V_x(i+1/2,bb)+V_x(i+1/2,bb+1)}{2}=0$$

or $V_x(i+1/2,bb+1)=-V_x(i+1/2,bb)$ For i = (fb+1) to (rb-1)

$V_y(i,bb+1/2)=0$ For i = (fb+1) to rb

For the constant wall temperature case:

$$\frac{T(i,bb)+T(i,bb+1)}{2}=1$$

or $T(i,bb+1)=2-T(i,bb)$ For i = (fb+2) to (rb-1)

3.3 Method of solution:

The SMAC-Implicit scheme:

As mentioned earlier, SMAC-Implicit scheme is used to solve the complete Navier-Stokes and energy equations. This scheme is implicit, but it may be noted that this scheme is implicit in diffusion and non-Newtonian terms while explicit in convective. It is noted that the computations of velocity and temperature fields are coupled. To start a computational cycle, guess fields for velocity, pressure, and temperature are used. First a predicted velocity is found from the implicit form of momentum equation using guessed or previous time level pressure and temperature field. From these, correct pressure and velocity fields are obtained by pressure and velocity iteration through continuity equations, which will be discussed in detail in the following section. From the initial or previous temperature field and the aforementioned corrected velocity field, a temperature distribution is calculated from the energy equation. This new temperature field and the foregoing corrected velocity and pressure fields are used to evaluate velocities for next timestep. As such, in the subsequent cycles, solutions for velocities are obtained from a temperature field lag by one time duration (δt). The time stepping is pseudo-transient, starting from an arbitrary initial conditions; the time stepping of the equations is continued until the steady state solution is achieved. The use of the implicit scheme here helps to avoid the commonly encountered numerical instability, especially at the low Reynolds number calculations. Advantage of SMAC-Implicit scheme over SMAC-explicit (which is explicit in convective and diffusive) scheme is in the use of larger time steps.

3.3.1 Velocity prediction

The velocity prediction equations are obtained as given below. Consider the Navier-Stokes equations (3.2) and (3.3) for cell (i, j). The center for discretisation of x and y-momentum equations are (i+1/2,j) and (i, j+1/2) respectively.

$$\left[\frac{\partial V_x}{\partial t}\right]_{i+1/2,j} + [Conv_x]_{i+1/2,j} = -\left[\frac{\partial p}{\partial x}\right]_{i+1/2,j} + \frac{\eta}{\mathrm{Re}}[Diff_x]_{i+1/2,j} + \frac{2}{\mathrm{Re}}[Non_x]_{i+1/2,j}$$

$$\left[\frac{\partial V_y}{\partial t}\right]_{i,j+1/2} + [Conv_y]_{i,j+1/2} = -\left[\frac{\partial p}{\partial y}\right]_{i,j+1/2} + \frac{\eta}{\mathrm{Re}}[Diff_y]_{i,j+1/2} + \frac{2}{\mathrm{Re}}[Non_y]_{i,j+1/2} + Ri[T]_{i,j+1/2}$$

the discretised form of the above equations is given by

$$\left[\frac{V_x^{n+1} - V_x^n}{\Delta t}\right]_{i+1/2,j} + [Conv_x]^n_{i+1/2,j} = -\left[\frac{\partial p}{\partial x}\right]^{n+1}_{i+1/2,j} + \frac{\eta}{\mathrm{Re}}[Diff_x]^{n+1}_{i+1/2,j} + \frac{2}{\mathrm{Re}}[Non_x]^{n+1}_{i+1/2,j} \quad (3.14)$$

$$\left[\frac{V_y^{n+1} - V_y^n}{\Delta t}\right]_{i,j+1/2} + [Conv_y]^n_{i,j+1/2} = -\left[\frac{\partial p}{\partial y}\right]^{n+1}_{i,j+1/2} + \frac{\eta}{\mathrm{Re}}[Diff_y]^{n+1}_{i,j+1/2} + \frac{2}{\mathrm{Re}}[Non_y]^{n+1}_{i,j+1/2} + Ri[T]^n_{i,j+1/2} \quad (3.15)$$

where the superscript n represents the current time step values which are known and (n+1) indicates the next time step values which are to be determined. Here the convective and buoyancy term are explicit while, the diffusion, non-Newtonian and pressure terms are implicit.

As mentioned above all terms except convective terms are at $(n+1)^{th}$ time step, that means it needs pressure field at $(n+1)^{th}$ time step to calculate the velocity field at $(n+1)^{th}$ time step. But we do not know pressure at $(n+1)^{th}$ time step. So we predict pressure field at $(n+1)^{th}$ time step. This predicted pressure field is pressure field at n^{th} time step. Therefore, here we predict velocity field at $(n+1)^{th}$ time step by predicting some pressure field which obviously will not satisfy continuity. Hence equations (3.14) and (3.15) leads to give prediction equations which can be written as.

$$\left[\frac{V_x^* - V_x^n}{\Delta t}\right]_{i,j+1/2} + [Conv_x]^n_{i,j+1/2} = -\left[\frac{\partial p}{\partial x}\right]^{n}_{i,j+1/2} + \frac{\eta}{\mathrm{Re}}[Diff_x]^*_{i,j+1/2} + \frac{2}{\mathrm{Re}}[Non_x]^*_{i,j+1/2} \quad (3.16)$$

$$\left[\frac{V_y^* - V_y^n}{\Delta t}\right]_{i,j+1/2} + [Conv_y]^n_{i,j+1/2} = -\left[\frac{\partial p}{\partial y}\right]^{n}_{i,j+1/2} + \frac{\eta}{\mathrm{Re}}[Diff_y]^*_{i,j+1/2} + \frac{2}{\mathrm{Re}}[Non_y]^*_{i,j+1/2} + Ri[T]^n_{i,j+1/2} \quad (3.17)$$

where V_x^* and V_y^* are the predicted velocities at the $(n+1)^{th}$ time step.

In equations (3.16) and (3.17) all variables at the n^{th} time step are known, while * values are unknown. Thus equations (3.16) and (3.17) are solved to get V_x^* and V_y^* by using Gauss-Siedel iterations.

It should noted that $[Diff_x]^*$ in equation (3.16), is a function of V_x^* only (see section 3.2), but $[Non_x]^*$ is a function of V_x^* and V_y^* (see section 3.2) . When V_x^* is predicted, the values of V_y^* is required, which it self is unknown. So for computational simplification V_y^* is lagged to V_y^n. But in equation (3.17), $[Diff_y]^*$ and $[Non_y]^*$ are functions of both V_x^* and V_y^*. There is no need of lagging here, since V_x^* is known for solving V_y^* . In the prediction we first find V_x^* and then V_y^*. However, this kind of lagging is not required in case of newtonian calculations, since $[Non_x]^*$ and $[Non_y]^*$ are identically zero.

3.3.2 Velocity correction

As mentioned in the previous section, velocity predictions are obtained from equations (3.16) and (3.17). In order to estimate the corrected velocity field at $(n+1)^{th}$ we need to find velocity correction which should be added to the velocity prediction. In this section we formulate the velocity correction equations. Subtracting (3.16) and (3.17) from (3.14) and (3.15) respectively one get,

$$\frac{V_x'(i+1/2,j)}{\Delta t} = -\left[\frac{\partial p'}{\partial x}\right]_{i+1/2,j} + \frac{\eta}{\mathrm{Re}}[Diff_x]'_{i+1/2,j} + \frac{2}{\mathrm{Re}}[Non_x]'_{i+1/2,j} \tag{3.18}$$

$$\frac{V_y'(i,j+1/2)}{\Delta t} = -\left[\frac{\partial p'}{\partial y}\right]_{i,j+1/2} + \frac{\eta}{\mathrm{Re}}[Diff_y]'_{i,j+1/2} + \frac{2}{\mathrm{Re}}[Non_y]'_{i,j+1/2} \tag{3.19}$$

where,

$$V_x'(i+1/2,j) = V_x^{n+1}(i+1/2,j) - V_x^*(i+1/2,j) \tag{3.20}$$

$$V_y'(i,j+1/2) = V_y^{n+1}(i,j+1/2) - V_y^*(i,j+1/2) \tag{3.21}$$

$$p'(i+1/2,j) = p^{n+1}(i+1/2,j) - p^n(i+1/2,j) \tag{3.22}$$

$$p'(i,j+1/2) = p^{n+1}(i,j+1/2) - p^n(i,j+1/2) \tag{3.23}$$

$$[Diff_x]'_{i+1/2,j} = [Diff_x]^{n+1}_{i+1/2,j} - [Diff_x]^{*}_{i+1/2,j} \tag{3.24}$$

$$[Diff_y]'_{i,j+1/2} = [Diff_y]^{n+1}_{i,j+1/2} - [Diff_y]^{*}_{i,j+1/2} \tag{3.25}$$

$$[Non_x]'_{i+1/2,j} = [Non_x]^{n+1}_{i+1/2,j} - [Non_x]^{*}_{i+1/2,j} \tag{3.26}$$

$$[Non_y]'_{i,j+1/2} = [Non_y]^{n+1}_{i,j+1/2} - [Non_y]^{*}_{i,j+1/2} \tag{3.27}$$

So in all above expressions, variables having superscript ' indicates corrections. We solve equations (3.18) and (3.19) by using Gauss-Siedel iterations but the difficulty is the non-availability of $p'(i,j)$, the pressure correction. Therefore before we calculate velocity corrections, pressure correction should be known, which is discussed in following section.

3.3.3 Pressure correction

Suppose V_x^{n+1} and V_y^{n+1} are the velocities at $(n+1)^{th}$ time step, then it must satisfy continuity equation i.e.

$$\frac{\partial V_x^{n+1}}{\partial x} + \frac{\partial V_y^{n+1}}{\partial y} = 0 \text{ or } \nabla . V^{n+1} = 0 \tag{3.28}$$

where V_x^{n+1} and V_y^{n+1} are given as:

$$V_x^{n+1} = V_x^{*} + V_x' \quad , \quad V_y^{n+1} = V_y^{*} + V_y' \tag{3.29}$$

Here V_x' and V_y' are given by equation (3.18) and (3.19) respectively. Thus equation (3.28) can be written as

$$\nabla . V' = -\nabla . V^{*} \tag{3.30}$$

Considering equations (3.18) and (3.19) for Newtonian case (i.e.η=1) and substituting in equation (3.30) one get

$$\Delta t\left[-\frac{\partial^2 p'}{\partial x^2} + \frac{1}{\mathrm{Re}}\frac{\partial [Diff_x']}{\partial x}\right] + \Delta t\left[-\frac{\partial^2 p'}{\partial y^2} + \frac{1}{\mathrm{Re}}\frac{\partial [Diff_y']}{\partial y}\right] = -\nabla . V^{*} \tag{3.31}$$

$$\text{or } \left(\frac{\partial^2 p'}{\partial x^2} + \frac{\partial^2 p'}{\partial y^2}\right) = \frac{1}{\Delta t}(\nabla . V^{*}) + \frac{1}{\mathrm{Re}}\left[\frac{\partial [Diff_x']}{\partial x} + \frac{\partial [Diff_y']}{\partial y}\right] \tag{3.32}$$

using equation (3.30), we get

$$\left[\frac{\partial[Diff_x^{'}]}{\partial x}+\frac{\partial[Diff_y^{'}]}{\partial y}\right]=\nabla.(\nabla^2 V^{'})=\nabla^2(\nabla.V^{'})=-\nabla^2(\nabla.V^{*}) \tag{3.33}$$

substituting equation (3.33) in (3.32)

$$\nabla^2 p^{'}=\frac{1}{\Delta t}(\nabla.V^{*})-\frac{1}{\mathrm{Re}}\nabla^2(\nabla.V^{*}) \tag{3.34}$$

Thus equation (3.34) is solved for $p^{'}$(i,j) with appropriate boundary conditions, then it is substituted to equations (3.18) and (3.19) to calculate $V_x^{'}$ and $V_y^{'}$ respectively.

Finally we get correct velocity and pressure (pseudo) field by

$$V_x^{n+1}(i+1/2,j)=V_x^{*}(i+1/2,j)+V_x^{'}(i+1/2,j) \tag{3.35a}$$

$$V_y^{n+1}(i,j+1/2)=V_y^{*}(i,j+1/2)+V_y^{'}(i,j+1/2) \tag{3.35b}$$

$$p^{n+1}(i,j)=p^{n}(i,j)+p^{'}(i,j) \tag{3.35c}$$

The equation (3.34) is for Newtonian case. However, the same equation is used for non-Newtonian case also. This is so as for diffusion terms one can eliminate the unknown values by continuity but it can not be extended to non-Newtonian terms. So just to avoid complications we neglect non-Newtonian terms and also there is justification as given below.

The equation (3.34) is continuity equation, so the ultimate aim of the pressure correction equation is to make the velocity fields satisfy the continuity, and as this being implemented here, this simplification is justified.

3.3.4 Discretisation of pressure correction equation:

Consider the pressure correction equation (3.34). This equation is discretised around center (i,j).

Let $D=\nabla.V^{*}$, therefore one can write equation (3.34) as

$$(\nabla^2 p^{'})_{i,j}=\frac{1}{\Delta t}D_{i,j}-\frac{1}{\mathrm{Re}}(\nabla^2 D)_{i,j} \tag{3.36}$$

equation (3.36) can be discretised as

$$(\nabla^2 p^{'})_{i,j}=\left[\frac{\partial^2 p^{'}}{\partial x^2}+\frac{\partial^2 p^{'}}{\partial y^2}\right]_{i,j}$$

$$\left[\frac{\partial^2 p'}{\partial x^2}\right]_{i,j} = \frac{p'(i+1,j)-2p'(i,j)+p'(i-1,j)}{(\Delta x)^2}$$

$$\left[\frac{\partial^2 p'}{\partial y^2}\right]_{i,j} = \frac{p'(i,j+1)-2p'(i,j)+p'(i,j-1)}{(\Delta y)^2}$$

$$D_{i,j} = \left[\frac{\partial V_x^*}{\partial x} + \frac{\partial V_y^*}{\partial y}\right]_{i,j}$$

$$\left[\frac{\partial V_x^*}{\partial x}\right]_{i,j} = \frac{V_x^*(i+1/2,j)-V_x^*(i-1/2,j)}{\Delta x}$$

$$\left[\frac{\partial V_y^*}{\partial x}\right]_{i,j} = \frac{V_y^*(i,j+1/2)-V_y^*(i,j-1/2)}{\Delta y}$$

$$(\nabla^2 D)_{i,j} = \left[\frac{\partial^2 D}{\partial x^2} + \frac{\partial^2 D}{\partial y^2}\right]_{i,j}$$

$$\left[\frac{\partial^2 D}{\partial x^2}\right]_{i,j} = \frac{D(i+1,j)-2D(i,j)+D(i-1,j)}{(\Delta x)^2}$$

$$\left[\frac{\partial^2 D}{\partial y^2}\right]_{i,j} = \frac{D(i,j+1)-2D(i,j)+D(i,j-1)}{(\Delta y)^2}$$

Thus by using the above discretized terms, equation (3.36) is solved by Gauss-Siedel iteration method for pressure correction.

This velocity field computed from Navier-Stokes solver is given as an input to the energy equation. The energy equation is solved by implicit scheme with Gauss-Siedel iterations and under-relaxation is used. The energy equation is discretised around center (i,j), Therefore equation (3.4) can be written as:

$$\frac{T_{i,j}^{n+1}-T_{i,j}^{n}}{\Delta t} + [Conv_T]_{i,j}^{n+1} = \frac{1}{Pe}[Diff_T]_{i,j}^{n+1} \qquad (3.37)$$

Here convergence criterion is achieved when the computed velocity and temperature fields in the domain reach steady state. The steady state criterion is defined as:

$$\max\left(\frac{(V_x^{n+1}-V_x^n)}{\Delta t},\frac{(V_y^{n+1}-V_y^n)}{\Delta t},\frac{(T^{n+1}-T^n)}{\Delta t}\right)\leq 10^{-3}$$

where maximum is with respect to each and every grid point in the domain.

3.4 Solution Algorithm:

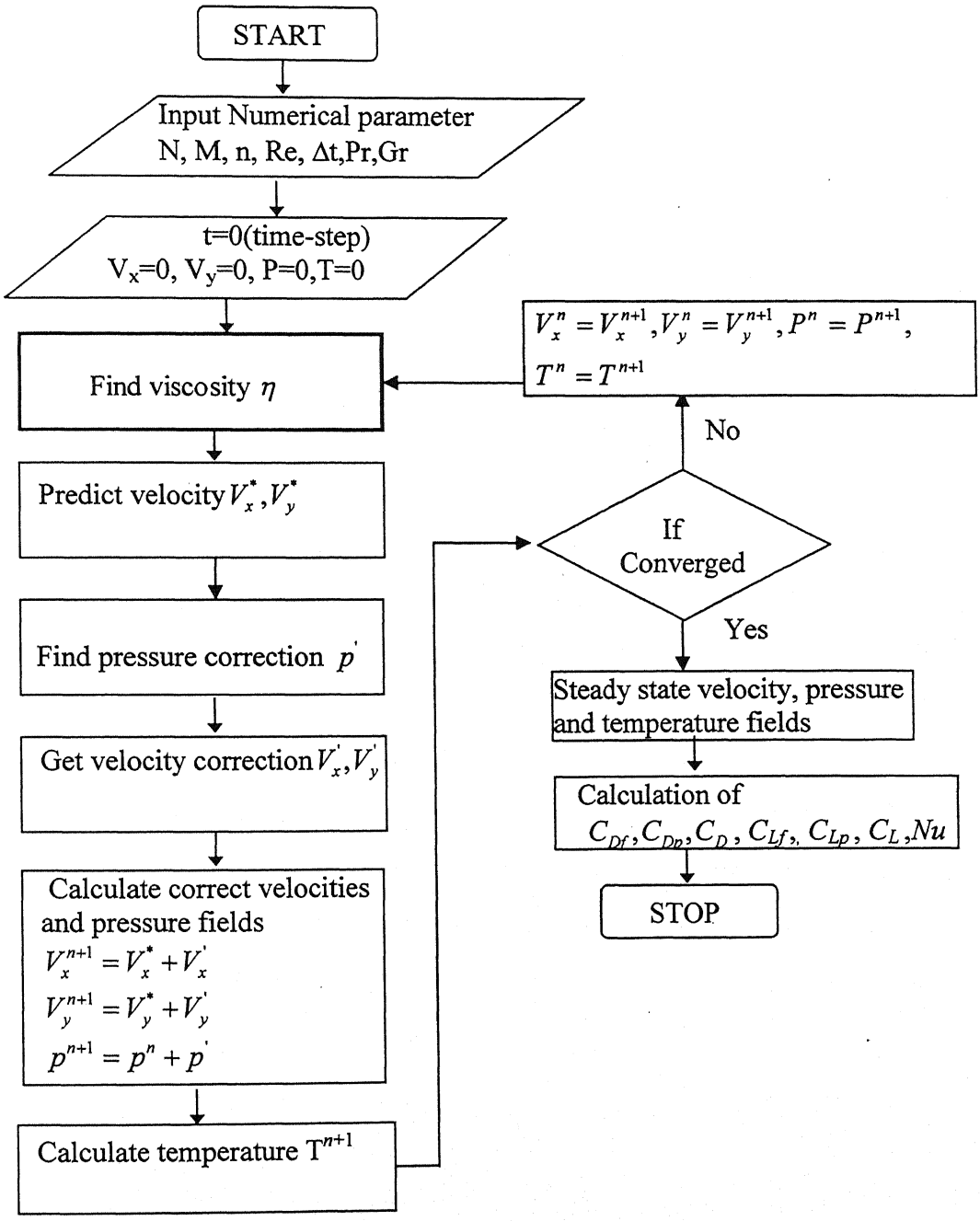

Figure 3.3 : Flow chart for the solution algorithm

The algorithm of the SMAC-implicit method is shown in Figure 3.3. Firstly, input parameters such as grid size, power-law index, Reynolds number, Prandtl number and Grashof number are given, followed by the initial assumed velocity, pressure and temperature fields. After the initial setting, viscosity is calculated using the power-law model at each grid in the computational domain. Now, velocity is predicted for the next time step after that pressure Poisson's equation is solved to find the corrected pressure. From these corrected pressure, velocity corrections are obtained. Finally, these velocity corrections are used to determine the pressure and velocity fields for the next time step. From the initial or previous temperature fields and the aforementioned corrected velocity field, a temperature distribution is calculated. Now convergence of velocities and temperature field is checked by convergence criteria. If these fields are not satisfying the convergence criteria then the velocity, pressure and temperature fields of this step are given as input for the next time step similar steps execute until convergence criteria is achieved. This converged velocity, pressure and temperature fields are used for further computation of drag, lift and Nusselt number.

3.4.1. Boundary conditions for velocity prediction equation:

The predicted velocities and the actual velocities should satisfy the same boundary conditions. Therefore the boundary condition described in section (3.2.4) applies to the velocity predictions i.e. V_x^* *and* V_y^* for solving equations (3.13) and (3.14) respectively.

3.4.2. Boundary conditions for the pressure correction equation:

The faces of the boundary where the normal velocity is known, the normal gradient of pressure correction is zero, which is the case at all boundaries except at the exit boundary, where pressure is known, i.e., $p'=0$.

The boundary conditions for equation (3.36) are as follows:

Along AA', FF', GG':

$$\frac{\partial p'}{\partial x}=0$$

$$\left(\frac{p'(2,j)-p'(1,j)}{\Delta x}\right)=0 \qquad \text{along AA'}$$

or $p'(1,j) = p'(2,j)$ for j =2 to (M-1) along AA'

similarly ,

$$p'(fb+1,j) = p'(fb,j) \quad \text{for j =(bb+2) to(tb-1) along FF'} \tag{3.38}$$

$$p'(rb,j) = p'(rb+1,j) \quad \text{for j =(bb+2) to(tb-1) along GG'}$$

Along AD, FG, F'G', A'D':

$$\frac{\partial p'}{\partial y} = 0$$

$$\left(\frac{p'(i,2) - p'(i,1)}{\Delta y}\right) = 0 \quad \text{along A'D'}$$

or $p'(i,1) = p'(i,2)$ for i =2 to (N-1)

similarly one can write

$p'(i,tb) = p'(i,tb+1)$ for i =(fb+2) to (rb-1) along FG (3.39)

$P'(i,bb+1) = P'(i,bb)$ for i = (rb+1) to (N-1) along F'G'

$p'(i,M) = p'(i,M-1)$ for i =2 to (N-1) along AD

Along DD':

$p'(N,j) = 0$ for j = 2 to (M-1)

the boundary condition of D as defined in equation (3.36) at all boundaries are given by

$$\frac{\partial D}{\partial n} = 0$$

where n represents the direction normal to face

3.4.3 Boundary conditions for velocity correction equation:

The boundary conditions for the velocity correction and prediction are the same except at inlet AA'. Since the inlet velocity profile is known, therefore along AA':

$V_x'(1+1/2,j) = 0$ for j = 2 to (M-1)

3.5 Treatment of boundary conditions at the corner of the square cylinder:

Some difficulties arise when boundary conditions of pressure correction and temperature are implemented along the surface of the square cylinder . As shown in Figure3.2, there is a dual prescription of values for the fictitious corner cells (F, F', G and G'). This is taken

care by assigning two values to the two corresponding real cells associated with it. When boundary conditions are given for the calculation of that real cell then in boundary condition the corresponding fictitious cell value is substituted. The procedure of the treatment of the boundary conditions at corner F for pressure correction is explained below:

In starting of Gauss-Siedel loop, if calculation of cell (fb,tb) is computed then assigned it as :

If (i =fb and j = tb)

Then $p'(fb+1,tb) = pc1$

If calculation of cell (fb+1,tb+1) is computed then assigned it as

If (i =fb+1 and j = tb+1)

Then $p'(fb+1,tb) = pc2$

where pc1,pc2 are any constants. Now when boundary conditions are applied then we assign the boundary condition for this fictitious cell according to equations (3.38) and (3.39) respectively as:

pc1= $p'(fb,tb)$

pc2= $p'(fb+1,tb+1)$

Same procedure is repeated for temperature boundary conditions at all corners of square cylinder.

3.5 Non-Newtonian viscosity:

The non-Newtonian viscosity is computed by using equations (2.47)-(2.51). The viscosity equation is discretised around center (i,j) as follows:

$$\varepsilon_{xx|_{i,j}} = \left[\frac{\partial V_x}{\partial x}\right]_{i,j} = \frac{[V_x(i+1/2,j) - V_x(i-1/2,j)]}{\Delta x}$$

$$\varepsilon_{yy|_{i,j}} = \left[\frac{\partial V_y}{\partial y}\right]_{i,j} = \frac{[V_y(i,j+1/2) - V_y(i,j-1/2)]}{\Delta y}$$

$$\varepsilon_{xy}\Big|_{i,j} = \left[\frac{\partial V_x}{\partial y} + \frac{\partial V_y}{\partial x}\right]_{i,j}$$

$$\left[\frac{\partial V_x}{\partial y}\right]_{i,j} = \frac{[V_x(i-1/2, j+1)+V_x(i+1/2, j+1)-V_x(i-1/2, j-1)-V_x(i+1/2, j-1)]}{4(\Delta y)}$$

$$\left[\frac{\partial V_y}{\partial x}\right]_{i,j} = \frac{[V_y(i+1, j+1/2)+V_y(i+1, j-1/2)-V_y(i-1, j+1/2)-V_y(i-1, j-1/2)]}{4(\Delta x)}$$

3.6 Stream function

Stream function Ψ is computed by discretising equation (2.52)

$$V_x(i+1/2, j) = \left(\frac{\partial \psi}{\partial y}\right)_{i+1/2, j}$$

$$V_x(i+1/2, j) = \left(\frac{\psi(i+1/2, j+1/2)-\psi(i+1/2, j-1/2)}{\Delta y}\right)$$

or $\psi(i+1/2, j+1/2) = \psi(i+1/2, j-1/2)+(V_x(i+1/2, j)\cdot \Delta y)$

where $\psi(i+1/2, 1+1/2)=0$ for (i =1to N-1)

For (i =1to N-1) and for (j = 2 to M-1) one can compute Ψ in the whole domain by knowing the steady state velocity field and marching in the upward direction on each vertical line in the domain after computing Ψ value.

3.7 Vorticity

The vorticity is computed by discrtising equation (2.54)

$$\omega_{i+1/2, j+1/2} = \left[\frac{\partial V_y}{\partial x} - \frac{\partial V_x}{\partial y}\right]_{i+1/2, j+1/2}$$

$$\left[\frac{\partial V_y}{\partial x}\right]_{i+1/2, j+1/2} = \frac{[V_y(i+1, j+1/2)-V_y(i, j+1/2)]}{\Delta x}$$

$$\left[\frac{\partial V_x}{\partial y}\right]_{i+1/2, j+1/2} = \frac{[V_x(i+1/2, j+1)-V_x(i+1/2, j)]}{\Delta y}$$

3.8 Drag

Friction drag

The friction drag on the top face (FG) is calculated by using equation (2.34) as:

$$(C_{Df})_{FG} = \frac{2}{\mathrm{Re}} \int_{F}^{G} \left(\eta \frac{\partial V_x}{\partial x} \right)_{i+1/2,tb+1/2} dx \qquad \text{for i = fb to rb} \tag{3.40}$$

where

$$\left(\eta \frac{\partial V_x}{\partial y} \right)_{i+1/2,tb+1/2} = \frac{[\eta(i+1/2,tb+1) \times V_x(i+1/2,tb+1)] - [\eta(i+1/2,tb) \times V_x(i+1/2,tb)]}{\Delta y}$$

$$\eta_{i+1/2,tb+1} = \frac{[\eta(i+1,tb+1) + \eta(i,tb+1)]}{2}$$

$$\eta_{i+1/2,tb} = \frac{[\eta(i+1,tb) + \eta(i,tb)]}{2}$$

Equation (3.40) is solved by numerical integration (Simpson1/3 rule) and similarly for bottom face F'G'.

Pressure Drag

Pressure drag on the front and rear faces (FF' and GG') is calculated by using equation (2.32) as:

$$(C_{DP})_{FF'andGG'} = 2\left[\int_{F'}^{F} p(fb, j)dy - \int_{G'}^{G} p(rb+1, j)dy \right] \qquad \text{for j = bb+1 to tb} \tag{3.41}$$

Equation (3.41) is solved by numerical integration as:

$$(C_{DP})_{FF'andGG'} = 2\left[\sum_{j=bb+1}^{j=tb} [p(fb, j) - p(rb+1, j)]\Delta y \right] \tag{3.41}$$

The total drag on square cylinder FGF'G' is calculated as:

$$[C_D]_{FGG'F'} = (C_{Df})_{FG} + (C_{Df})_{F'G'} + (C_{Dp})_{FF'andGG'}$$

3.9 Lift

Friction lift

The friction lift on the front face (FF') is calculated by using equation (2.35) as:

$$(C_{Lf})_{F'F} = \frac{2}{\mathrm{Re}} \int_{F'}^{F} \left(\eta \frac{\partial V_y}{\partial x} \right)_{fb+1/2, j+1/2} dy \quad \text{for j = bb to tb} \tag{3.42}$$

where

$$\left(\eta \frac{\partial V_y}{\partial x} \right)_{fb+1/2, j+1/2} = \frac{\left[\eta(fb, j+1/2) \times V_y(fb, j+1/2)\right] - \left[\eta(fb+1, j+1/2) \times V_y(fb+1, j+1/2)\right]}{\Delta x}$$

$$\eta_{fb, j+1/2} = \frac{\left[\eta(fb, j+1) + \eta(fb, j)\right]}{2}$$

$$\eta_{fb+1, j+1/2} = \frac{\left[\eta(fb+1, j+1) + \eta(fb+1, j)\right]}{2}$$

Equation (3.42) is solved by numerical integration (Simpson1/3 rule) and similarly for rear face G'G.

Pressure lift

The pressure lift on the top and bottom faces (FG and F'G') is calculated by using equation (2.33) as:

$$(C_{LP})_{FGandF'G'} = 2\left[\int_{F'}^{G'} p(i, bb)dx - \int_{F}^{G} p(i, tb+1)dx \right] \quad \text{for i = fb+1 to rb} \tag{3.43}$$

Equation (3.42) is solved by numerical integration as:

$$(C_{LP})_{FGandF'G'} = 2\left[\sum_{i=fb+1}^{i=rb} \left[p(i, bb) - p(i, tb+1) \right] dx \right] \tag{3.44}$$

The total lift on the square cylinder FGF'G' is calculated as:

$$[C_L]_{FGG'F'} = (C_{Lf})_{F'F} + (C_{Lf})_{G'G} + (C_{Lp})_{FGandF'G'}$$

3.9 Nusselt number

Constant wall temperature condition:

The local Nusselt number for the faces FF', FG, GG', G'F' are calculated by using equations (2.40)-(2.42) as

$$[Nu(j)]_{FF'} = -\left[\frac{T(fb, j) - T(fb+1, j)}{\Delta x} \right]$$

from equation(3.13),

$$\text{or}\left[Nu(j)\right]_{FF'} = -\left[\frac{T(fb,j)-(2-T(fb,j))}{\Delta x}\right] \quad \text{for j = (bb+1) to tb} \tag{3.45}$$

Similarly for the top (FG) , rear (GG') and bottom (G'F') faces, one can write

$$\left[Nu(i)\right]_{FG} = -\left[\frac{T(i,tb+1)-(2-T(i,tb+1))}{\Delta y}\right] \text{for i = (fb+1) to rb} \tag{3.46}$$

$$\left[Nu(j)\right]_{GG'} = -\left[\frac{T(rb+1,j)-(2-T(rb+1,j))}{\Delta x}\right] \text{for j = (bb+1) to tb} \tag{3.47}$$

$$\left[Nu(i)\right]_{G'F} = -\left[\frac{T(i,bb)-(2-T(i,bb))}{\Delta y}\right] \text{for i = (fb+1) to rb} \tag{3.48}$$

The average Nusselt number for front, top and rear faces are calculated by using equation (2.62) to (2.65) as

For front face (FF'):

$$< Nu >_{FF'} = \sum_{j=bb+1}^{j=tb} Nu(j).\Delta y \tag{3.49}$$

Similarly for top (FG) , rear (GG') and bottom (G'F') faces one can write

$$< Nu >_{FG} = \sum_{i=fb+1}^{i=rb} Nu(i).\Delta x \tag{3.50}$$

$$< Nu >_{GG'} = \sum_{j=bb+1}^{j=tb} Nu(j).\Delta y \tag{3.51}$$

$$< Nu >_{G'F'} = \sum_{i=fb+1}^{i=rb} Nu(i).\Delta x \tag{3.52}$$

The overall Nusselt number for the square cylinder FGF'G' is evaluated as:

$$\left[< Nu >\right]_{FGG'F'} = \frac{\left[< Nu >_{FF'} + < Nu >_{FG} + < Nu >_{GG'} + < Nu >_{G'F'}\right]}{4} \tag{3.53}$$

3.10 Influence of Blockage (b/H):

In the present work for unconfined flow case the upper and lower boundaries are treated as friction-free walls, i.e. symmetric boundaries. The influence of different blockages are investigated for n=1.0, Re=40.0, Pr=10,Ri=0.5,L_u=6.0, L_d=12.0 on total drag, pressure drag, average Nusselt numbers of different faces and overall Nusselt number to decide the appropriate blockage ratio for present study. The blockage ratio (b/H) studied here is in the range of 1/10-1/25

Table 3.1 Influence of blockage on drag for n=1.0, Re=40, L_u=6, L_d=12 Pr=10, Ri=0.5

b/H	C_{Df}	C_{Dp}	C_D	%Diff. In C_D w.r.t. b/H=1/25
1/10	0.3242	1.7003	2.0244	7.37
1/15	0.3067	1.6051	1.9118	1.40
1/20	0.3033	1.5849	1.8882	0.15
1/25	0.3032	1.5821	1.8854	-

Table 3.2 Influence of blockage on Nusselt number for n=1.0, Re=40, L_u=6, L_d =12, Pr=10, Ri =0.5

b/H	$<Nu>_f$	$<Nu>_r$	$<Nu>_t$	$<Nu>_b$	$<Nu>_m$	%Diff. In $<Nu>_m$ w.r.t. b/H=1/25
1/10	11.9056	2.8161	7.0424	6.5348	7.0747	1.86
1/15	11.7951	2.8259	6.9424	6.3404	6.9740	0.47
1/20	11.7699	2.8160	6.8930	6.3280	6.9518	0.10
1/25	11.7653	2.7999	6.8600	6.3559	6.9453	-

The results are given in Table 3.1 and 3.2 for drag coefficient and Nusselt number respectively at different blockage ratios and % difference is also given for comparison purpose of the value of total drag and mean Nusselt number with respect to blockage ratio of 1/25. It has been found that the difference in the value of C_D and $<Nu>_m$ at B/H=1/15 and 1/25 is very small i.e. 1.40 % and 0.47 % respectively. Thus B/H=1/15 has been used in further computations.

3.11 Influence of upstream length (L_u):

In present work, the influence of different upstream lengths L_u are studied for n=1.0, Re=40.0, Pr=10, Ri=0.5, L_d=12 and blockage ratio of 1/15 to decide the appropriate upstream length for present study .The influence of different upstream lengths are investigated on total drag, pressure drag, average Nusselt numbers of different faces and overall Nusselt number. The upstream length (L_u) studied here is in the range of 6.0-10.0.

Table 3.3 Influence of up-stream length on drag for n=1.0, Re=40, H=15, L_d=12 Pr=10, Ri=0.5

L_u	C_{Df}	C_{Dp}	C_D	%Diff. In C_D w.r.t. L_u=10
6	0.3067	1.6051	1.9118	3.10
7	0.3045	1.5815	1.8860	1.71
8	0.3033	1.5670	1.8703	0.86
10	0.3020	1.5523	1.8543	-

Table 3.4 Influence of up-stream length on Nusselt number for n=1.0, Re=40, H=15, L_d=12,Pr=10 ,Ri=0.5

L_u	$<Nu>_f$	$<Nu>_r$	$<Nu>_t$	$<Nu>_b$	$<Nu>_m$	%Diff. In $<Nu>_m$ w.r.t. L_u=10
6	11.7951	2.8259	6.9424	6.3404	6.9760	0.87
7	11.7515	2.8080	6.9315	6.3098	6.9502	0.49
8	11.7239	2.7927	6.9173	6.2994	6.9333	0.25
10	11.6949	2.7764	6.9002	6.2914	6.9157	-

The results are given in Table 3.3 and 3.4 for drag coefficient and Nusselt number respectively at different upstream lengths and % difference is also presented for the comparison purpose the value of total drag and mean Nusselt number with respect to upstream length of 10.0. It has been found that the difference in the value of C_D and $< Nu>_m$ at L_u = 6.0 and 10.0 are 3.10 % and 0.87 % respectively. Thus L_u = 6.0 has been finally used in further computations.

3.12 Grid dependence:

A uniform mesh has been used throughout the domain. The grid dependence study are also done for n=1.0, Re=40.0, Pr=10, Ri=0.5, L_u =6.0, L_d=12.0 and blockage ratio of 1/15 to obtain reliable results for the present study .The effects of different grid size on total drag, pressure drag, average Nusselt numbers of different faces and overall Nusselt number are given in Table 3.8-3.13.

Table 3.5 Grid Dependence on drag for Re=40 Pr=10 n=1 Ri=0.5 H=15 L_u=6 L_d=12

Grid size (N-2)× (M-2)	C_{Df}	C_{Dp}	C_D	%Diff. In C_D w.r.t. finest grid
190× 150	0.3388	1.6373	1.9760	2.55
304×150	0.3448	1.6490	1.9939	3.48
190× 240	0.3067	1.6051	1.9118	-0.78
304×240	0.3143	1.6126	1.9269	-

Table 3.6 Grid Dependence on Nusselt number for Re=40 Pr=10 n=1 Ri=0.5 H=15 L_u=6 L_d=12

Grid size (N-2) ×(M-2)	$\langle Nu \rangle_f$	$\langle Nu \rangle_r$	$\langle Nu \rangle_t$	$\langle Nu \rangle_b$	$\langle Nu \rangle_m$	%Diff. In $\langle Nu \rangle_m$ w.r.t. finest grid
190× 150	11.6529	2.8659	7.5688	6.7124	7.2004	3.74
304×150	12.6963	2.4250	7.7364	6.9985	7.4641	7.54
190× 240	11.7951	2.8259	6.9424	6.3404	6.9760	0.50
304×240	12.1991	2.8230	6.8008	5.9412	6.9410	-

It is clearly seen from tables that the grid size of 190×240 is sufficiently fine to obtain the flow and heat transfer parameters that are essentially grid independent. Thus, this grid size has been finally used in all further computations.

3.12 Choice of time step:

The conditions necessary to prevent numerical instabilities are determined from the Courant-Friedrichs-Lewy (CFL) condition and the restriction on the grid Fourier numbers.

According to the CFL conditions, the distance the fluid travels in one time increment must be less than one space increment:

$$\Delta t < \min\left(\frac{\Delta x}{|V_x|}, \frac{\Delta y}{|V_y|}\right) \tag{3.95}$$

When the viscous diffusion terms are more important, the condition necessary to ensure stability is dictated by the restriction of the grid Fourier numbers, which is given by

$$\nu \Delta t < \left(\frac{1}{2}\frac{\Delta x^2 \Delta y^2}{\Delta x^2 + \Delta y^2}\right) \tag{3.96}$$

where $\nu = 1/\mathrm{Re}$ for momentum equation solver and $\nu = 1/\mathrm{Pe}$ for energy equation.

The final Δt is for each time increment is the minimum of the Δt obtained from equation (3.95) and (3.96).

Chapter 4

RESULTS AND DISCUSSION

In this work, the governing equations presented in chapter 3 have been solved numerically by using Coupled method. A SMAC–type implicit scheme has been implemented on a staggered grid to solve complete Navier-Stokes and Energy equations. It has been known that flow and heat transfer characteristics in a particular mixed convection problem depends on Reynolds number, Re, Grashof number, Gr, Prandtl number, Pr. So the Parametric calculations have been performed on both confined and unconfined flow situations to determine the effect of Reynolds number (Re = 5,10 and 40), Richardson number ($0 \leq Ri \leq 0.5$), Prandtl number ($Pr \leq 10$) and power law index ($0.5 \leq n \leq 1.4$) on hydrodynamic and thermal conditions for a blockage ratio of 1/15.For these computations, a 190×240 uniform grid has been used. Computations have been carried out for a blockage ratio (b/H) of 1/15. The upstream (L_u) and downstream (L_d) distances are kept 6 and 12 respectively throughout entire computations.

4.1 Validation of Results

As mentioned in Chapter 1, no numerical results are available to explore the effect of buoyancy on the flow and heat transfer characteristics from a square cylinder placed normally to approaching steady flow even for Newtonian fluids. And no prior study is available for the simplest type of non-Newtonian fluid behavior, namely, shear thinning and shear thickening modeled by the usual two-parameter power-law model therefore, the solution procedure has been validated by comparing the present results with the literature values for unsteady flow for Newtonian fluids. For unsteady flow, some results on drag , lift and Nusselt number have been reported by Sharma et al. [20] and Turki et al. [22]. From a careful scrutiny of the available literature on mixed convection heat transfer from a horizontal cylinder it is found that for $Ri < 0.5$ the predominant heat transfer mechanism is forced convection and increase in the average Nusselt number will be $\approx$ 5%. Turki results are contradicting with this statement by showing a huge increment in the average Nusselt number (>25%) for $Ri < 0.1$ therefore validation of the numerical

solution procedure used for the present analysis is done with the unpublished results of Sharma et al. which are in good agreement the previous studies.

Validation with unsteady results

Sharma et al. [20] investigated various flow and heat transfer parameters such as drag coefficient, Strouhal number, lift coefficient etc. for flow around a square cylinder for Newtonian fluids for Reynolds number 100, $0 \leq Ri \leq 1$ and Pr=0.7. They have used a combination of uniform and non-uniform grid structure with fine grids clustered around the cylinder and uniform coarse grid far away from the cylinder on a grid size of 323×132, L_u=8.5, L_d=16.5 and the blockage ratio of 1/20. They used QUICK scheme for discretisation of convective terms.

Table 4.1 Benchmarking of drag and lift coefficients of the present work with Sharma et al .[20] for Re=100,Pr=0.7,n=1

Ri		C_{Dp}	C_D	C_{Lp}	C_L
0	Atul	1.4463	1.4936	-	-
	Present	1.5567	1.6528	-	-
	%error	7.2	9.6	-	-
0.25	Atul	1.4573	1.5051	-0.4124	-0.4096
	Present	1.5412	1.6398	-0.4503	-0.4479
	%error	5.7	8.9	9.19	9.35
0.5	Atul	1.5039	1.5532	-0.7671	-0.7573
	Present	1.5223	1.6128	-0.8727	-0.8695
	%error	1.2	3.8	13.8	14.8
1.0	Atul	1.6445	1.7011	-1.3138	-1.2794
	Present	1.5345	1.6174	-1.5018	-1.4551
	%error	6.7	4.9	14.3	13.7

Table 4.2 Benchmarking of Nusselt number of the present work with Sharma et al .[20] for Re=100,Pr=0.7,n=1

Ri		$\langle Nu \rangle_f$	$\langle Nu \rangle_r$	$\langle Nu \rangle_t$	$\langle Nu \rangle_b$	$\langle Nu \rangle_m$
0	Atul	7.4290	1.7190	3.5139	3.5139	4.0439
	Present	7.1037	1.5477	3.4975	3.4975	3.9377
	%error	4.3	9.9	0.5	0.5	2.6
0.25	Atul	7.4134	1.8787	3.7136	3.3057	4.0778
	Present	7.0893	1.6290	3.7134	3.3384	3.9425
	%error	4.4	13.2	0.01	0.989	3.32
0.5	Atul	7.3943	2.1729	3.8974	3.1180	4.2118
	Present	7.0452	1.8938	3.8650	3.0971	3.9753
	%error	4.7	12.8	0.8	0.67	5.62
1.0	Atul	7.3188	2.7538	4.1896	2.8370	4.2748
	Present	6.9348	2.5115	4.1838	2.7569	4.0967
	%error	5.24	8.7	0.14	2.82	4.16

It is seen from the results shown in Tables 4.1 and 4.2, the maximum difference in the values of the drag, lift and Nusselt number is 9.6%, 14.8% and 5.62% correspondingly with the results obtained by Sharma et al. [20]. It is found that the coefficient of lift has great sensitivity to the number of grid points in the domain as compared to the other parmeters. Even though Sharma et al. [20] have used a non-uniform grid and QUICK scheme, our results are very closer using first order upwind scheme and uniform grid

Comparison with circular cylinder results

Ahmad [2], Badr [3]have investigated the problem of combined convection heat transfer from a circular cylinder placed with its axis horizontal and perpendicular to the free stream direction. They have reported the effect of buoyancy parameter on drag and Nusselt number with in the steady flow regime .The results are mostly of qualitative relevance to the present work.

Table 4.3 comparison of drag coefficients of the present work with Ahmad [2] for Re=5,Pr=0.7,n=1

Gr	ahmad	Present work
0	3.74	4.8144
12.5	3.43	4.7344
%difference	8.2	1.66

Table 4.4 Benchmarking of Nusselt number of the present work with Badr [3] for Re=40,Pr=0.7,n=1

Gr	Badr	Present work
0	3.48	3.041395
400	3.49	3.047115
%difference	0.29	0.20

From Table 4.3 and 4.4 it can be observed that influence of buoyancy parameter on the drag co-efficient and Nusselt number is similar for circular and square cylinder at low Reynolds numbers.

4.2 Results for Mixed convection Heat Transfer in Power-law fluids

A detailed analysis on the variations of drag, lift , Local and average Nusselt number with Power law index, Prandtl and Richardson numbers at different Reynolds numbers are presented for both unconfined and confined cases. Also, the dynamics of flow and heat transfer are made visible by means of Stream line and iso-vorticity contour plots.

4.2.1 Drag and Lift

The most important flow characteristics quantities of the flow around square cylinder are the drag and lift coefficients. The values of drag and coefficients are presented in Tables A.1 – A.18 for $5 \leq Re \leq 40$, $5 \leq Pe \leq 400$, $0 \leq Ri \leq 0.5$ and $0.5 \leq n \leq 1.4$.

Variation of drag with power law index

Paliwal et al have presented the variation of drag with power law index in forced flow case. In order to elucidate the effect of n in mixed convection flow case, the drag coefficient has been normalized with using the corresponding value for Newtonian liquids at the same value of Reynolds number, Prandtl number and Richardson number. Figure 4.1-4.3 shows the variation of the individual and the total drag coefficient with power index for Pr=1,5 and 10,Ri=0,0.25and 0.5 at Re=5,10 and 40. From these figures it is observed that the variation of the individual and the total drag with power law index in

the mixed convection is similar to the forced convection case for both confined and unconfined flows except for total drag in the confined flow at Re=40.

Variation of drag with Richardson number

In order to elucidate the effect of Ri for constant value of power law index and Prandtl number, the drag coefficient has been normalized with using the corresponding value for Ri=0 at the same value of Reynolds number, Prandtl number and Power law index. Figure 4.4 shows the variation of the individual and the total drag coefficient with Richardson number at $0.5 \leq n \leq 1.4$, $1 < Pr < 10$ and Re=40 for both confined and unconfined flow situations. From this figure it is observed that the values of individual and the total drag coefficients vary from one case to another case with out any particular order. This complicated behavior is expected because of cross stream buoyancy. Similar type of effect can be observed for Re=5 and 10.

Variation of Lift with Richardson number

It is known that incase of forced convection flow lift is zero with in the steady flow regime because of symmetric pressure on the top and bottom surfaces of the cylinder. However in the case of mixed convection because of asymmetry in the flow some lift is possible on the cylinder. The total lift comprising the frictional and pressure components, frictional term has insignificant contribution in the total lift. So only the variation of pressure lift and total lift with Richardson is studied. From tables it is observed that lift coefficient acts down ward due to the lower pressure on the bottom side as compared to the top surface. The lift coefficient can not be normalized with using the corresponding value for Ri=0 at the same value of Reynolds number, Prandtl number and Power law index because lift at Ri=0 is zero. Figure 4.5 shows the variation of the Pressure and the total lift coefficient with Richardson number at $0.5 \leq n \leq 1.4$, $1 < Pr < 10$ and Re= 40 for both confined and unconfined flow situations. From this figure it is observed that the values of pressure and the total lift coefficients increases with increasing Ri and Pr. Similar type of effect can be observed for Re=5 and 10.

4.2.2 Average Nusselt number

Heat transfer rates are commonly represented in terms of the local and average Nusselt numbers. The values of surface average Nusselt numbers for front, rear, top and bottom faces and overall Nusselt number for the entire square cylinder are presented in Tables A.19 – A.36 for $5 \leq Re \leq 40$, $5 \leq Pe \leq 400$, $0 \leq Ri \leq 0.5$ and $0.5 \leq n \leq 1.4$ for the constant wall temperature at the surface of square cylinder

Variation of Average Nusselt number with power law index

Paliwal et al have presented the variation of average Nusselt numbers for front, top, rear faces and overall Nusselt number for square cylinder with power law index in forced flow case. The value of average Nusselt numbers is normalized with respect to the Nusselt number for a Newtonian liquid at the same value of the Reynolds number, Prandtl number and the Richardson number. Figure 4.6-4.7 shows the variation of the average Nusselt numbers for all faces and the overall mean Nusselt number for the square cylinder with power index for Pr=1,5 and 10,Ri=0,0.25 at Re= 40. From this figure it is observed that the variation of the average Nusselt numbers in the mixed convection is similar to the forced convection case for both confined and unconfined flow situations.

Variation of average Nusselt number with Richardson number

In order to elucidate the effect of Ri for constant value of power law index and Prandtl number, the average Nusselt number has been normalized with using the corresponding value for Ri=0 at the same value of Reynolds number, Prandtl number and Power law index. Figure 4.8-4.9 shows the variation of the average Nusselt numbers for all faces and the overall mean Nusselt number for the square cylinder with Richardson number at $0.5 \leq n \leq 1.4$, $1 < Pr < 10$ and Re= 40 for both confined and unconfined flow situations. From this figure it is observed that for unconfined flow a monotonic increase in the top and rear face Nusselt number where as there is a monotonic decrease in the front and bottom face Nusselt number with increasing Ri and for confined flow a monotonic increase in the top, rear and front face Nusselt number where as there is a monotonic decrease in the bottom face Nusselt number with increasing Ri. However, the cylinder average Nusselt number increases with increasing Ri. From the data given in tables A.19-A.36 it is observed that for Re=5 unconfined flow front face Nusselt number is increased for n=0.6 and the cyiinder average Nusselt number decreased for n=0.6 and

0.8 with increasing Ri and for Re=10 unconfined flow front face Nusselt number is increased for n=0.5 and the cylinder average Nusselt number decreased for n <1 and increases for n>1 with increasing Ri.

4.2.3 Streamline plots

Further insights in to the underlying flow mechanics can be gained by studying the streamline plots shown in Figure-4.10, for n=1 at Reynolds number of 40 and for Pr=1 and 10, $0 \leq Ri \leq 0.5$. From stream function plots it is observed that mixed convection can initiate the asymmetry. As the value of the buoyancy parameter increases stream lines ahead of the cylinder have a downward slope. The lines behind the cylinder have a positive slope and rise more in comparison with upstream lines because of greater influence of the buoyancy parameter in the wake. The vortices start to disappear as Ri increases.

4.2.4 Isotherms

The effect of Richardson number on the thermal boundary layer is presented by plotting the lines of equal temperature (iso therms). Fig 4.11shows that for Ri=0 the temperature field is symmetric about centerline, with increase in the Ri isotherm patterns become asymmetric.

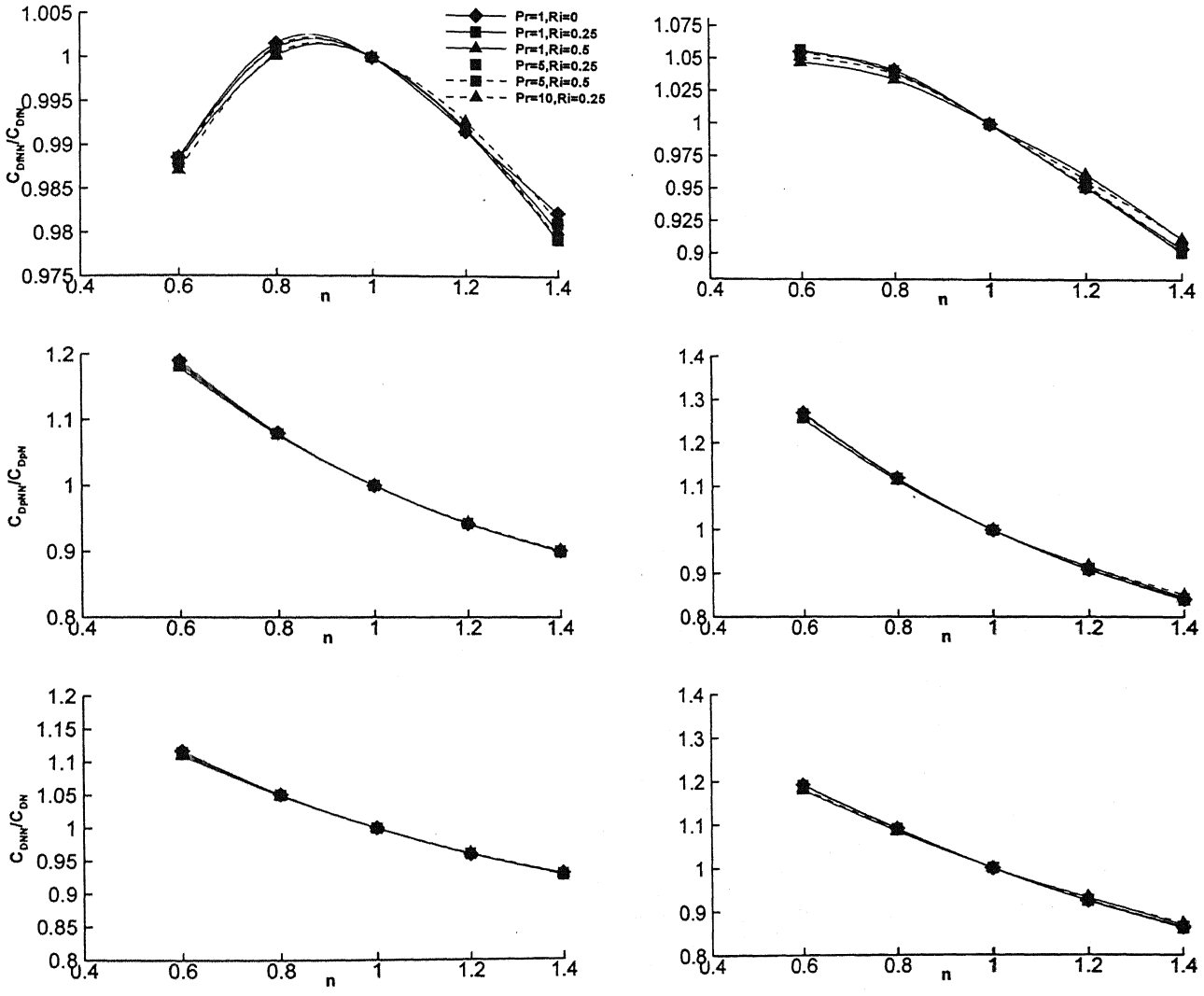

Fig 4.1: Variation of drag with power law index (a) and (b) for unconfined and confined cases respectively for Re=5

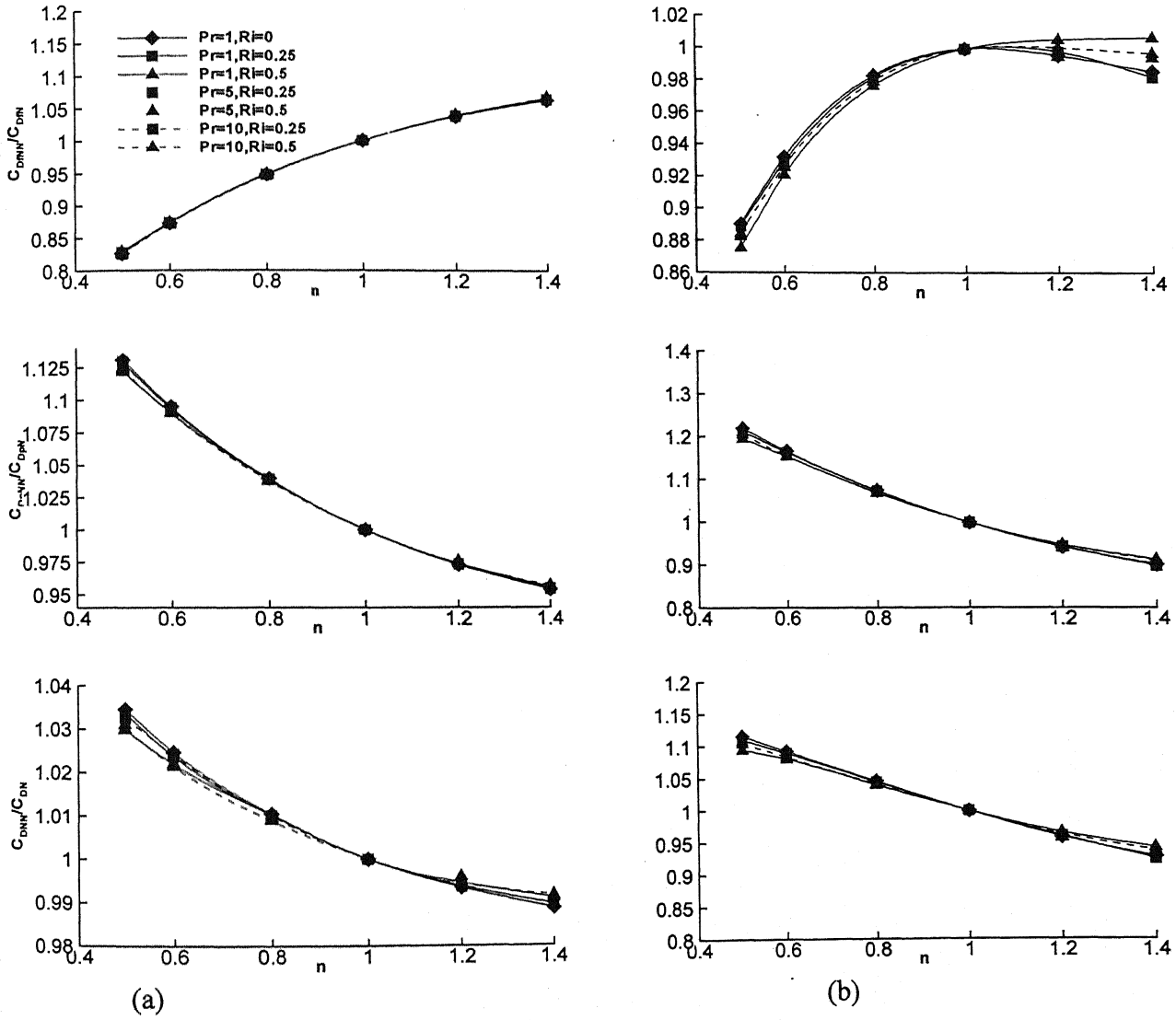

Fig 4.2: Variation of drag with power law index for Re=10

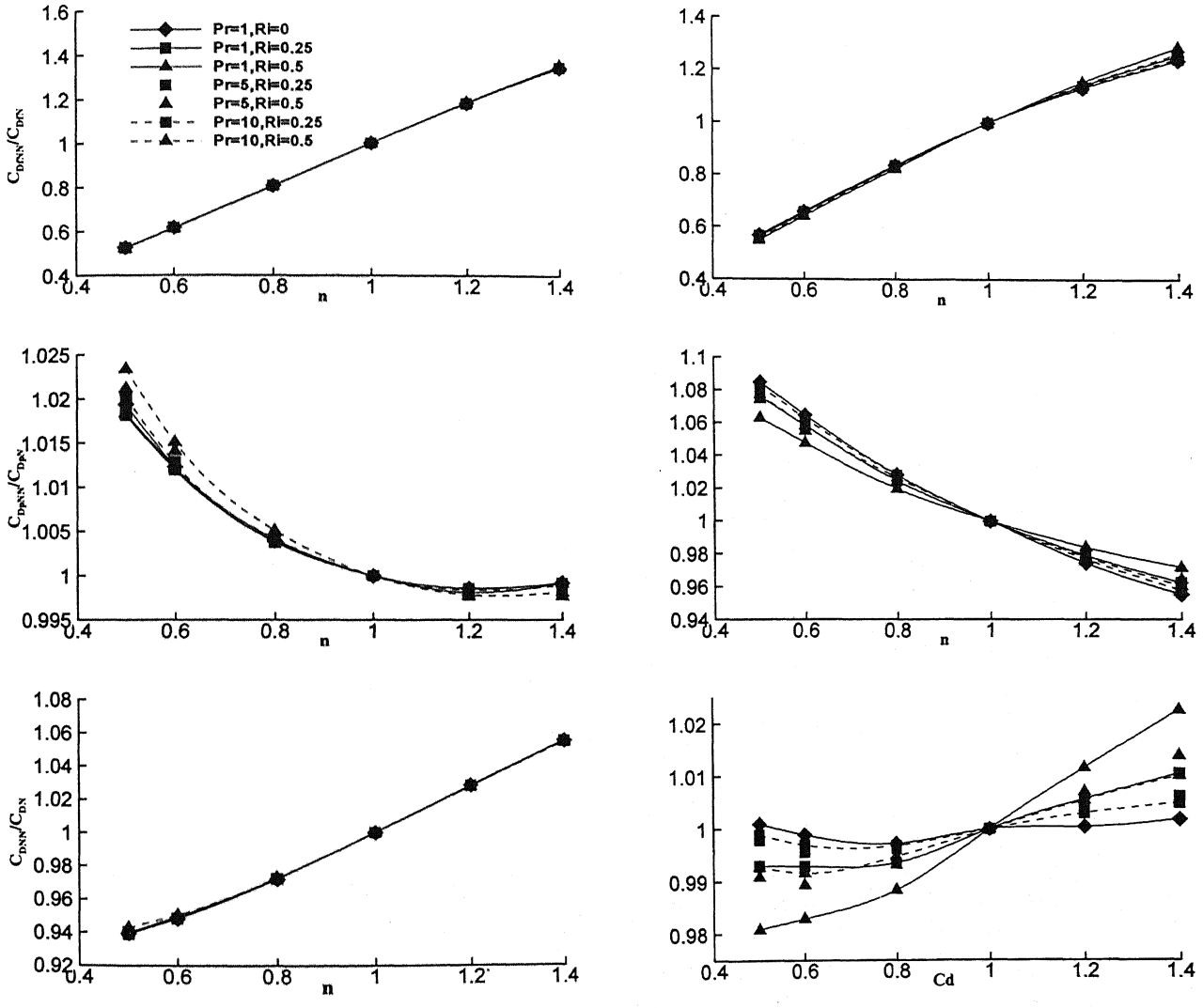

Fig 4.3: Variation of drag with power law index Re=40

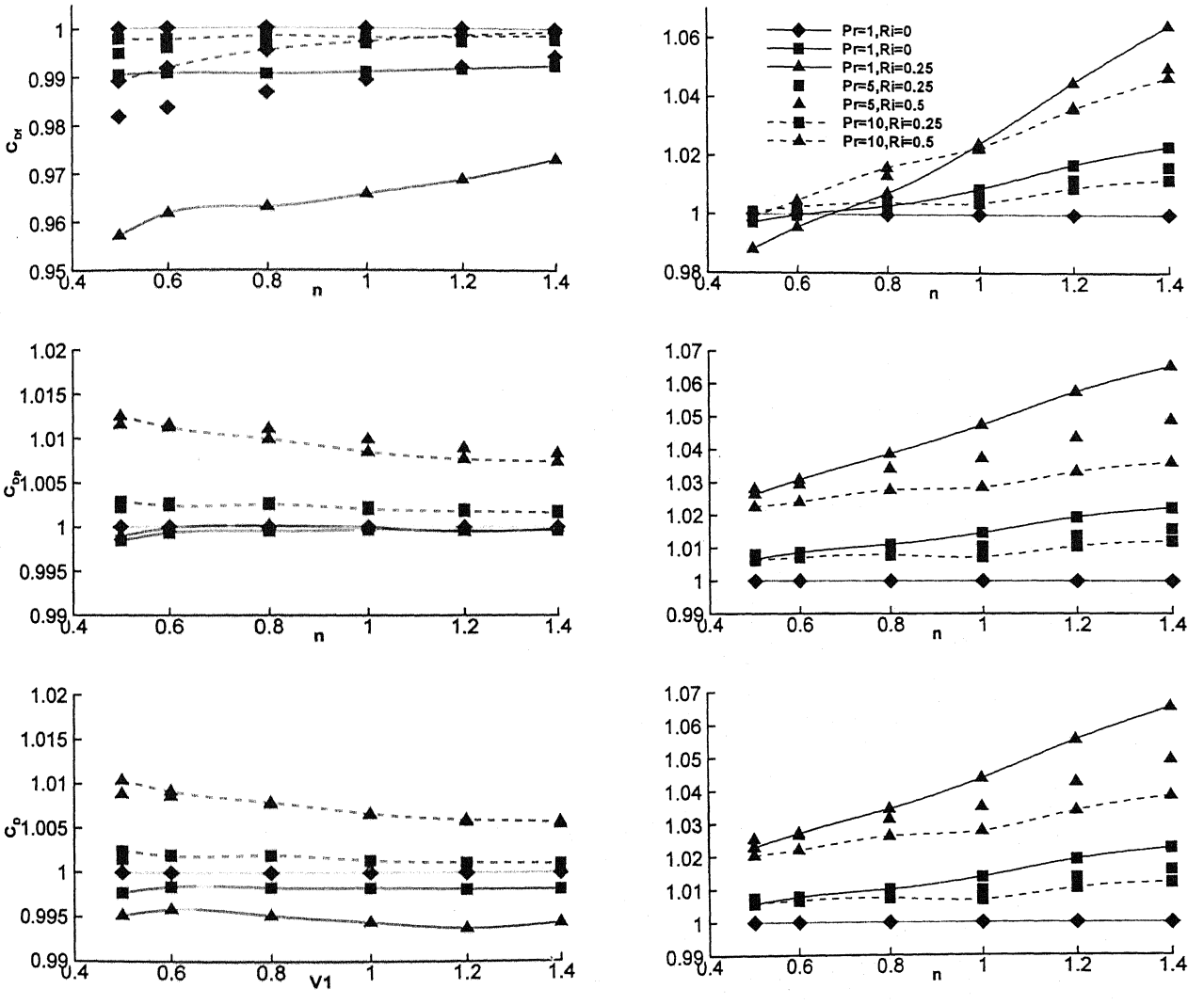

(a) (b)

Fig 4.4 : Variation of drag with Richardson number for Re=40

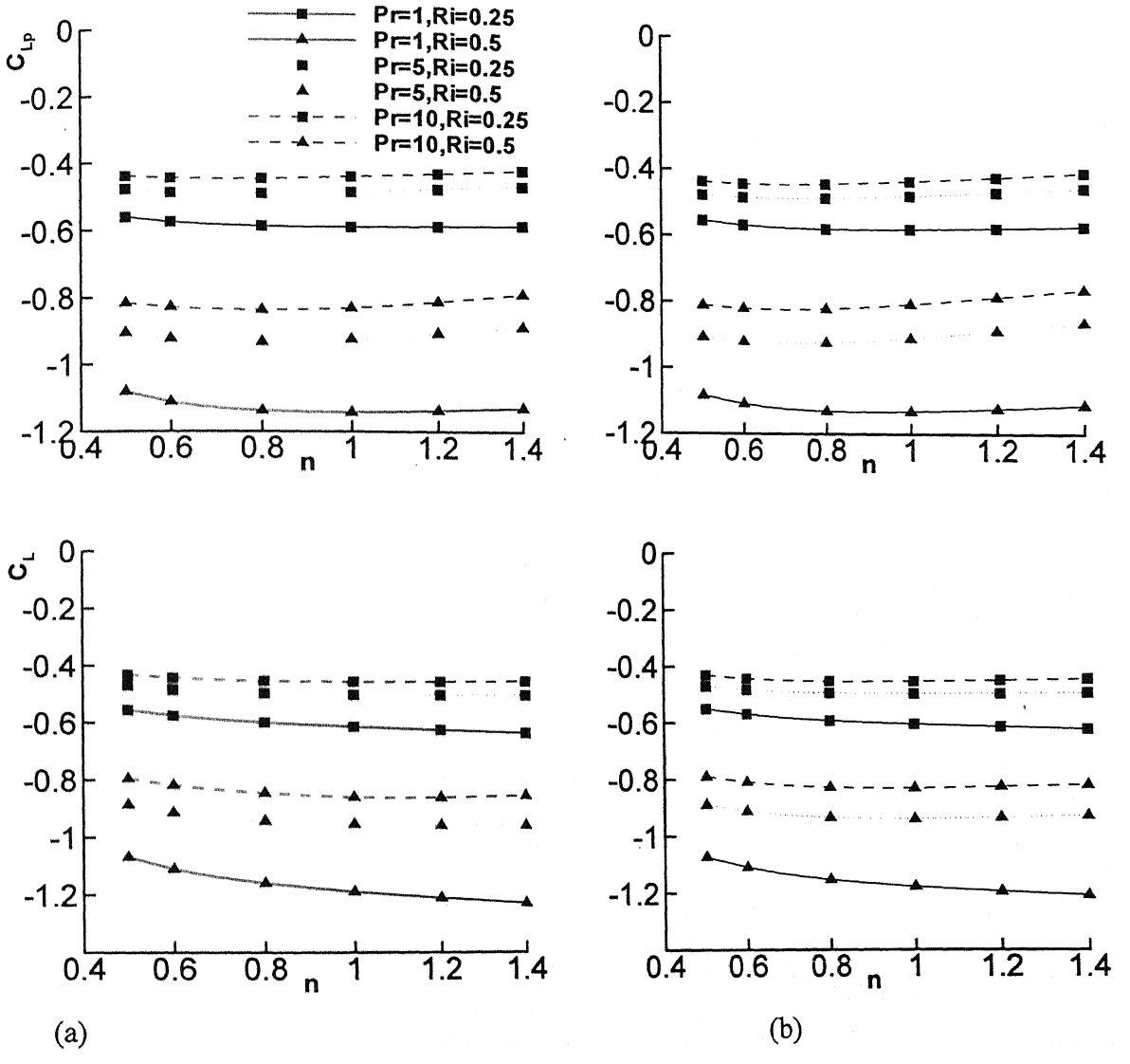

Fig 4.5 : Variation of lift with Richardson number for Re=40

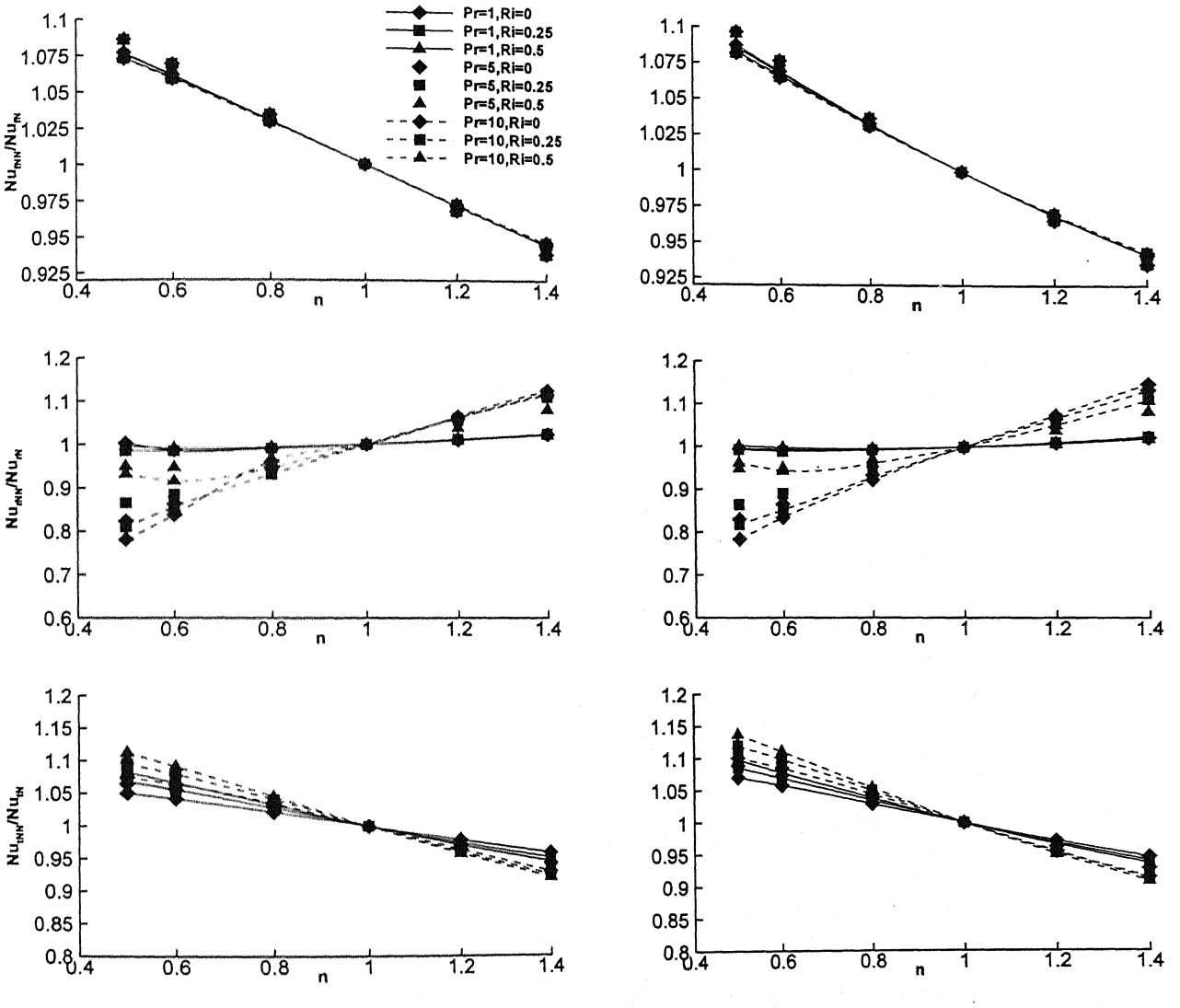

Fig 4.6 : Variation of Nusselt number with power law index for Re=40

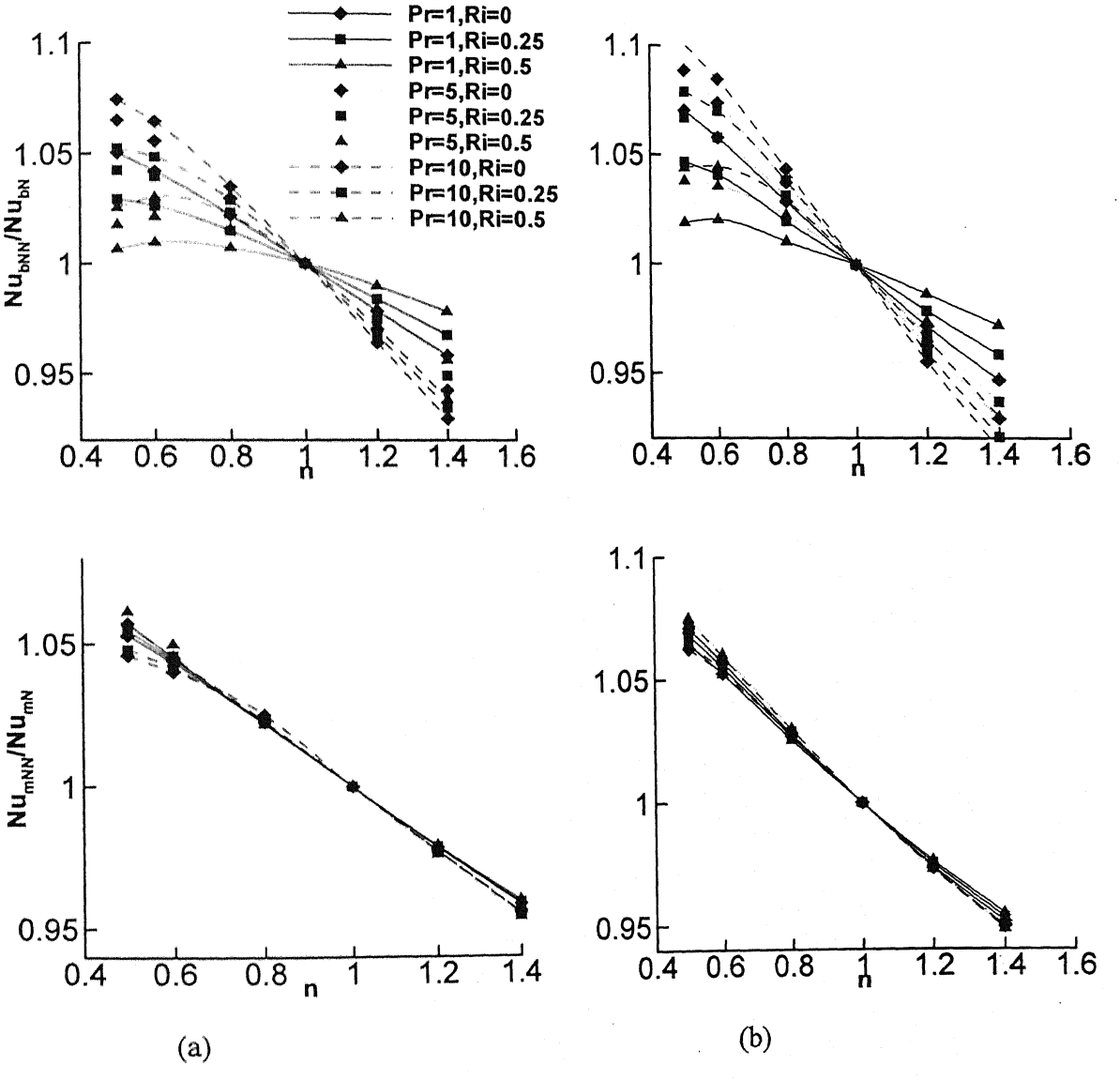

Fig 4.7 : Variation of Nusselt number with power law index for Re=40

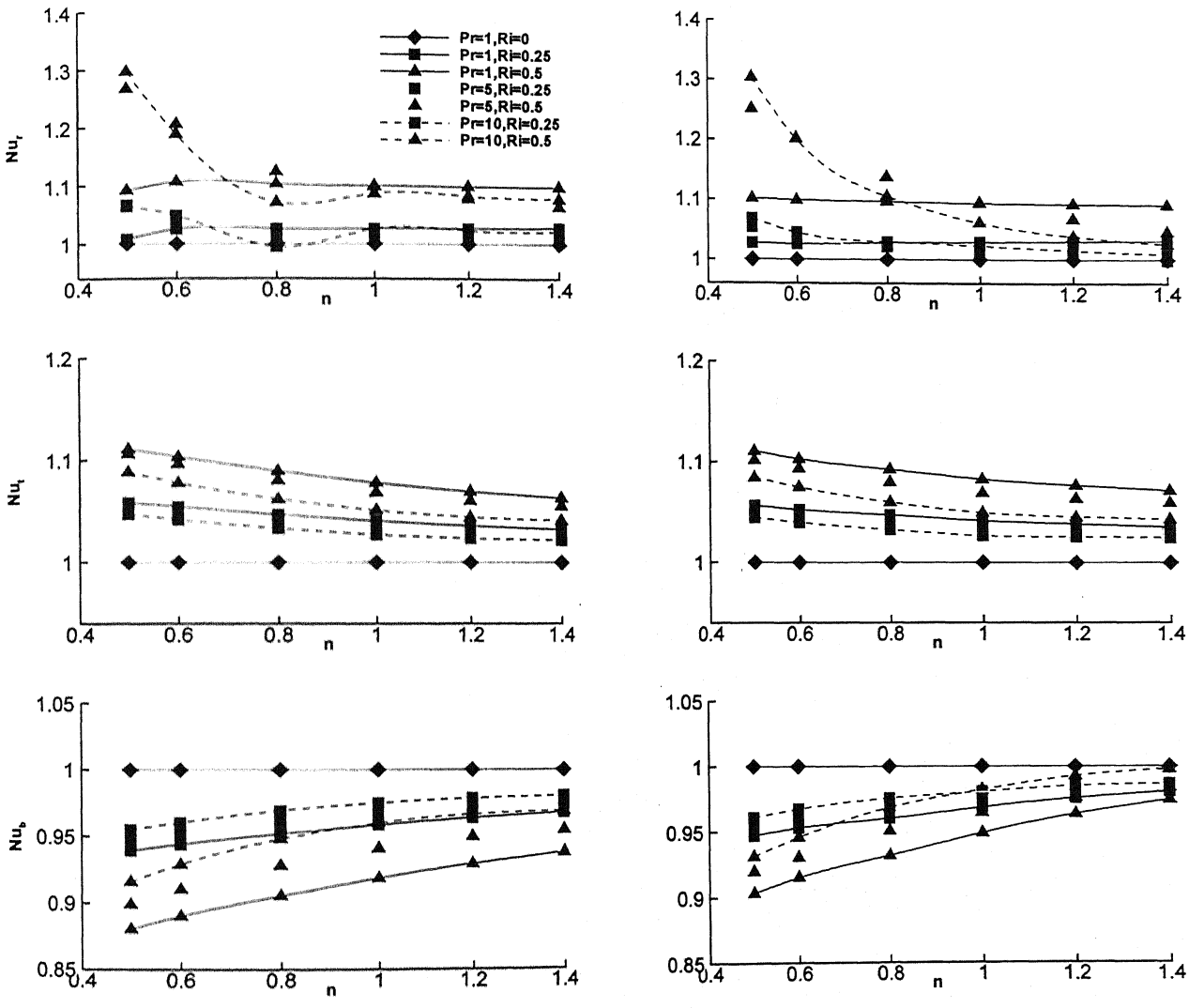

Fig 4.8 : Variation of Nusselt number with Richardson number for Re=40

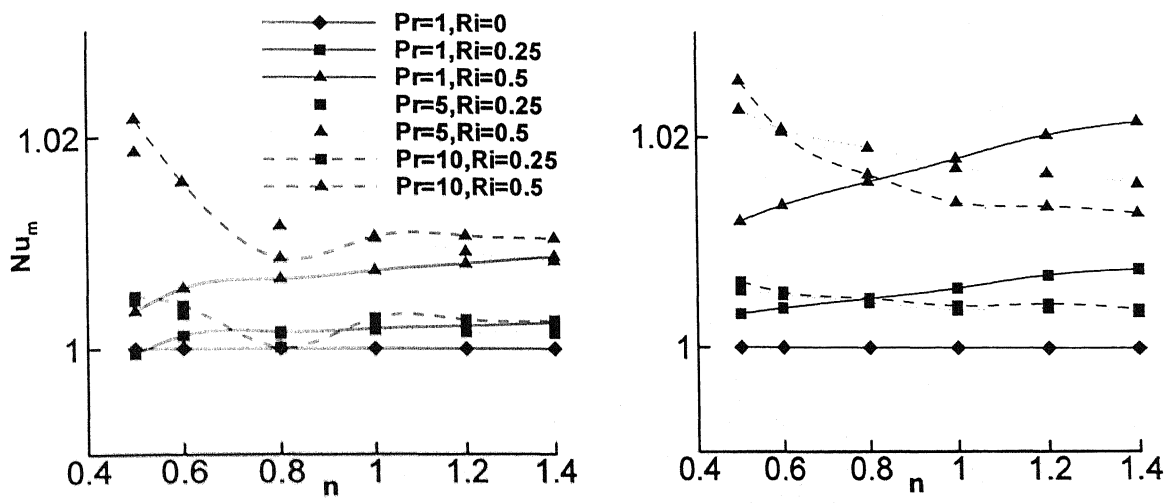

Fig 4.9 : Variation of Nusselt number with Richardson number for Re=40

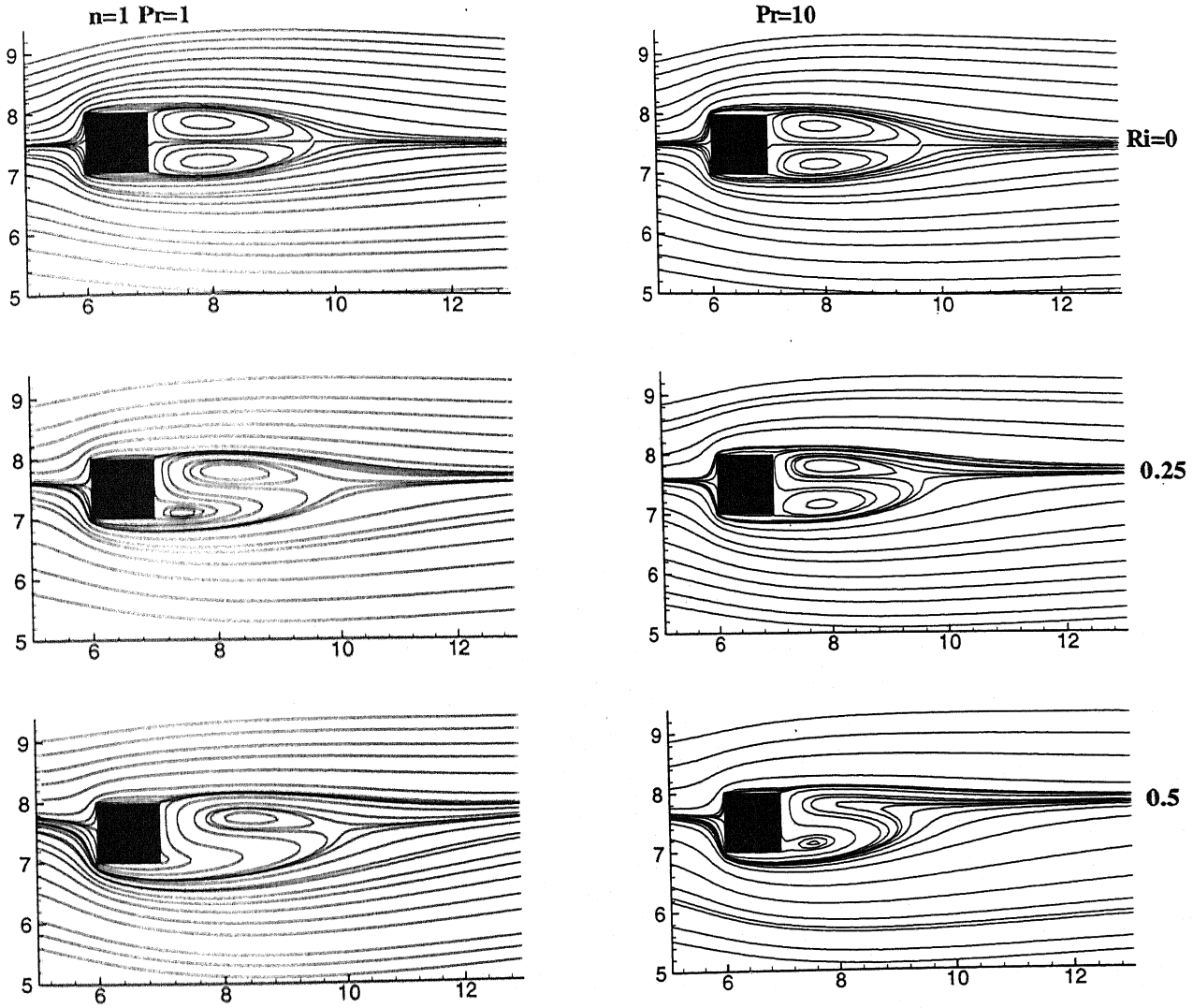

Fig 4.10 : Stream lines for Re=40

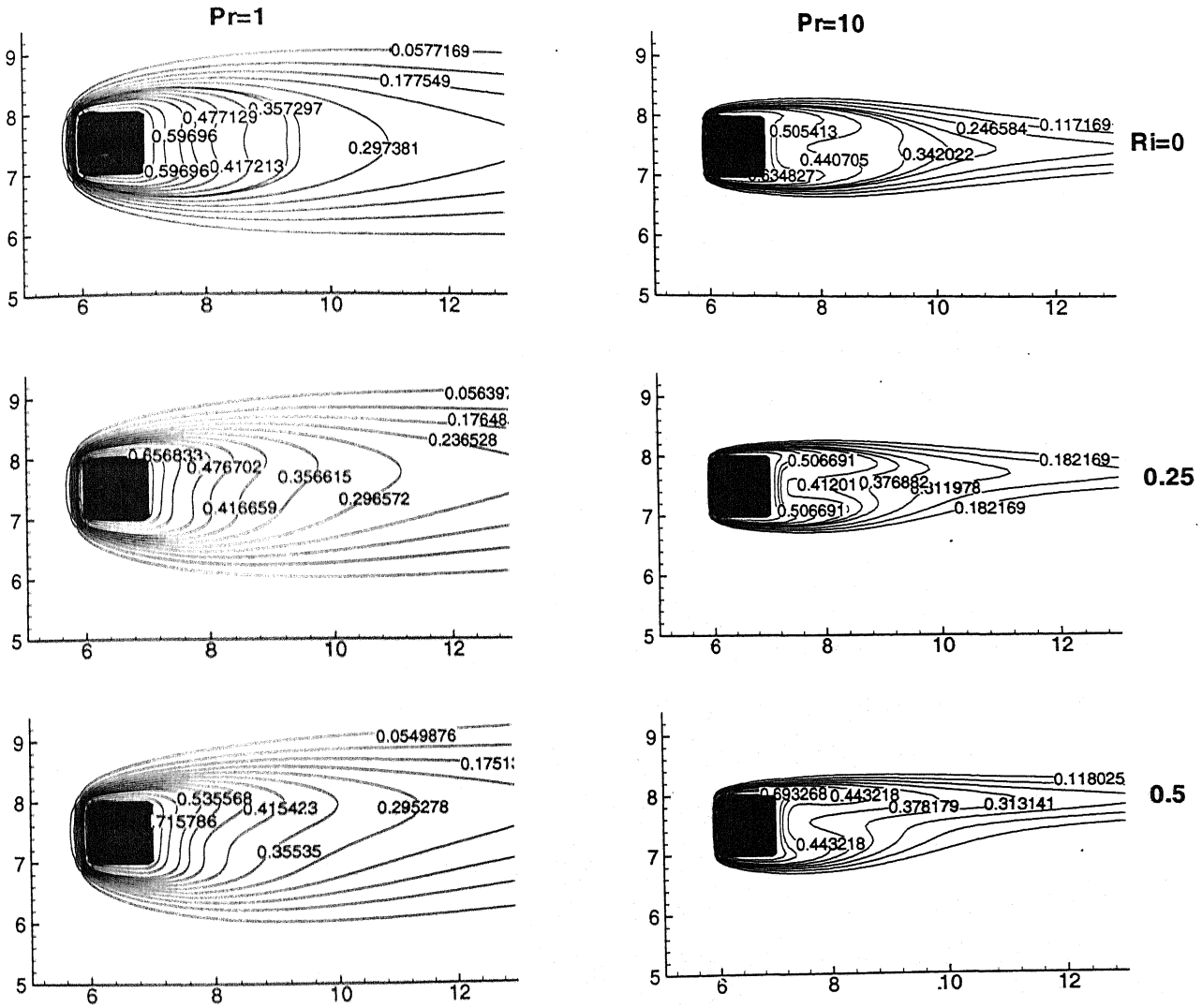

Fig 4.11 : isotherms for Re=40

Chapter 5

Conclusions and suggestions for future work

5.1 Conclusions

In this study, the effect of combined forced and natural convection (mixed convection) on flow and heat transfer characteristics of steady, incompressible flow of power law fluids over a heated square cylinder placed normally to the approaching fluid is analyzed. A SMAC–type implicit scheme has been implemented on a staggered grid to solve complete Navier-Stokes and Energy equations for a two-dimensional laminar flow of a Boussinesq fluid over a square cylinder. Parametric calculations have been performed to determine the effect of Reynolds number (Re =5, 10 and 40), Richardson number ($0 \leq Ri \leq 0.5$), Prandtl number ($Pr \leq 10$), power law index ($0.5 \leq n \leq 1.4$) and Wall effects on hydrodynamic and thermal conditions for a blockage ratio of 1/15, L_u=6 and L_d=12. The dynamics of flow and heat transfer are made visible by means of contour plots.

It is observed that the variation of the individual, total drag and average Nusselt numbers with the power law index and Reynolds number in the mixed convection is similar to the forced convection case for both confined and unconfined flow situations. The variation of the individual, total drag with Richardson number is not following any trend, this is expected because of cross stream buoyancy.

It is found that the Lift coefficient acts downward due to the lower pressure on the bottom as compared to the top surface of the cylinder. Both the Pressure and total Lift coefficient increases with increasing Ri.

It is also observed that for unconfined flow a monotonic increase in the top and rear face Nusselt number where as there is a monotonic decrease in the front and bottom face Nusselt number with increasing Ri and for confined flow a monotonic increase in the top, rear and front face Nusselt number where as there is a monotonic decrease in the bottom face Nusselt number with increasing Ri. However, the cylinder average Nusselt number increases with increasing Ri.

A considerable change in the flow and heat transfer fields is observed. From stream function and isotherm plots it is observed that mixed convection can initiate the asymmetry in flow and temperature fields. As the value of the buoyancy parameter

increases stream lines ahead of the cylinder have a downward slope. The lines behind the cylinder have a positive slope and rise more in comparison with upstream lines because of greater influence of the buoyancy parameter in the wake. The vortices start to disappear as Ri increases.

5.2 Suggestions for the future work

The present work has explored the steady flow and heat transfer to power law liquids from a isothermal square cylinder for the range of Reynolds number 5-40 and Richardson number 0-0.5. Considerable scope exists to extend this work; therefore some of the possibilities are mentioned here.

- The present work can be extended in many ways: first, for the cylinder dissipating constant heat flux; second for the channel walls with uniform heat flux and constant temperature boundary conditions.
- In the present work , first order upwind scheme has been used for the discretisation of the convective terms of momentum equations, which has only for the first order accuracy. QUICK scheme can be used for the discretisation of the convective terms to increase the accuracy.
- The present work has been carried out using power law fluid model. Thus one can use more realistic model such as Ellis or the Carreau equations.
- In the present work only uniform grids have been used through out. Accuracy of the numerical results can be increased by using non-uniform grid with clustering near the cylinder.

References

[1] Abbasi H., Turki S., Ben Nasrallah S., Channel flow past bluff-body: outlet boundary condition, vortex shedding and effects of buoyancy, Computational mechanics, **28**, 10-16, 2002.

[2] Ahmad R.A. and Qureshi Z.H. , Laminar mixed convection from a uniform heat flux horizontal cylinder in a cross flow, Journal of Thermophysics and heat transfer, **6**(2), 277-287, 1992.

[3] Badr H.M., A Theoretical study of laminar mixed convection from a horizontal cylinder in a cross stream , Int. J. Heat and Mass transfer, **26** , 639-653, 1983.

[4] Bassam A., Abu-Hijleh K., Laminar Mixed convection correlations for an isothermal cylinder in cross flow a different angles of attack, Int. J. Heat and Mass transfer, **42**, 1383-1388, 1999

[5] Bennon W.D. and Incropera F.P., Mixed convection heat transfer from horizontal cylinders in the crossflow of a finite water layer, ASME, J. Heat transfer, **103**, 540-545, 1981.

[6] Biswas G., Laschefski H., Mitra N.K. and Fiebg M., Numerical Investigation of Mixed convection Heat transfer in a channel with a built in square cylinder, numerical Heat transfer, A , **18**, 173-188, 1990.

[7] Chhabra R.P., Richardson J.F., Non-Newtonian flow in the process industries, Butterworth-Heimemam, Oxford, 1999.

[8] Denn M.M., Boundary layer flows for a class of elastic fluids , Chem. Engg. Sci., **22**(3), 395, 1967.

[9] Dhiman A.K, Sharma A., Chhabra R.P. &Eswaran V., Effects of Reynolds and Prandtl numbers on the heat transfer across a square cylinder in the steady flow regime, Numerical Heat Transfer Part A, communicated, 2004.

[10] Dhiman A.K, Chhabra R.P. &Eswaran V., Flow and Heat Transfer Across a Confined Square Cylinder in the Steady Flow Regime, Int. J. Heat Mass Transfer, In press, 2005.

[11] Fand R.M. , Keswani K.K , Combined natural and forced convection heat transfer from horizontal cylinders to water, Int. J. Heat Mass Transfer, **16**, 1175-1191, 1973.

[12] Gupta A.K., Sharma A., Chhabra R.P. &Eswaran V., Two-Dimensional steady flow of a power law fluid past a square cylinder in a plane channel: momentum and heat transfer characteristics, Ind. Eng. Chem. Res., **42** , 5674-5686, 2003.

[13] Hatton A.P., James D.D. and Swire H.W., Combined forced and natural convection with low speed air flow over horizontal cylinders, J. Fluid. Mech., **42**(1), 17-31, 1970.

[14] Juma A.K.A. and Richardson J.F., Heat transfer from horizontal cylinders to liquids, Chem. Eng. sci., **37**(11), 1681-1688, 1992.

[15] Nitin S., CFD Modeling of Two-Dimensional flows of Newtonian and power law fluids , M.Tech Thesis, IITKanpur,2004.

[16] Paliwal B., Sharma A., Chhabra R.P. &Eswaran V., Power law fluid flow past a square cylinder: momentum and heat transfer characteristics, Chem. Eng. Sci., **58**, 5315-5329, 2003..

[17] Saha A.K., Dynamical characteristics of the wake of a square cylinder at low and high Reynolds numbers, PhD. Thesis, IIT Kanpur, 1999.

[18] Sharma A. and Eswaran V., Heat and fluid flow across a square cylinder in the two-dimensional laminar flow regime, Numerical Heat Transfer, Part A , **44** , 1-23, 2003.

[19] Sharma A., Numerical Investigation of unconfined and channel confined flow across a square cylinder with forced and mixed convection heat transfer, PhD. Thesis, IIT Kanpur, 2003.

[20] Sharma A. and Eswaran V., Effect of buoyancy on the vortex shedding from a heated /cooled square cylinder in cross flow, Proc 6th Annual CFD Symposium, Bangalore, 2003.

[21] Sharma G.K. and Sukumathe S.P., Combined free and forced convection from a heated tube to a transverse air stream, J. Heat transfer, **91** , 457-459,1969.

[22] Turki S., Abbasi H., Ben Nasrallah S., Two-dimensional laminar fluid flow and heat transfer in a channel with a built-in square cylinder, Int. J. of thermal sciences, **42**, 1105-1113, 2003.

[23] Wang A.B., Travnicek Z. and Chia K.C., On the relationship of effective Reynolds number and Strouhal number for the laminar vortex shedding of a heated circular cylinder, Phys.Fluids, **12**, 1401-1410, 2000.

Appendix A

Unconfined Flow Results:

Table A.1 Drag and Lift Coefficients for Re=5,Pr=1

n	Ri	Drag coefficients			Lift coefficients		
		C_{Df}	C_{Dp}	C_D	C_{Lf}	C_{Lp}	C_L
0.6	0	1.721856	3.654922	5.376777	-0.000384	0.000056	-0.000328
	0.25	1.714692	3.623699	5.338391	-0.083677	-0.663997	-0.747674
	0.5	1.693921	3.559104	5.253024	-0.154629	-1.309247	-1.463876
0.8	0	1.744536	3.316604	5.061140	-0.000179	0.000017	-0.000163
	0.25	1.736395	3.297850	5.034245	-0.114644	-0.680747	-0.795391
	0.5	1.714248	3.250889	4.965137	-0.225777	-1.353409	-1.579186
1.0	0	1.741914	3.072522	4.814437	-0.000091	-0.000125	-0.000216
	0.25	1.734786	3.059118	4.793904	-0.143399	-0.689592	-0.832991
	0.5	1.714217	3.020238	4.734455	-0.28484	-1.373514	-1.658354
1.2	0	1.727308	2.894735	4.622044	0.000107	-0.000024	0.000083
	0.25	1.720472	2.882862	4.603334	-0.167405	-0.693439	-0.860844
	0.5	1.700510	2.846728	4.547239	-0.331814	-1.379656	-1.711470
1.4	0	1.711134	2.770059	4.481193	0.000204	0.000022	0.000226
	0.25	1.698820	2.752374	4.451194	-0.185616	-0.692703	-0.878319
	0.5	1.680495	2.718815	4.399311	-0.370899	-1.380857	-1.751756

Table A.2 Drag and Lift Coefficients for Re=5,Pr=5

n	Ri	Drag coefficients			Lift cpefficients		
		C_{Df}	C_{Dp}	C_D	C_{Lf}	C_{Lp}	C_L
0.6	0	1.721838	3.654887	5.376726	-0.000396	0.000038	-0.000358
	0.25	1.720880	3.650717	5.371597	-0.018647	-0.455073	-0.473719
	0.5	1.720167	3.645809	5.365976	-0.035698	-0.896066	-0.931764
0.8	0	1.744536	3.316605	5.061141	-0.000179	0.000017	-0.000162
	0.25	1.743373	3.316358	5.059731	-0.048545	-0.485388	-0.533932
	0.5	1.740326	3.318683	5.059010	-0.095027	-0.963105	-1.058132
1.0	0	1.741962	3.072591	4.814552	0	0	0
	0.25	1.741308	3.074547	4.815855	-0.078062	-0.511654	-0.589716
	0.5	1.739544	3.080764	4.820308	-0.152449	-1.014452	-1.166901
1.2	0	1.727171	2.894547	4.621718	0.000123	0.000002	0.000126
	0.25	1.726966	2.897375	4.624341	-0.104275	-0.531909	-0.636184
	0.5	1.726495	2.906014	4.632509	-0.201513	-1.050341	-1.251854
1.4	0	1.705116	2.763292	4.468408	0.000178	-0.000038	0.000140
	0.25	1.708434	2.769972	4.478406	-0.124477	-0.542765	-0.667242

Table A.3 Drag and Lift Coefficients for Re=5,Pr=10

n	Ri	Drag coefficients			Lift cpefficients		
		C_{Df}	C_{Dp}	C_D	C_{Lf}	C_{Lp}	C_L
0.6	0	1.721829	3.654871	5.376700	-0.000402	0.000010	-0.000392
	0.25	1.721505	3.656266	5.377771	0.006428	-0.368213	-0.361785
	0.5	1.722018	3.668091	5.390109	0.014261	-0.727071	-0.712810
0.8	0	1.744536	3.316604	5.061140	-0.000179	0.000017	-0.000163
	0.25	1.744663	3.321795	5.066458	-0.021062	-0.399750	-0.420812
	0.5	1.745089	3.338840	5.083929	-0.039320	-0.787337	-0.826657
1.0	0	1.741936	3.072694	4.81463	-0.000004	0.000003	-0.000001
	0.25	1.742663	3.080023	4.822687	-0.049662	-0.429503	-0.479164
	0.5	1.744667	3.101571	4.846238	-0.092721	-0.841915	-0.934636
1.2	0	1.727155	2.894444	4.621599	-0.000660	-0.002319	-0.002979
	0.25	1.728724	2.903650	4.632374	-0.075834	-0.453901	-0.529735
	0.5	1.732071	2.927896	4.659967	-0.139847	-0.882390	-1.022238
1.4	0	1.705423	2.763652	4.469075	-0.000249	-0.000501	-0.000750
	0.25	1.706954	2.772434	4.479388	-0.097890	-0.471885	-0.569774
	0.5	1.712277	2.798483	4.510760	-0.183768	-0.918484	-1.102252

Table A.4 Drag and Lift Coefficients for Re=10,Pr=1

n	Ri	Drag coefficients			Lift cpefficients		
		C_{Df}	C_{Dp}	C_D	C_{Lf}	C_{Lp}	C_L
0.5	0	0.865628	2.568036	3.433664	-0.000043	0.000074	0.000031
	0.25	0.862119	2.550601	3.412720	-0.036409	-0.659462	-0.695870
	0.5	0.849422	2.499707	3.349129	-0.074156	-1.315593	-1.389749
0.6	0	0.914541	2.486221	3.400763	-0.000029	0.000051	0.000022
	0.25	0.909510	2.470331	3.379841	-0.047261	-0.660289	-0.707550
	0.5	0.894823	2.428770	3.323593	-0.097733	-1.316116	-1.413849
0.8	0	0.992688	2.361123	3.353810	-0.000006	0.000007	0.000000
	0.25	0.987165	2.348090	3.335255	-0.071960	-0.659441	-0.731400
	0.5	0.971080	2.314334	3.285414	-0.143087	-1.309857	-1.452944
1.0	0	1.048050	2.271030	3.319080	0.000000	0.000000	0.000000
	0.25	1.041769	2.259962	3.301731	-0.095468	-0.662220	-0.757688
	0.5	1.023844	2.228607	3.252452	-0.188399	-1.315742	-1.504141
1.2	0	1.087614	2.209380	3.296994	-0.000337	-0.000358	-0.000695
	0.25	1.081638	2.199282	3.280919	-0.115152	-0.661179	-0.776331
	0.5	1.064009	2.170608	3.234617	-0.226567	-1.311382	-1.537950
1.4	0	1.114982	2.166402	3.281384	0.000022	0.000046	0.000068
	0.25	0.954917	2.157542	3.112459	-0.096556	-0.656255	-0.752811
	0.5	0.941010	2.130321	3.071332	-0.191908	-1.305498	-1.497406

Table A.5 Drag and Lift Coefficients for Re=10,Pr=5

n	Ri	Drag coefficients			Lift cpefficients		
		C_{Df}	C_{Dp}	C_D	C_{Lf}	C_{Lp}	C_L
0.5	0	0.865648	2.568087	3.433735	-0.000043	0.000074	0.000031
	0.25	0.864853	2.568850	3.433703	-0.005154	-0.500640	-0.505794
	0.5	0.863052	2.569569	3.432621	-0.014482	-0.998647	-1.013129
0.6	0	0.914519	2.486162	3.400681	-0.000028	0.000051	0.000023
	0.25	0.913490	2.488465	3.401955	-0.015439	-0.507588	-0.523027
	0.5	0.910997	2.491670	3.402667	-0.033785	-1.008551	-1.042336
0.8	0	0.992654	2.361050	3.353704	-0.000006	0.000007	0.000000
	0.25	0.991644	2.363290	3.354933	-0.038242	-0.519847	-0.558089
	0.5	0.989036	2.371400	3.360437	-0.074180	-1.024652	-1.098832
1.0	0	1.048112	2.271338	3.319450	0.000003	0.000014	0.000017
	0.25	1.047030	2.274372	3.321403	-0.060509	-0.531898	-0.592407
	0.5	1.044492	2.284966	3.329458	-0.114920	-1.044298	-1.159218
1.2	0	1.087422	2.209067	3.296489	0.000009	0.000018	0.000027
	0.25	1.086832	2.213177	3.300009	-0.079029	-0.539186	-0.618215
	0.5	1.086305	2.229688	3.315993	-0.140373	-1.030953	-1.171327
1.4	0	1.115251	2.166727	3.281977	0.000042	0.000051	0.000093
	0.25	1.114960	2.170837	3.285796	-0.095132	-0.542848	-0.637980
	0.5	1.115376	2.185345	3.300721	-0.181105	-1.057864	-1.238969

Table A.6 Drag and Lift Coefficients for Re=10,Pr=10

n	Ri	Drag coefficients			Lift coefficients		
		C_{Df}	C_{Dp}	C_D	C_{Lf}	C_{Lp}	C_L
0.5	0	0.865626	2.568029	3.433655	-0.000043	0.000074	0.000031
	0.25	0.864797	2.571578	3.436375	0.009327	-0.431657	-0.422330
	0.5	0.865058	2.588526	3.453584	0.011047	-0.856724	-0.845677
0.6	0	0.914541	2.486222	3.400763	-0.000029	0.000051	0.000022
	0.25	0.914324	2.493990	3.408314	-0.002260	-0.442008	-0.444268
	0.5	0.913878	2.510731	3.424609	-0.005668	-0.865633	-0.871301
0.8	0	0.992689	2.361122	3.353811	-0.000006	0.000006	0.000000
	0.25	0.992629	2.368780	3.361409	-0.023729	-0.456340	-0.480070
	0.5	0.992533	2.390214	3.382747	-0.041387	-0.880888	-0.922275
1.0	0	1.048050	2.271030	3.319080	0.000000	0.000000	0.000000
	0.25	1.048263	2.280128	3.328391	-0.045086	-0.470435	-0.515522
	0.5	1.048702	2.304311	3.353013	-0.077730	-0.897789	-0.975518
1.2	0	1.088180	2.210277	3.298457	0.000009	0.000017	0.000026
	0.25	1.088495	2.219549	3.308043	-0.062978	-0.479852	-0.542830
	0.5	1.090111	2.243960	3.334071	-0.109915	-0.920732	-1.030647
1.4	0	1.115307	2.166774	3.282081	0.000031	0.000045	0.000076
	0.25	1.116421	2.176702	3.293124	-0.078567	-0.485286	-0.563853
	0.5	1.120102	2.204828	3.324930	-0.137272	-0.909056	-1.046328

Table A.7 Drag and Lift Coefficients for Re=40,Pr=1

n	Ri	Drag coefficients			Lift cpefficients		
		C_{Df}	C_{Dp}	C_D	C_{Lf}	C_{Lp}	C_L
0.5	0	0.161561	1.622510	1.784071	0.000073	-0.000096	-0.000023
	0.25	0.160010	1.619992	1.780002	0.005266	-0.561071	-0.555805
	0.5	0.154636	1.620797	1.775433	0.012822	-1.080668	-1.067846
0.6	0	0.189499	1.611281	1.800779	0.000062	-0.000081	-0.000019
	0.25	0.187732	1.610161	1.797892	-0.000684	-0.574545	-0.575228
	0.5	0.182237	1.611050	1.793287	0.001579	-1.111278	-1.109698
0.8	0	0.248199	1.597942	1.846141	0.000038	-0.000042	-0.000004
	0.25	0.245832	1.597190	1.843022	-0.012655	-0.586757	-0.599412
	0.5	0.239034	1.598184	1.837218	-0.021279	-1.137287	-1.158567
1.0	0	0.307552	1.591718	1.899269	0.000000	0.000001	0.000001
	0.25	0.304756	1.591196	1.895952	-0.025522	-0.588285	-0.613807
	0.5	0.297015	1.591614	1.888629	-0.046120	-1.142359	-1.188479
1.2	0	0.363798	1.589467	1.953265	-0.000044	0.000049	0.000005
	0.25	0.360753	1.588870	1.949623	-0.039254	-0.585181	-0.624434
	0.5	0.352447	1.588564	1.941012	-0.072546	-1.137077	-1.209623
1.4	0	0.414343	1.590429	2.004772	-0.000076	0.000105	0.000029
	0.25	0.411177	1.589823	2.000999	-0.053433	-0.581017	-0.634450
	0.5	0.403175	1.590238	1.993414	-0.099539	-1.128651	-1.228189

Table A.8 Drag and Lift Coefficients for Re=40,Pr=5

n	Ri	Drag coefficients			Lift cpefficients		
		C_{Df}	C_{Dp}	C_D	C_{Lf}	C_{Lp}	C_L
0.5	0	0.161563	1.622530	1.784093	0.000073	-0.000096	-0.000023
	0.25	0.160730	1.626076	1.786806	0.008025	-0.477563	-0.469538
	0.5	0.158615	1.641227	1.799842	0.019306	-0.905142	-0.885836
0.6	0	0.189496	1.611246	1.800743	0.000061	-0.000073	-0.000012
	0.25	0.188723	1.615662	1.804385	0.002377	-0.487474	-0.485097
	0.5	0.186380	1.629818	1.816198	0.008974	-0.922436	-0.913462
0.8	0	0.248114	1.597554	1.845668	0.000039	-0.000044	-0.000005
	0.25	0.247272	1.601939	1.849211	-0.008051	-0.489751	-0.497802
	0.5	0.244815	1.615166	1.859981	-0.010683	-0.931878	-0.942560
1.0	0	0.307513	1.591567	1.899080	0.000000	0.000000	0.000000
	0.25	0.306533	1.595221	1.901754	-0.018655	-0.483646	-0.502302
	0.5	0.304228	1.607247	1.911475	-0.030745	-0.923210	-0.953955
1.2	0	0.363755	1.589327	1.953082	-0.000047	0.000041	-0.000006
	0.25	0.362762	1.592532	1.955294	-0.029415	-0.473448	-0.502864
	0.5	0.360853	1.603470	1.964323	-0.051159	-0.905513	-0.956672
1.4	0	0.414293	1.590296	2.004589	-0.000078	0.000098	0.000020
	0.25	0.413354	1.593260	2.006614	-0.040184	-0.462746	-0.502931
	0.5	0.411940	1.603559	2.015500	-0.071386	-0.885125	-0.956512

Table A.9 Drag and Lift Coefficients for Re=40,Pr=10

n	Ri	Drag coefficients			Lift cpefficients		
		C_{Df}	C_{Dp}	C_D	C_{Lf}	C_{Lp}	C_L
0.5	0	0.161546	1.622375	1.783921	0.000072	-0.000103	-0.000031
	0.25	0.161193	1.627103	1.788296	0.006745	-0.439145	-0.432400
	0.5	0.159786	1.642638	1.802424	0.021683	-0.816329	-0.794646
0.6	0	0.189499	1.611282	1.800781	0.000062	-0.000081	-0.000019
	0.25	0.189051	1.615109	1.804160	0.001167	-0.444278	-0.443111
	0.5	0.187932	1.629339	1.817271	0.010282	-0.827961	-0.817679
0.8	0	0.248116	1.597562	1.845678	0.000039	-0.000045	-0.000007
	0.25	0.247690	1.601597	1.849288	-0.008973	-0.445356	-0.454329
	0.5	0.246958	1.613341	1.860299	-0.009444	-0.835789	-0.845233
1.0	0	0.307552	1.591718	1.899269	0.000000	0.000001	0.000001
	0.25	0.306942	1.594885	1.901827	-0.018760	-0.437891	-0.456651
	0.5	0.306694	1.605159	1.911854	-0.029737	-0.829793	-0.859530
1.2	0	0.363798	1.589466	1.953265	-0.000044	0.000049	0.000005
	0.25	0.363175	1.592276	1.955451	-0.028532	-0.427208	-0.455739
	0.5	0.363267	1.601630	1.964897	-0.049072	-0.810666	-0.859738
1.4	0	0.414343	1.590429	2.004772	-0.000076	0.000105	0.000028
	0.25	0.413739	1.593031	2.006770	-0.038064	-0.415516	-0.453580
	0.5	0.414068	1.602156	2.016224	-0.066794	-0.785940	-0.852734

Confined Flow Results:

Table A.10 Drag and Lift Coefficients for Re=5,Pr=1

n	Ri	Drag coefficients			Lift cpefficients		
		C_{Df}	C_{Dp}	C_D	C_{Lf}	C_{Lp}	C_L
0.6	0	1.712913	3.660474	5.373388	-0.000405	0.000062	-0.000343
	0.25	1.719600	3.664104	5.383703	-0.078340	-0.646146	-0.724486
	0.5	1.716818	3.658121	5.374939	-0.159056	-1.326908	-1.485964
0.8	0	1.690249	3.227534	4.917783	-0.000191	0.000015	-0.000176
	0.25	1.691403	3.231255	4.922657	-0.117388	-0.683805	-0.801193
	0.5	1.695492	3.244537	4.940029	-0.229438	-1.358329	-1.587767
1.0	0	1.622974	2.881368	4.504342	0.000000	0.000000	0.000000
	0.25	1.627254	2.889832	4.517086	-0.149625	-0.692835	-0.842461
	0.5	1.639400	2.913632	4.553032	-0.291602	-1.371396	-1.662998
1.2	0	1.544856	2.619905	4.164761	-0.000133	-0.000507	-0.000640
	0.25	1.548500	2.627506	4.176006	-0.174742	-0.696975	-0.871717
	0.5	1.575508	2.667521	4.243029	-0.342572	-1.375114	-1.717686
1.4	0	1.467113	2.42387	3.890982	0.000176	-0.000068	0.000108
	0.25	1.46631	2.425072	3.891382	-0.199118	-0.698947	-0.898064
	0.5	1.494207	2.459918	3.954125	-0.38585	-1.376297	-1.762147

Table A.11 Drag and Lift Coefficients for Re=5,Pr=5

n	Ri	Drag coefficients			Lift coefficients		
		C_{Df}	C_{Dp}	C_D	C_{Lf}	C_{Lp}	C_L
0.6	0	1.712696	3.660035	5.372731	-0.000411	0.000042	-0.000370
	0.25	1.714532	3.664421	5.378953	-0.016726	-0.449764	-0.466491
	0.5	1.720767	3.689092	5.409859	-0.017956	-0.854716	-0.872671
0.8	0	1.690253	3.227537	4.917789	-0.000192	0.000015	-0.000177
	0.25	1.692355	3.236096	4.928451	-0.045423	-0.476164	-0.521586
	0.5	1.698409	3.262906	4.961315	-0.087027	-0.940878	-1.027905
1.0	0	1.622974	2.881365	4.504339	0.000000	-0.000001	-0.000001
	0.25	1.625409	2.890713	4.516122	-0.077644	-0.504483	-0.582126
	0.5	1.635910	2.924103	4.560012	-0.146316	-0.989104	-1.135420
1.2	0	1.544827	2.619944	4.164771	-0.000129	-0.000447	-0.000576
	0.25	1.550928	2.635098	4.186026	-0.102392	-0.520091	-0.622483
	0.5	1.572895	2.686073	4.258968	-0.186057	-1.004570	-1.190627
1.4	0	1.461752	2.418282	3.880035	-0.000105	-0.000401	-0.000506
	0.25	1.46926	2.435562	3.904822	-0.122099	-0.530907	-0.653006
	0.5	1.488764	2.477055	3.965819	-0.242701	-1.054735	-1.297437

Table A.12 Drag and Lift Coefficients for Re=5,Pr=10

n	Ri	Drag coefficients			Lift coefficients		
		C_{Df}	C_{Dp}	C_D	C_{Lf}	C_{Lp}	C_L
0.6	0	1.712913	3.660464	5.373377	-0.000404	0.000060	-0.000344
	0.25	1.714125	3.666386	5.380511	0.008477	-0.361956	-0.353479
	0.5	1.719132	3.692389	5.411521	0.018438	-0.713186	-0.694747
0.8	0	1.690249	3.227534	4.917783	-0.000191	0.000015	-0.000176
	0.25	1.692254	3.238325	4.93058	-0.016859	-0.387975	-0.404834
	0.5	1.69741	3.269917	4.967327	-0.030096	-0.761805	-0.7919
1.0	0	1.622708	2.880959	4.503667	0.000000	0.000000	0.000000
	0.25	1.626170	2.895193	4.521363	-0.046388	-0.417290	-0.463678
	0.5	1.635158	2.934375	4.569533	-0.083031	-0.810465	-0.893496
1.2	0	1.544859	2.619955	4.164814	-0.000186	-0.000582	-0.000768
	0.25	1.550194	2.637936	4.188130	-0.071848	-0.438916	-0.510764
	0.5	1.565987	2.688791	4.254778	-0.125046	-0.839451	-0.964497
1.4	0	1.461917	2.418461	3.880378	-0.000132	-0.000455	-0.000587
	0.25	1.469313	2.438793	3.908107	-0.096117	-0.460787	-0.556904
	0.5	1.491159	2.496695	3.987854	-0.167935	-0.873227	-1.041162

Table A.13 Drag and Lift Coefficients for Re=10,Pr=1

n	Ri	Drag coefficients			Lift cpefficients		
		C_{Df}	C_{Dp}	C_D	C_{Lf}	C_{Lp}	C_L
0.5	0	0.861119	2.554969	3.416088	-0.000050	0.000061	0.000011
	0.25	0.861327	2.547916	3.409243	-0.036615	-0.660191	-0.696806
	0.5	0.852875	2.536977	3.389852	-0.082278	-1.346775	-1.429053
0.6	0	0.901465	2.443558	3.345023	-0.000030	0.000050	0.000019
	0.25	0.900501	2.445807	3.346308	-0.049571	-0.664777	-0.714348
	0.5	0.897322	2.448797	3.346120	-0.101686	-1.326803	-1.428490
0.8	0	0.951133	2.251957	3.203091	-0.000013	0.000008	-0.000005
	0.25	0.951746	2.256323	3.208069	-0.074986	-0.660048	-0.735034
	0.5	0.951874	2.268584	3.220458	-0.147171	-1.310769	-1.457940
1.0	0	0.967340	2.095329	3.062669	-0.000001	-0.000001	-0.000001
	0.25	0.969331	2.102956	3.072287	-0.099907	-0.663572	-0.763480
	0.5	0.974415	2.123202	3.097617	-0.193219	-1.311190	-1.504409
1.2	0	0.963488	1.974208	2.937696	0.000015	0.000016	0.000031
	0.25	0.967839	1.983925	2.951763	-0.120740	-0.662837	-0.783577
	0.5	0.980256	2.012151	2.992407	-0.233009	-1.306017	-1.539027
1.4	0	0.953846	1.888964	2.842810	0.001032	0.000620	0.001652
	0.25	0.952415	1.889191	2.841607	-0.140665	-0.664043	-0.804708
	0.5	0.981461	1.938494	2.919954	-0.264498	-1.293535	-1.558032

Table A.14 Drag and Lift Coefficients for Re=10,Pr=5

n	Ri	Drag coefficients			Lift cpefficients		
		C_{Df}	C_{Dp}	C_D	C_{Lf}	C_{Lp}	C_L
0.5	0	0.860788	2.554219	3.415007	-0.000044	0.000032	-0.000012
	0.5	0.861201	2.590813	3.452015	-0.020079	-1.023663	-1.043741
0.6	0	0.879494	2.443477	3.322971	0.000000	0.000051	0.000051
	0.25	0.901895	2.452764	3.354658	-0.015321	-0.505589	-0.520911
	0.5	0.903301	2.474052	3.377352	-0.033207	-1.004296	-1.037502
0.8	0	0.951082	2.251840	3.202922	-0.000011	0.000008	-0.000003
	0.25	0.952906	2.262957	3.215863	-0.038092	-0.515157	-0.553249
	0.5	0.956082	2.289301	3.245383	-0.072141	-1.010197	-1.082337
1.0	0	0.967271	2.095200	3.062471	-0.000002	-0.000005	-0.000007
	0.25	0.969183	2.106187	3.075371	-0.061881	-0.529461	-0.591342
	0.5	0.975934	2.140461	3.116395	-0.113346	-1.028210	-1.141556
1.2	0	0.963395	1.974050	2.937445	0.000014	0.000016	0.000030
	0.25	0.966689	1.986568	2.953257	-0.082294	-0.539756	-0.622049
	0.5	0.971444	2.014148	2.985592	-0.154628	-1.049265	-1.203892
1.4	0	0.950912	1.884631	2.835544	-0.000193	-0.001336	-0.001529
	0.25	0.955021	1.898968	2.853989	-0.098605	-0.544224	-0.642829
	0.5	0.970676	1.942565	2.913242	-0.181443	-1.043440	-1.224883

Table A.15 Drag and Lift Coefficients for Re=10,Pr=10

n	Ri	Drag coefficients			Lift cpefficients		
		C_{Df}	C_{Dp}	C_D	C_{Lf}	C_{Lp}	C_L
0.5	0	0.861127	2.554965	3.416092	-0.000049	0.000059	0.000011
	0.5	0.863218	2.591108	3.454326	0.012092	-0.853933	-0.841841
0.6	0	0.901466	2.443570	3.345036	-0.000030	0.000048	0.000019
	0.25	0.902179	2.456124	3.358302	-0.001265	-0.437419	-0.438685
	0.5	0.904225	2.484980	3.389205	-0.003238	-0.855602	-0.858840
0.8	0	0.951133	2.251957	3.203091	-0.000013	0.000008	-0.000004
	0.25	0.952613	2.265055	3.217669	-0.022304	-0.448839	-0.471144
	0.5	0.956538	2.300286	3.256824	-0.036865	-0.860630	-0.897495
1.0	0	0.967343	2.095337	3.062679	-0.000002	-0.000006	-0.000008
	0.25	0.969851	2.111071	3.080922	-0.044356	-0.463864	-0.50822
	0.5	0.976254	2.151884	3.128138	-0.072602	-0.874174	-0.946775
1.2	0	0.963485	1.974201	2.937686	0.000014	0.000015	0.000029
	0.25	0.967531	1.992099	2.959630	-0.063808	-0.476173	-0.539981
	0.5	0.977131	2.036949	3.014081	-0.105000	-0.883121	-0.988121
1.4	0	0.951162	1.884956	2.836118	-0.000060	-0.001188	-0.001248
	0.25	0.958363	1.907071	2.865434	-0.078713	-0.481503	-0.560216
	0.5	0.973678	1.959868	2.933547	-0.128869	-0.877437	-1.006306

Table A.16 Drag and Lift Coefficients for Re=40,Pr=1

n	Ri	Drag coefficients			Lift cpefficients		
		C_{Df}	C_{Dp}	C_D	C_{Lf}	C_{Lp}	C_L
0.5	0	0.158592	1.567557	1.726149	0.000073	-0.00009	-0.000017
	0.25	0.15815	1.577846	1.735996	0.005607	-0.555421	-0.549814
	0.5	0.156694	1.608947	1.765641	0.011807	-1.084126	-1.072319
0.6	0	0.184088	1.53857	1.722658	0.000007	-0.000117	-0.00011
	0.25	0.184035	1.551867	1.735901	-0.000186	-0.567234	-0.567421
	0.5	0.183271	1.586016	1.769287	0.001081	-1.108869	-1.107788
0.8	0	0.233727	1.486053	1.719779	0.000037	-0.000041	-0.000005
	0.25	0.234415	1.502656	1.737071	-0.012091	-0.577901	-0.589992
	0.5	0.235435	1.543709	1.779143	-0.021275	-1.130388	-1.151663
1.0	0	0.279451	1.445105	1.724556	-0.000055	-0.00028	-0.000335
	0.25	0.281916	1.466411	1.748327	-0.024267	-0.576886	-0.601153
	0.5	0.286211	1.513848	1.800059	-0.044863	-1.131101	-1.175964
1.2	0	0.317137	1.408123	1.72526	-0.00003	0.000092	0.000063
	0.25	0.322625	1.435754	1.758379	-0.037048	-0.572152	-0.6092
	0.5	0.331545	1.489572	1.821117	-0.069475	-1.122888	-1.192363
1.4	0	0.347283	1.380491	1.727774	-0.000114	-0.000122	-0.000236
	0.25	0.355466	1.411413	1.766879	-0.049893	-0.566668	-0.616561
	0.5	0.369885	1.47114	1.841025	-0.094031	-1.111808	-1.205839

Table A.17 Drag and Lift Coefficients for Re=40,Pr=5

n	Ri	Drag coefficients			Lift cpefficients		
		C_{Df}	C_{Dp}	C_D	C_{Lf}	C_{Lp}	C_L
0.5	0	0.158624	1.567899	1.726523	0.000073	-0.000091	-0.000017
	0.25	0.15872	1.58053	1.73925	0.008024	-0.47786	-0.469836
	0.5	0.158425	1.611755	1.77018	0.019087	-0.90756	-0.888473
0.6	0	0.183985	1.537757	1.721741	0.000061	-0.000083	-0.000022
	0.25	0.184293	1.550914	1.735207	0.002682	-0.483991	-0.481309
	0.5	0.184411	1.582966	1.767377	0.00922	-0.919743	-0.910522
0.8	0	0.233779	1.486345	1.720125	0.000035	-0.000044	-0.000009
	0.25	0.234859	1.501459	1.736318	-0.007454	-0.484426	-0.49188
	0.5	0.236893	1.537376	1.774269	-0.009428	-0.922604	-0.932032
1.0	0	0.279732	1.446209	1.725941	-0.000018	-0.00005	-0.000067
	0.25	0.281472	1.461419	1.742891	-0.017487	-0.475974	-0.49346
	0.5	0.286035	1.500394	1.786429	-0.027953	-0.908692	-0.936645
1.2	0	0.31722	1.408391	1.725611	-0.000036	0.00004	0.000004
	0.25	0.321059	1.427991	1.74905	-0.027482	-0.463943	-0.491425
	0.5	0.328955	1.470212	1.799166	-0.046065	-0.885237	-0.931302
1.4	0	0.346832	1.379261	1.726092	-0.000041	0.000151	0.00011
	0.25	0.352519	1.401288	1.753807	-0.037119	-0.45104	-0.488159
	0.5	0.364381	1.447169	1.81155	-0.063452	-0.860204	-0.923656

Table A.18 Drag and Lift Coefficients for Re=40,Pr=10

n	Ri	Drag coefficients			Lift cpefficients		
		C_{Df}	C_{Dp}	C_D	C_{Lf}	C_{Lp}	C_L
0.5	0	0.158591	1.567557	1.726149	0.000073	-0.00009	-0.000017
	0.25	0.158723	1.577377	1.7361	0.006949	-0.437385	-0.430436
	0.5	0.158438	1.602823	1.76126	0.021558	-0.810484	-0.788926
0.6	0	0.183945	1.537428	1.721373	0.000064	-0.000062	0.000002
	0.25	0.184391	1.548365	1.732756	0.001454	-0.443227	-0.441774
	0.5	0.184796	1.574459	1.759255	0.011709	-0.819543	-0.807834
0.8	0	0.233726	1.486051	1.719777	0.000037	-0.000041	-0.000005
	0.25	0.234683	1.497841	1.732525	-0.008479	-0.44142	-0.449898
	0.5	0.237489	1.527338	1.764827	-0.005845	-0.819704	-0.825549
1.0	0	0.279792	1.446461	1.726253	-0.00003	-0.000112	-0.000142
	0.25	0.280911	1.457148	1.73806	-0.017801	-0.431363	-0.449164
	0.5	0.286276	1.487878	1.774155	-0.022977	-0.804591	-0.827568
1.2	0	0.317136	1.408122	1.725259	-0.00003	0.000092	0.000063
	0.25	0.320077	1.423237	1.743314	-0.026789	-0.417948	-0.444737
	0.5	0.328693	1.455213	1.783906	-0.039564	-0.781731	-0.821295
1.4	0	0.346756	1.379055	1.725811	-0.00005	0.000169	0.00012
	0.25	0.350942	1.39583	1.746772	-0.035243	-0.403326	-0.43857
	0.5	0.363153	1.429083	1.792236	-0.05585	-0.759205	-0.815055

Heat Transfer Results for Unconfined flow:

Table A.19 Nusselt number for Re=5,Pr=1

n	Ri	Nusselt Number				
		$\langle Nu \rangle_f$	$\langle Nu \rangle_r$	$\langle Nu \rangle_t$	$\langle Nu \rangle_b$	$\langle Nu \rangle_m$
0.6	0	2.027034	0.764346	1.467677	1.467696	1.431688
	0.25	2.025798	0.764463	1.488115	1.444205	1.430645
	0.5	2.022800	0.765001	1.501581	1.423469	1.428213
0.8	0	1.971496	0.759858	1.416771	1.416774	1.391225
	0.25	1.971835	0.760033	1.437331	1.395110	1.391077
	0.5	1.974205	0.760602	1.455133	1.374627	1.391142
1.0	0	1.929519	0.757234	1.383331	1.383219	1.363326
	0.25	1.930594	0.757396	1.40399	1.362358	1.363585
	0.5	1.933811	0.757858	1.424006	1.341898	1.364393
1.2	0	1.896969	0.755750	1.359821	1.359814	1.343088
	0.25	1.897942	0.755768	1.380618	1.339021	1.343337
	0.5	1.900582	0.756213	1.401024	1.318931	1.344188
1.4	0	1.871809	0.756161	1.343763	1.343757	1.328873
	0.25	1.871753	0.754895	1.362947	1.322138	1.327933
	0.5	1.873702	0.755429	1.383766	1.302406	1.328826

Table A.20 Nusselt number for Re=5,Pr=5

n	Ri	Nusselt Number				
		$\langle Nu \rangle_f$	$\langle Nu \rangle_r$	$\langle Nu \rangle_t$	$\langle Nu \rangle_b$	$\langle Nu \rangle_m$
0.6	0	3.490556	1.020434	2.578541	2.578675	2.417051
	0.25	3.491167	1.022736	2.599693	2.557034	2.417658
	0.5	3.495179	1.030184	2.618272	2.538877	2.420628
0.8	0	3.386450	0.998354	2.426630	2.426640	2.309519
	0.25	3.388220	1.000752	2.447930	2.406186	2.310772
	0.5	3.393630	1.008293	2.468230	2.388592	2.314686
1.0	0	3.302595	0.981023	2.327843	2.327843	2.234826
	0.25	3.304571	0.983751	2.350186	2.307174	2.236421
	0.5	3.310331	0.992	2.373136	2.289139	2.241152
1.2	0	3.235016	0.967261	2.258979	2.258976	2.180058
	0.25	3.236754	0.970516	2.282733	2.237491	2.181874
	0.5	3.241674	0.980454	2.307344	2.219402	2.187218
1.4	0	3.180163	0.956581	2.208205	2.208208	2.138289
	0.25	3.182360	0.961260	2.234314	2.187232	2.141291

Table A.21 Nusselt number for Re=5,Pr=10

n	Ri	Nusselt Number				
		$\langle Nu \rangle_f$	$\langle Nu \rangle_r$	$\langle Nu \rangle_t$	$\langle Nu \rangle_b$	$\langle Nu \rangle_m$
0.6	0	4.343875	1.165773	3.289562	3.289664	3.022218
	0.25	4.344415	1.170995	3.306314	3.272403	3.023532
	0.5	4.348432	1.187789	3.321235	3.259334	3.029198
0.8	0	4.226465	1.132207	3.064390	3.064413	2.871869
	0.25	4.228257	1.138604	3.082016	3.048282	2.874290
	0.5	4.233469	1.158472	3.099533	3.035066	2.881635
1.0	0	4.127441	1.104005	2.91961	2.919622	2.76767
	0.25	4.12936	1.112285	2.939398	2.902253	2.770824
	0.5	4.13473	1.136497	2.960189	2.88823	2.779912
1.2	0	4.045570	1.080589	2.818906	2.820118	2.691296
	0.25	4.047405	1.091234	2.841862	2.800672	2.695293
	0.5	4.051931	1.121664	2.865430	2.785712	2.706184
1.4	0	3.978474	1.062144	2.746611	2.745872	2.633275
	0.25	3.979797	1.074809	2.771251	2.724970	2.637707
	0.5	3.983540	1.110159	2.797507	2.709722	2.650232

Table A.22 Nusselt number for Re=10,Pr=1

n	Ri	Nusselt Number				
		$\langle Nu \rangle_f$	$\langle Nu \rangle_r$	$\langle Nu \rangle_t$	$\langle Nu \rangle_b$	$\langle Nu \rangle_m$
0.5	0	2.846323	0.854129	1.975741	1.975811	1.913001
	0.25	2.845955	0.854580	2.026166	1.922554	1.912314
	0.5	2.844670	0.854629	2.063728	1.869661	1.908172
0.6	0	2.797181	0.849853	1.927133	1.927174	1.875335
	0.25	2.797406	0.849962	1.973952	1.876730	1.874513
	0.5	2.798579	0.850309	2.009754	1.827680	1.871580
0.8	0	2.716869	0.858731	1.854899	1.854915	1.821354
	0.25	2.717490	0.843464	1.895696	1.810205	1.816714
	0.5	2.721465	0.844395	1.932013	1.767101	1.816243
1.0	0	2.650268	0.838934	1.801667	1.801667	1.773134
	0.25	2.651681	0.839269	1.839872	1.761997	1.773205
	0.5	2.656001	0.840537	1.875117	1.722890	1.773636
1.2	0	2.593041	0.836149	1.761824	1.761651	1.738166
	0.25	2.594165	0.836734	1.798592	1.724349	1.738460
	0.5	2.597028	0.838409	1.831750	1.689181	1.739092
1.4	0	2.543866	0.834251	1.730134	1.730096	1.709587
	0.25	2.544511	0.835097	1.764678	1.695747	1.710009
	0.5	2.546202	0.837332	1.797718	1.662403	1.710914

Table A.23 Nusselt number for Re=10,Pr=5

n	Ri	Nusselt Number				
		$\langle Nu \rangle_f$	$\langle Nu \rangle_r$	$\langle Nu \rangle_t$	$\langle Nu \rangle_b$	$\langle Nu \rangle_m$
0.5	0	4.991705	1.116785	3.508566	3.508835	3.281973
	0.25	4.994121	1.118149	3.572771	3.445373	3.282604
	0.5	5.003566	1.135696	3.632160	3.389766	3.290297
0.6	0	4.889170	1.104998	3.380096	3.380269	3.188633
	0.25	4.892246	1.104654	3.438320	3.322512	3.189433
	0.5	4.901432	1.124655	3.492083	3.271782	3.197488
0.8	0	4.730401	1.081176	3.189203	3.189254	3.047509
	0.25	4.732968	1.082559	3.239651	3.140272	3.048862
	0.5	4.741223	1.107699	3.287731	3.097283	3.058484
1.0	0	4.599546	1.064029	3.053011	3.052979	2.942391
	0.25	4.602254	1.066775	3.099290	3.009309	2.944407
	0.5	4.610078	1.098346	3.145386	2.971520	2.956332
1.2	0	4.484361	1.044048	2.950899	2.950886	2.857549
	0.25	4.486195	1.057160	2.995235	2.910314	2.862226
	0.5	4.490681	1.103302	3.032970	2.883530	2.877621
1.4	0	4.384811	1.048396	2.872070	2.872061	2.794335
	0.25	4.385760	1.053099	2.915286	2.833155	2.796825
	0.5	4.388990	1.097575	2.959789	2.802749	2.812276

Table A.24 Nusselt number for Re=10,Pr=10

n	Ri	Nusselt Number				
		$\langle Nu \rangle_f$	$\langle Nu \rangle_r$	$\langle Nu \rangle_t$	$\langle Nu \rangle_b$	$\langle Nu \rangle_m$
0.5	0	6.307561	1.250539	4.472643	4.473043	4.125947
	0.25	6.309175	1.263826	4.556883	4.388176	4.129515
	0.5	6.318592	1.308999	4.600352	4.356224	4.146042
0.6	0	6.172275	1.231125	4.290125	4.290384	3.995977
	0.25	6.175537	1.246250	4.350202	4.233008	4.001249
	0.5	6.184494	1.300970	4.406253	4.184979	4.019174
0.8	0	5.970093	1.194891	4.020096	4.020182	3.801316
	0.25	5.972680	1.219634	4.072202	3.971661	3.809044
	0.5	5.980380	1.291766	4.121971	3.931882	3.831500
1.0	0	5.805467	1.168332	3.828413	3.828413	3.657656
	0.25	5.808210	1.202770	3.876944	3.784880	3.668201
	0.5	5.815091	1.293482	3.923955	3.750541	3.695767
1.2	0	5.659482	1.154717	3.686659	3.686637	3.546874
	0.25	5.661044	1.196771	3.733094	3.645520	3.559107
	0.5	5.665304	1.304450	3.778989	3.614698	3.590860
1.4	0	5.531826	1.153347	3.576451	3.576438	3.459516
	0.25	5.532652	1.201728	3.623770	3.536355	3.473626
	0.5	5.535205	1.322320	3.668768	3.510307	3.509150

Table A.25 Nusselt number for Re=40,Pr=1

n	Ri	Nusselt Number				
		$<Nu>_f$	$<Nu>_r$	$<Nu>_t$	$<Nu>_b$	$<Nu>_m$
0.5	0	5.572744	1.059983	3.114282	3.114470	3.215370
	0.25	5.565161	1.068742	3.295917	2.925098	3.213730
	0.5	5.547824	1.157310	3.459267	2.742147	3.226637
0.6	0	5.493294	1.041855	3.089261	3.089430	3.178460
	0.25	5.488082	1.067890	3.257098	2.916227	3.182324
	0.5	5.475785	1.152716	3.407965	2.749907	3.196593
0.8	0	5.332804	1.047674	3.029917	3.030013	3.110102
	0.25	5.329990	1.074535	3.171568	2.883952	3.115011
	0.5	5.322965	1.155654	3.300362	2.743146	3.130531
1.0	0	5.176872	1.057278	2.965715	2.965715	3.041395
	0.25	5.174977	1.085026	3.086150	2.842307	3.047115
	0.5	5.170072	1.163607	3.197018	2.724272	3.063742
1.2	0	5.029356	1.069200	2.902298	2.902224	2.975769
	0.25	5.027526	1.098064	3.006426	2.796710	2.982181
	0.5	5.022735	1.175570	3.103795	2.696742	2.999711
1.4	0	4.890971	1.082634	2.842899	2.842800	2.914826
	0.25	4.888867	1.113061	2.934886	2.750771	2.921897
	0.5	4.883245	1.190004	3.022288	2.665501	2.940259

Table A.26 Nusselt number for Re=40,Pr=5

n	Ri	Nusselt Number				
		$<Nu>_f$	$<Nu>_r$	$<Nu>_t$	$<Nu>_b$	$<Nu>_m$
0.5	0	10.232597	1.547432	5.357693	5.357869	5.623898
	0.25	10.226218	1.650917	5.650371	5.069882	5.649347
	0.5	10.212039	1.960582	5.923760	4.817133	5.728379
0.6	0	10.070095	1.621636	5.309856	5.310038	5.577906
	0.25	10.065572	1.687470	5.574998	5.055363	5.595851
	0.5	10.054367	1.955510	5.819296	4.833392	5.665641
0.8	0	9.741405	1.778049	5.179549	5.179549	5.469638
	0.25	9.738431	1.798063	5.396211	4.975770	5.477119
	0.5	9.730254	1.999066	5.595005	4.806579	5.532726
1.0	0	9.423307	1.879284	5.031702	5.031706	5.341500
	0.25	9.420092	1.908350	5.210813	4.864598	5.350963
	0.5	9.412335	2.065687	5.376323	4.733763	5.397027
1.2	0	9.123374	1.991007	4.882877	4.882797	5.220014
	0.25	9.119590	2.016289	5.036154	4.741075	5.228277
	0.5	9.110872	2.146619	5.177930	4.635885	5.267826
1.4	0	8.842224	2.096955	4.743130	4.742989	5.106324
	0.25	8.837860	2.120719	4.879133	4.617747	5.113865
	0.5	8.828182	2.234225	5.004880	4.527469	5.148689

Table A.27 Nusselt number for Re=40,Pr=10

n	Ri	Nusselt Number				
		$\langle Nu \rangle_f$	$\langle Nu \rangle_r$	$\langle Nu \rangle_t$	$\langle Nu \rangle_b$	$\langle Nu \rangle_m$
0.5	0	12.656296	2.029566	7.095910	7.095946	7.219430
	0.25	12.655125	2.159990	7.429731	6.775910	7.255189
	0.5	12.649072	2.631966	7.721638	6.500608	7.375821
0.6	0	12.486721	2.176049	7.029536	7.029549	7.180464
	0.25	12.485614	2.281269	7.321466	6.750288	7.209659
	0.5	12.482326	2.585565	7.575091	6.530058	7.293260
0.8	0	12.140311	2.496431	6.834944	6.834781	7.076617
	0.25	12.139603	2.482686	7.062342	6.624378	7.077252
	0.5	12.137384	2.673934	7.256954	6.478934	7.136801
1.0	0	11.800777	2.600055	6.605888	6.605888	6.903152
	0.25	11.798482	2.668106	6.785251	6.440298	6.923034
	0.5	11.795145	2.825951	6.942451	6.340461	6.976002
1.2	0	11.476155	2.769448	6.368896	6.36888	6.745845
	0.25	11.472442	2.83371	6.518915	6.232045	6.764278
	0.5	11.465995	2.999416	6.651261	6.154534	6.817802
1.4	0	11.167730	2.926069	6.141690	6.141629	6.594279
	0.25	11.162759	2.988815	6.275670	6.019654	6.611725
	0.5	11.153404	3.155711	6.393635	5.950061	6.663203

Heat Transfer Results For Confined flow:

Table A.28 Nusselt number for Re=5,Pr=1

n	Ri	Nusselt Number				
		$\langle Nu \rangle_f$	$\langle Nu \rangle_r$	$\langle Nu \rangle_t$	$\langle Nu \rangle_b$	$\langle Nu \rangle_m$
0.6	0	2.020922	0.761558	1.458941	1.458947	1.425092
	0.25	2.025177	0.763588	1.477280	1.447414	1.428365
	0.5	2.030077	0.765715	1.497645	1.431997	1.431359
0.8	0	1.951262	0.754515	1.397229	1.397229	1.375059
	0.25	1.954414	0.755637	1.416464	1.381818	1.377083
	0.5	1.963426	0.759365	1.43751	1.371997	1.383075
1.0	0	1.897423	0.748737	1.353347	1.353347	1.338214
	0.25	1.900817	0.750216	1.373878	1.337930	1.340710
	0.5	1.910170	0.754567	1.396685	1.329219	1.347660
1.2	0	1.856995	0.745430	1.322899	1.322819	1.312036
	0.25	1.859579	0.745894	1.340790	1.308387	1.313663
	0.5	1.869551	0.752079	1.368669	1.300486	1.322696
1.4	0	1.82656	0.743919	1.301286	1.30143	1.293299
	0.25	1.828112	0.743071	1.321142	1.282518	1.293711
	0.5	1.836089	0.74906	1.346941	1.275318	1.301852

Table A.29 Nusselt number for Re=5,Pr=5

n	Ri	Nusselt Number				
		$\langle Nu \rangle_f$	$\langle Nu \rangle_r$	$\langle Nu \rangle_t$	$\langle Nu \rangle_b$	$\langle Nu \rangle_m$
0.6	0	3.480536	1.020841	2.566506	2.566544	2.408607
	0.25	3.483766	1.024223	2.584806	2.552019	2.411204
	0.5	3.490194	1.035854	2.591542	2.553898	2.417872
0.8	0	3.352996	0.995876	2.393862	2.393875	2.284153
	0.25	3.356159	0.999691	2.41089	2.381066	2.286951
	0.5	3.36517	1.011312	2.43015	2.373802	2.295109
1.0	0	3.250100	0.973614	2.275203	2.275200	2.193529
	0.25	3.253053	0.977860	2.294496	2.260205	2.196403
	0.5	3.262082	0.991886	2.316333	2.253808	2.206027
1.2	0	3.170651	0.956239	2.193283	2.193002	2.128294
	0.25	3.173656	0.962455	2.212218	2.181200	2.132382
	0.5	3.182364	0.982536	2.233891	2.182330	2.145280
1.4	0	3.108482	0.941511	2.132269	2.131738	2.0785
	0.25	3.110942	0.949202	2.150621	2.121046	2.082953
	0.5	3.118041	0.968795	2.180784	2.112374	2.094999

Table A.30 Nusselt number for Re=5,Pr=10

n	Ri	Nusselt Number				
		$\langle Nu \rangle_f$	$\langle Nu \rangle_r$	$\langle Nu \rangle_t$	$\langle Nu \rangle_b$	$\langle Nu \rangle_m$
0.6	0	4.331169	1.168371	3.275606	3.275706	3.012713
	0.25	4.333749	1.174609	3.288506	3.265418	3.015570
	0.5	4.341759	1.194170	3.303898	3.259450	3.024819
0.8	0	4.184759	1.131679	3.022813	3.022838	2.840522
	0.25	4.187469	1.139836	3.035046	3.01456	2.844228
	0.5	4.194986	1.164314	3.049981	3.009965	2.854811
1.0	0	4.062435	1.097435	2.851888	2.851888	2.715912
	0.25	4.065234	1.108539	2.866790	2.842464	2.720757
	0.5	4.072620	1.140372	2.884794	2.838621	2.734102
1.2	0	3.966436	1.069349	2.735082	2.734688	2.626389
	0.25	3.969045	1.084685	2.750547	2.726352	2.632657
	0.5	3.975885	1.127930	2.769590	2.727242	2.650162
1.4	0	3.890729	1.045115	2.64857	2.647853	2.558067
	0.25	3.893101	1.064414	2.666797	2.638845	2.565789
	0.5	3.89934	1.118746	2.689459	2.641459	2.587251

Table A.31 Nusselt number for Re=10,Pr=1

n	Ri	Nusselt Number				
		$\langle Nu \rangle_f$	$\langle Nu \rangle_r$	$\langle Nu \rangle_t$	$\langle Nu \rangle_b$	$\langle Nu \rangle_m$
0.5	0	2.841171	0.851924	1.967312	1.967376	1.906946
	0.25	2.845228	0.854195	2.025546	1.921162	1.911532
	0.5	2.855901	0.854788	2.067078	1.869370	1.911784
0.6	0	2.782119	0.845905	1.910611	1.910656	1.862323
	0.25	2.787390	0.847336	1.957622	1.867949	1.865074
	0.5	2.799736	0.851471	2.001347	1.833056	1.871403
0.8	0	2.684986	0.835816	1.822614	1.822621	1.791509
	0.25	2.689446	0.837755	1.865120	1.785734	1.794514
	0.5	2.702920	0.843269	1.907030	1.759014	1.803058
1.0	0	2.606040	0.827858	1.757386	1.757382	1.737166
	0.25	2.611051	0.830434	1.797946	1.724592	1.741006
	0.5	2.624370	0.837379	1.839184	1.703645	1.751144
1.2	0	2.540485	0.821659	1.707498	1.707491	1.694283
	0.25	2.544837	0.824679	1.747267	1.676867	1.698413
	0.5	2.556826	0.833145	1.788467	1.660634	1.709768
1.4	0	2.487745	0.818697	1.669786	1.672646	1.662219
	0.25	2.489566	0.820097	1.708787	1.637088	1.663885
	0.5	2.502029	0.831719	1.748912	1.632528	1.678797

Table A.32 Nusselt number for Re=10,Pr=5

n	Ri	Nusselt Number				
		$\langle Nu \rangle_f$	$\langle Nu \rangle_r$	$\langle Nu \rangle_t$	$\langle Nu \rangle_b$	$\langle Nu \rangle_m$
0.5	0	4.980455	1.112601	3.493187	3.493341	3.269896
	0.5	5.030547	1.132820	3.638397	3.377888	3.294913
0.6	0	4.860070	1.102390	3.351072	3.351238	3.166193
	0.25	4.866249	1.103603	3.405405	3.302678	3.169484
	0.5	4.883509	1.127145	3.460896	3.264051	3.183900
0.8	0	4.672648	1.073667	3.132058	3.132109	3.002620
	0.25	4.677875	1.077638	3.179498	3.092371	3.006845
	0.5	4.691905	1.109093	3.227718	3.064560	3.023319
1.0	0	4.522470	1.050263	2.972474	2.972454	2.879415
	0.25	4.527362	1.056611	3.017546	2.936301	2.884455
	0.5	4.540965	1.098006	3.064128	2.916688	2.904947
1.2	0	4.395366	1.033326	2.852547	2.852531	2.783443
	0.25	4.399197	1.041901	2.897510	2.818602	2.789303
	0.5	4.407839	1.092485	2.948675	2.791094	2.810023
1.4	0	4.290423	1.024566	2.762035	2.763568	2.710148
	0.25	4.293532	1.034169	2.804483	2.732624	2.716202
	0.5	4.302001	1.097234	2.854954	2.720742	2.743733

Table A.33 Nusselt number for Re=10,Pr=10

n	Ri	Nusselt Number				
		$\langle Nu \rangle_f$	$\langle Nu \rangle_r$	$\langle Nu \rangle_t$	$\langle Nu \rangle_b$	$\langle Nu \rangle_m$
0.5	0	6.293124	1.250945	4.454435	4.454829	4.113333
	0.5	6.314140	1.313763	4.579974	4.355363	4.140810
0.6	0	6.132844	1.229903	4.253226	4.253482	3.967363
	0.25	6.138600	1.246731	4.306605	4.206893	3.974707
	0.5	6.154487	1.306173	4.361254	4.171354	3.998317
0.8	0	5.894026	1.187960	3.946992	3.947072	3.744013
	0.25	5.898827	1.216152	3.992368	3.910099	3.754362
	0.5	5.911270	1.298026	4.039315	3.885395	3.783502
1.0	0	5.705824	1.153041	3.725242	3.725226	3.577333
	0.25	5.710489	1.193967	3.768323	3.693213	3.591498
	0.5	5.721802	1.300670	3.813446	3.675696	3.627904
1.2	0	5.545397	1.129775	3.559770	3.559763	3.448676
	0.25	5.549161	1.182379	3.603450	3.530240	3.466307
	0.5	5.557641	1.314243	3.649763	3.516906	3.509638
1.4	0	5.412700	1.122536	3.435376	3.437978	3.352147
	0.25	5.416749	1.183932	3.477891	3.415206	3.373445
	0.5	5.424635	1.338586	3.523814	3.410774	3.424453

Table A.34 Nusselt number for Re=40,Pr=1

n	Ri	Nusselt Number				
		$\langle Nu \rangle_f$	$\langle Nu \rangle_r$	$\langle Nu \rangle_t$	$\langle Nu \rangle_b$	$\langle Nu \rangle_m$
0.5	0	5.53364	1.033952	3.08007	3.080291	3.181989
	0.25	5.534811	1.062207	3.254166	2.917587	3.192193
	0.5	5.538587	1.13905	3.421178	2.782534	3.220337
0.6	0	5.441909	1.032284	3.044832	3.04481	3.140959
	0.25	5.445893	1.059002	3.204646	2.901677	3.152805
	0.5	5.454644	1.134991	3.358077	2.786886	3.18365
0.8	0	5.258661	1.03297	2.961286	2.961398	3.053579
	0.25	5.265306	1.06203	3.101149	2.84337	3.067964
	0.5	5.280231	1.133304	3.235296	2.759757	3.102147
1.0	0	5.088978	1.039464	2.877942	2.877965	2.971087
	0.25	5.097524	1.069874	2.997683	2.78759	2.988168
	0.5	5.114891	1.137838	3.11656	2.731062	3.025088
1.2	0	4.932581	1.049573	2.796778	2.796691	2.893906
	0.25	4.94268	1.081847	2.903949	2.728541	2.914254
	0.5	4.959876	1.147425	3.011264	2.694624	2.953297
1.4	0	4.791368	1.063506	2.725405	2.725325	2.826401
	0.25	4.800615	1.097036	2.821344	2.672682	2.847919
	0.5	4.815545	1.161023	2.920317	2.655453	2.888084

Table A.35 Nusselt number for Re=40,Pr=5

n	Ri	Nusselt Number				
		$\langle Nu \rangle_f$	$\langle Nu \rangle_r$	$\langle Nu \rangle_t$	$\langle Nu \rangle_b$	$\langle Nu \rangle_m$
0.5	0	10.164526	1.522881	5.288704	5.288909	5.566255
	0.25	10.16794	1.604776	5.563318	5.050915	5.596737
	0.5	10.172526	1.906396	5.826304	4.864947	5.692543
0.6	0	9.978644	1.587286	5.217434	5.217632	5.500249
	0.25	9.983445	1.652891	5.46657	5.008563	5.527867
	0.5	9.990895	1.909835	5.704656	4.854861	5.615062
0.8	0	9.610377	1.713755	5.041997	5.042093	5.352056
	0.25	9.617417	1.751532	5.248582	4.883382	5.375229
	0.5	9.629922	1.951731	5.444515	4.792906	5.454769
1.0	0	9.26804	1.83469	4.859402	4.858765	5.205224
	0.25	9.27414	1.857485	5.030979	4.734282	5.224221
	0.5	9.287825	2.010081	5.19593	4.687085	5.29523
1.2	0	8.951966	1.95747	4.676778	4.676714	5.065732
	0.25	8.960319	1.968245	4.832115	4.580288	5.085242
	0.5	8.973831	2.09069	4.974781	4.56425	5.150888
1.4	0	8.66562	2.08253	4.51472	4.514589	4.944365
	0.25	8.67367	2.080256	4.656646	4.435424	4.961499
	0.5	8.686625	2.179127	4.783837	4.44096	5.022637

Table A.36 Nusselt number for Re=40,Pr=10

n	Ri	Nusselt Number				
		$\langle Nu \rangle_f$	$\langle Nu \rangle_r$	$\langle Nu \rangle_t$	$\langle Nu \rangle_b$	$\langle Nu \rangle_m$
0.5	0	12.583446	1.988829	6.996218	6.99631	7.141201
	0.25	12.588367	2.12437	7.307392	6.723635	7.185941
	0.5	12.595889	2.594047	7.586195	6.516134	7.323066
0.6	0	12.38817	2.117764	6.895181	6.895261	7.074094
	0.25	12.394845	2.212293	7.168989	6.66976	7.111472
	0.5	12.40499	2.544664	7.410461	6.520326	7.22011
0.8	0	11.997495	2.3421	6.635146	6.6352	6.902485
	0.25	12.004636	2.41157	6.85088	6.472979	6.935016
	0.5	12.019014	2.590664	7.032816	6.425904	7.017099
1.0	0	11.62979	2.539039	6.357347	6.356426	6.72065
	0.25	11.633886	2.597249	6.527184	6.232573	6.747723
	0.5	11.64879	2.695551	6.672294	6.241411	6.814512
1.2	0	11.28447	2.730733	6.072477	6.072374	6.540013
	0.25	11.290776	2.772333	6.227021	5.981059	6.567797
	0.5	11.305392	2.836638	6.347165	6.027229	6.629106
1.4	0	10.968124	2.917258	5.816282	5.816038	6.379425
	0.25	10.973319	2.942034	5.95991	5.737872	6.403284
	0.5	10.987342	2.991991	6.066266	5.80392	6.46238